LBL-4506

MASTER FILE

CARBON-13 NMR STUDIES OF LIQUID CRYSTALS

Stuart Anthony Allison
(M. S. thesis)

June 1975

Prepared for the U. S. Energy Research and
Development Administration under Contract W-7405-ENG-48

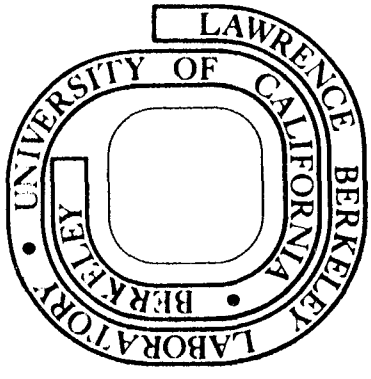

LBL-4506

ABSTRACT

High resolution, proton decoupled ^{13}C nmr are observed for a series of neat nematic liquid crystals, the p-alkoxyazoxybenzenes, and a smectic-A liquid crystal, diethylazoxydibenzoate in a magnetic field of 23 kG. The (uniaxial) order parameters $S = \langle P_2(\cos\theta)\rangle$ are found to be about 0.4 and 0.9 for the nematic and smectic-A phase respectively at the clearing points. The order parameter increases with decreasing temperature in the nematic phase but is constant, or nearly so, with temperature in the smectic-A phase. In the nematic series studied, the ordering exhibits an even-odd alternation along the series and qualitative agreement with a recent theory due to Marčelja is found. In both phases, the spectra show that the molecule rotates rapidly about its long axis. Tentative conclusions about molecular conformational motion and ^{14}N spin relaxation are presented for both nematic and smectic-A phases. In the smectic-A phase, the sample is rotated about an axis perpendicular to H_0 and the resulting spectra are discussed.

The theory of observed chemical shifts in liquid crystals is treated in an appendix. Equations are derived which relate the nmr spectra of liquid-crystals to the order parameters. A model for the smectic-C phase due to Luz and Meiboom and Doane is described and lineshapes are determined on the basis of this model for special cases. Experiments on smectic-C liquid crystals are currently underway for comparison with the theory.

Also treated in an appendix is the dependence of the order parameters on the molecular potential which give rise to the various

degrees of order in the different liquid crystalline phases. To a good approximation the functional dependence of the order parameters on the molecular potential is shown to be a simple one in the limit of small tilt angle in the smectic-C phase.

DEDICATION

To my parents - Dr. & Mrs. Bruce A. Allison

ACKNOWLEDGMENTS

The author wishes to thank Professor Alexander Pines for his guidance and direction of this research work. His example, both as a research director and as a teacher, has set a standard for my own career.

The author is grateful to Dr. James Chang, Dr. David Ruben, Dr. Alfred Hohener, Thomas Shattuck, and David Wemmer for their assistance with the experiments and for the many helpful discussions we had together. Also, thanks are due the Department of Chemistry, Materials and Molecular Research Division of the Lawrence Berkeley Laboratory, and the National Science Foundation through a traineeship for financial assistance. This work was performed under the auspices of the U.S. Energy Research and Development Administration.

Finally, the author would like to thank his fellow graduate students for their friendship and Carol Hacker for typing this thesis.

TABLE OF CONTENTS

I. INTRODUCTION

The aim of this research has been the study of nematic and smectic liquid crystals using ^{13}C nuclear magnetic resonance (nmr). In the past, nmr has played an important role in the study of liquid crystals although its application has not been straightforward.[1] The primary reason for this is the fact that the molecules comprising liquid crystals are long and rod-like and contain aromatic and/or highly conjugated systems. As a consequence, in addition to the isotropic liquid phase ordered liquid phases exist. In the isotropic liquid phase, rapid isotropic molecular reorientation takes place thereby averaging to zero the direct magnetic dipolar couplings between nuclear spins. In the liquid crystalline phases, however, varying degrees of long range orientational order lead to severely broadened, normally intractable nmr spectra. The common high temperature liquid crystal phases are depicted in Figure 1.

In our experiments proton decoupled ^{13}C nmr was used. Due to the decoupling of the protons and the low isotopic abundance of ^{13}C nuclei, high resolution spectra were obtained. This method, which was first applied in our laboratory during the spring of 1974[2] circumvents the need for a foreign probe molecule or the costliness of isotopically enriched samples.

The study of liquid crystals is extremely important for several reasons: (a) they serve as models for phase transitions and critical phenomena, e.g. superconductivity, ferromagnetism, (b) they provide

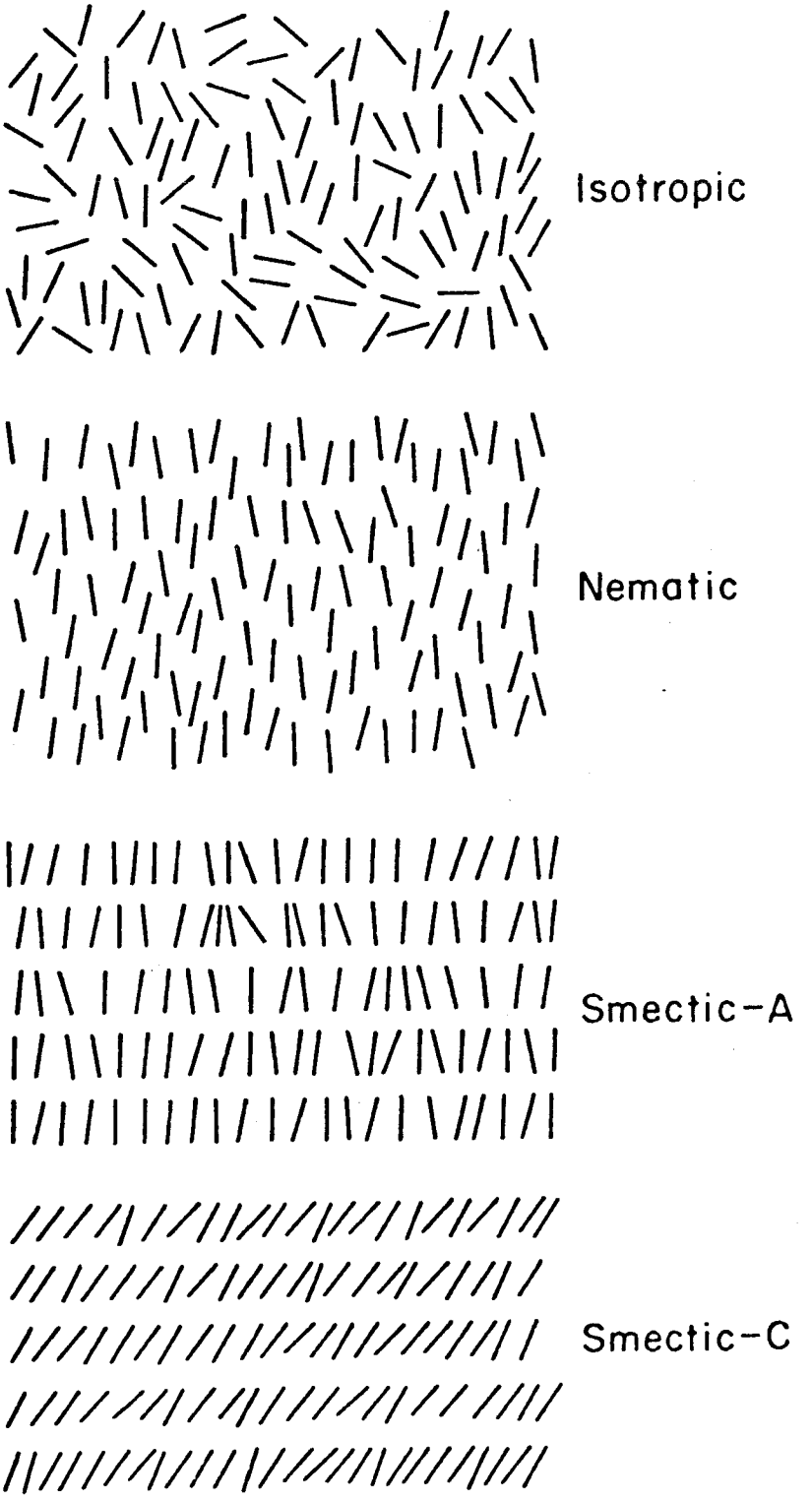

Figure 1

well defined orienting environments for chemistry, (c) technological importance in displays, nonlinear optical devices, etc., and (d) models for biological membranes.

In the last year, a series of nematic liquid crystals (n-alkoxyazoxybenzenes) and a smectic-A liquid crystal (diethylazoxydibenzoate) were studied. At the present time, experiments on smectic-C liquid crystals are under way.

In nematics, information was obtained concerning: (a) ordering as a function of temperature and as a function of chain length in a homologous series, (b) molecular conformational motion, and (c) spin relaxation of other nuclei, e.g. ^{14}N. In the smectic-A liquid crystal studied, diethylazoxydibenzoate (DEAB), the same kind of information was extracted. Here, though, we were able to rotate the sample which provided additional information. Although the conclusions about the liquid crystal are not novel, in particular because of the simple structure of the smectic-A phase, the results are testimony to the simple and direct interpretation the method provides.

Though the current lack of experimental data makes it difficult to draw many conclusions concerning the smectic-C phases, the theory of observed chemical shifts is extended to this phase. Line shapes have been generated and it is shown that they are sensitive to long range orientational order and internal molecular conformational motion. The theory also demonstrates the advantages of sample rotation.

The main body of this thesis describes the experiments and the conclusions drawn from them. The instrumentation relevant to the experiments and the preparation of samples are discussed in Section II-A. In Sections II-B and II-C, the experiments are discussed in detail. The observable of greatest importance in the interpretation of data is the chemical shift. A thorough treatment of it is placed in the appendices to avoid lengthy digressions from the discussion of experiments.

In appendix A, the chemical shielding tensor and its transformational properties in cartesian coordinates are discussed. In appendix B, equations are derived which relate the chemical shift to the order parameters in the various liquid crystal phases. The program used to generate lineshapes for a rotated smectic C is given in appendix C. Appendices E and F relate the various order parameters to the molecular field potentials responsible for the partial ordering in liquid crystals.

II. EXPERIMENTAL

A. Instrumentation and Samples

1. Spectrometer

The spectrometer is a homebuilt double resonance device described briefly elsewhere[3]. A schematic of the spectrometer is shown in Figure 2. The main features of relevance to the present experiments are:

(a) High power proton spin-decoupling amplifier,

(b) probe (see below),

(c) sensitive ^{13}C detector system with efficient rejection of spin-decoupling induced noise,

(d) features for signal enhancement and Fourier-transformation.

The proton and carbon amplifiers are modified Millen radio amateur transmitters capable of producing several hundred watts of continuous rf power at 106 MHz into a matched 50 ohm load. A schematic drawing appears in Figure 3. For operation into the probe, rf power bursts exceedingly .15 sec caused severe problems of heat dissipation and the device was normally operated with a duty cycle of < 20%. The ^{13}C detector consists of a narrow-band preamplifier and complex phase detector with an intermediate frequency of 30 MHz. Tuned diodes and narrowband filters precede the preamplifier to provide protection from the rf pulses and rejection of noise introduced by the proton spin-decoupling. Since the ^{13}C signals are extremely weak, care was taken to eliminate radiated noise by physically separating the low level

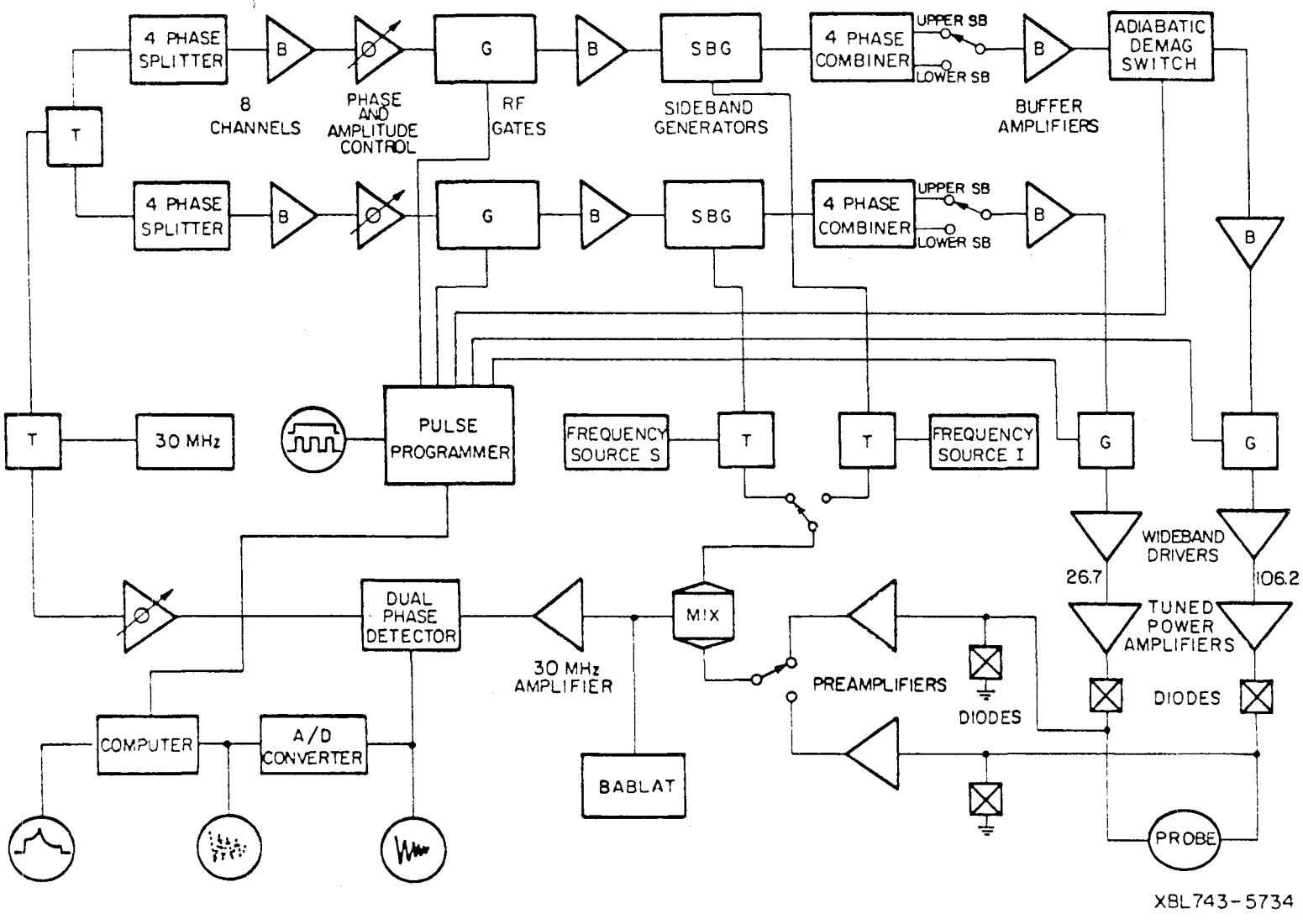
4 PHASE SPLITTER
B
G
SBG
4 PHASE COMBINER
UPPER SB
LOWER SB
ADIABATIC DEMAG SWITCH
8 CHANNELS
PHASE AND AMPLITUDE CONTROL
RF GATES
SIDEBAND GENERATORS
BUFFER AMPLIFIERS
T
30 MHz
PULSE PROGRAMMER
FREQUENCY SOURCE S
FREQUENCY SOURCE I
WIDEBAND DRIVERS
26.7
106.2
TUNED POWER AMPLIFIERS
DUAL PHASE DETECTOR
MIX
30 MHz AMPLIFIER
PREAMPLIFIERS
DIODES
COMPUTER
A/D CONVERTER
BABLAT
PROBE
XBL743-5734

Figure 2

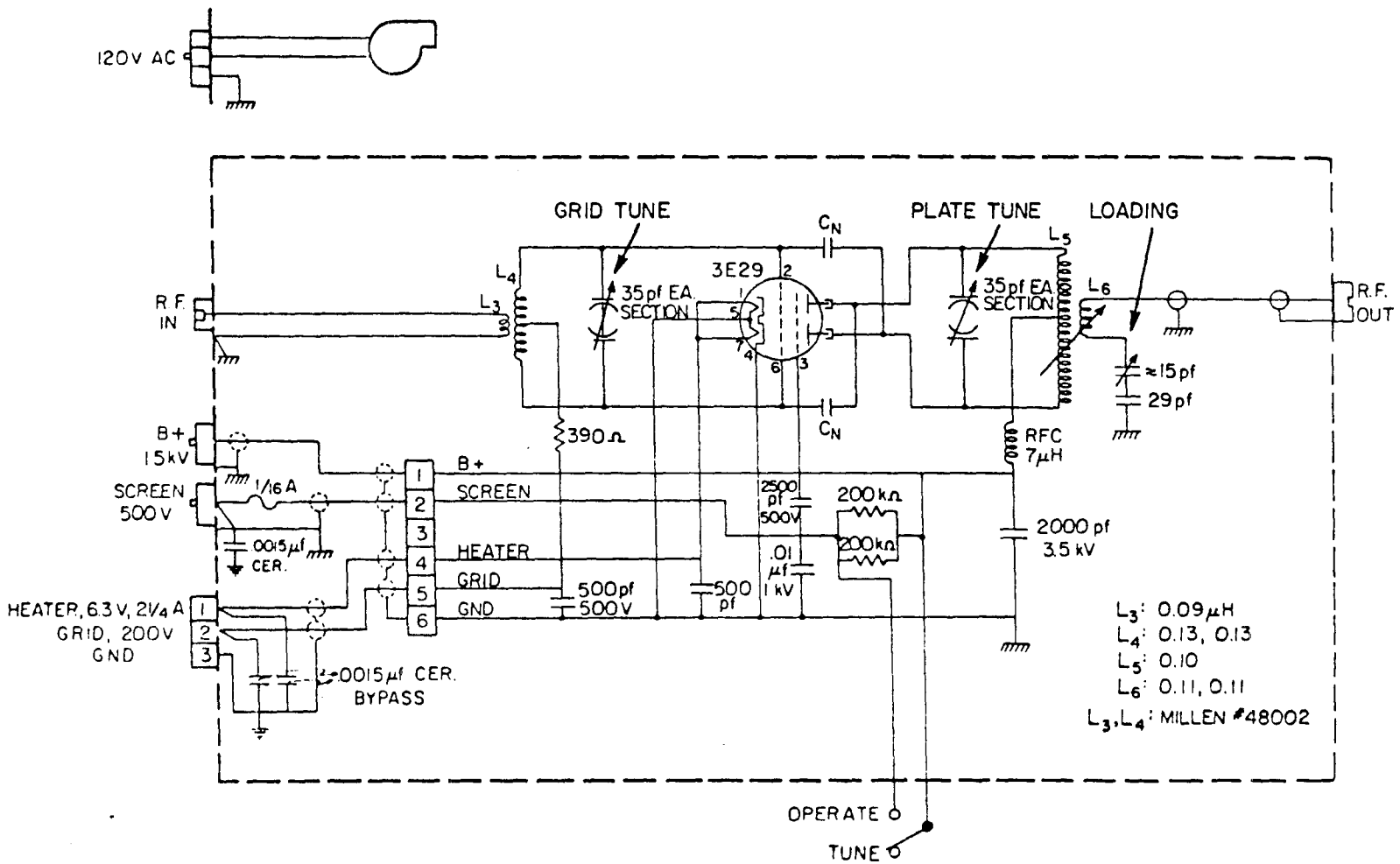

106 MHz TRANSMITTER

WILKINSON

XBL 766-6945

Figure 3

rf phase and amplitude modulation sections from the transmitter sections, and shielding all detector cables, connectors, and components. Ground loops were minimized with heavy copper strips distributed behind the instrument panels.

The pulse sequences used in the experiments are depicted in Figure 4. The first is a simple proton spin decoupled free induction decay which yields the high resolution ^{13}C nmr spectrum on Fourier-transformation. Decoupling fields of 15 - 20 G in the rotating frame were found to suffice. The second is similar except that it is preceeded by a cross-polarization step which provides an enhancement of the ^{13}C signal/noise. This was designed for solids, but we showed previously that it also functions in liquid crystals. The latter sequence was used wherever possible, and was found to yield rapid and efficient data accumulation. Two instances when it could not be used were:

(a) in the isotropic phase,

(b) in the rotated smectic-A phase at and near the magic angle (54.7°).

In both these cases the ^{13}C-^{1}H magnetic-dipolar coupling vanishes, and thus cross-polarization proceeds very inefficiently through the isotropic electron-coupled nuclear spin interactions.[4] In these cases, the normal free induction decay was used with longer accumulation times.

Data acquisition is performed by a Biomation analog-digital recorder with direct transfer to the memory of a PDP 8/E computer.

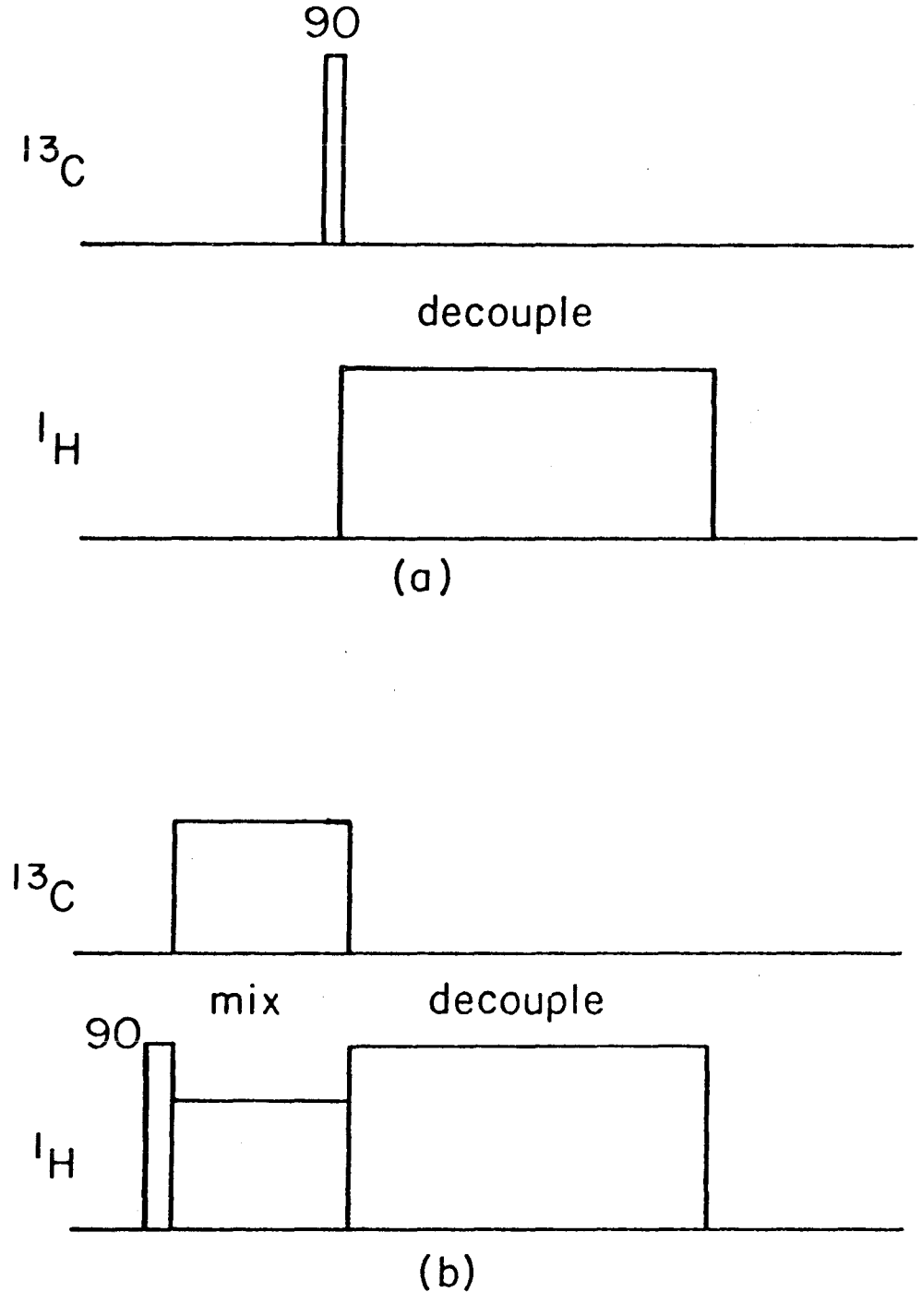

XBL 766 1987

Figure 4

The latter served for signal averaging, data storage and plotting, Fourier transformation and other data processing. One thousand complex points can be accumulated and transformed, certainly sufficient for the constraints imposed by the magnet homogeneity. Acquisition times for our experiments varied from several minutes to several hours. Timing is provided by a homebuilt pulse programmer; computer controlled for rf pulse sequences, acquisition pulses, and general purpose peripheral supervision.

2. Probe

A schematic diagram of the probe designed for the superconducting geometry is shown in Figure 5. A photograph is shown in Figure 6. The double-resonance rf coil system contains an inner horizontal solenoidal coil for ^{13}C and an outer Helmholtz-pair for ^{1}H, and is mounted on a teflon/glass base. Tuning is achieved by series resonance circuits with home-built high voltage capacitors. These consist of polished copper tubes with teflon/glass dielectric. The capacitors are varied remotely (outside the magnet bore) by threaded valves which control the position of a length rigid coaxial cable connected to one pole of the capacitors. Matching to 50 ohms is accomplished with low power fixed commercial capacitors. Both entire capacitor arrangements are shielded with grounded tubes to prevent capacitive coupling between the two resonance circuits.

Sample orientation is provided by a goniometer consisting of a vertical shaft passing through the base and attached to a worm gear. The latter is arranged through two gears to rotate the gear

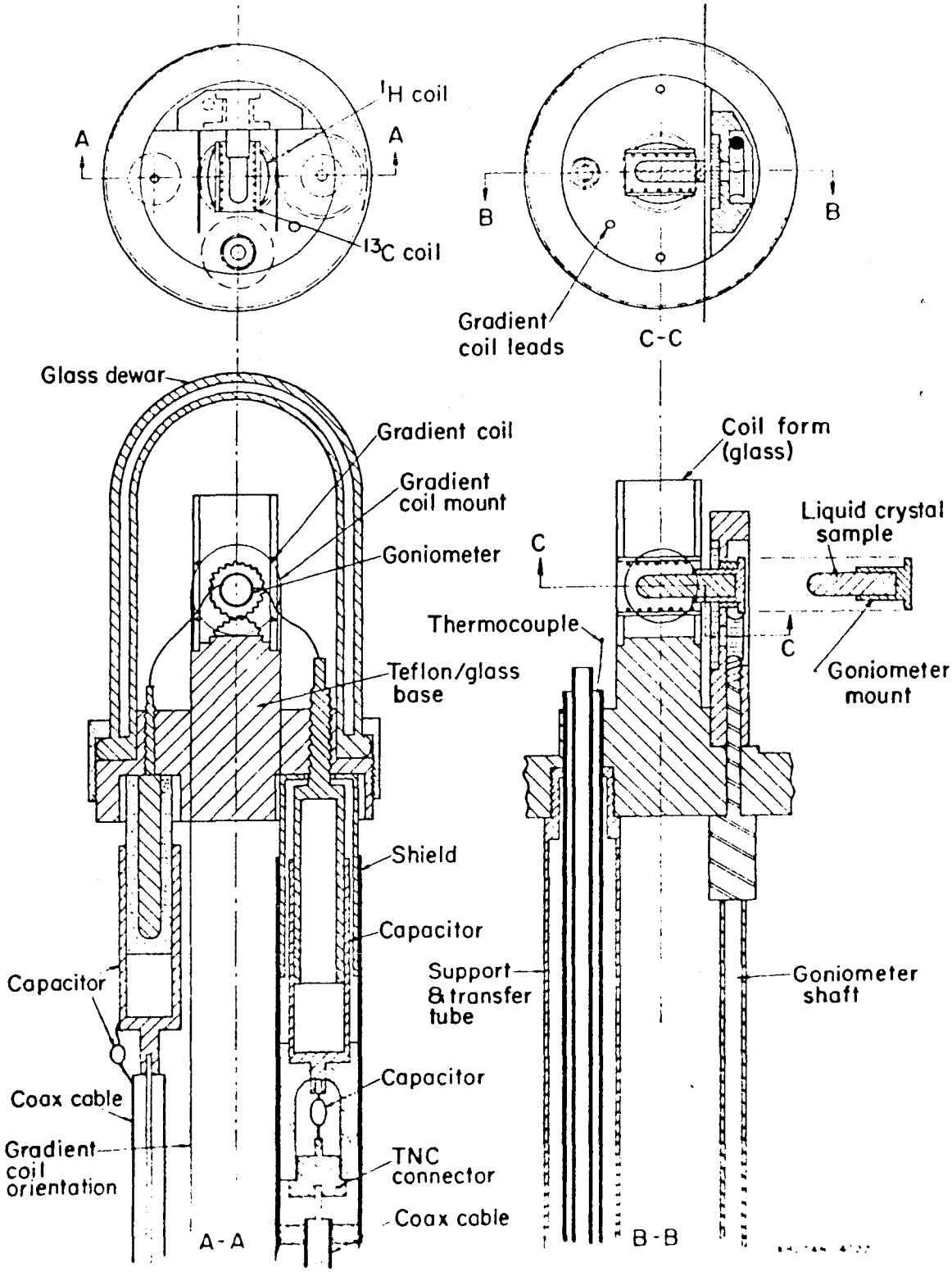
^{1}H coil
^{13}C coil
A
A
B
B
Gradient coil leads
C-C
Glass dewar
Gradient coil
Gradient coil mount
Goniometer
Teflon/glass base
Shield
Capacitor
Capacitor
Coax cable
Gradient coil orientation
Capacitor
TNC connector
Coax cable
A-A
Coil form (glass)
Liquid crystal sample
C
C
Thermocouple
Goniometer mount
Support & transfer tube
Goniometer shaft
B-B

Figure 5

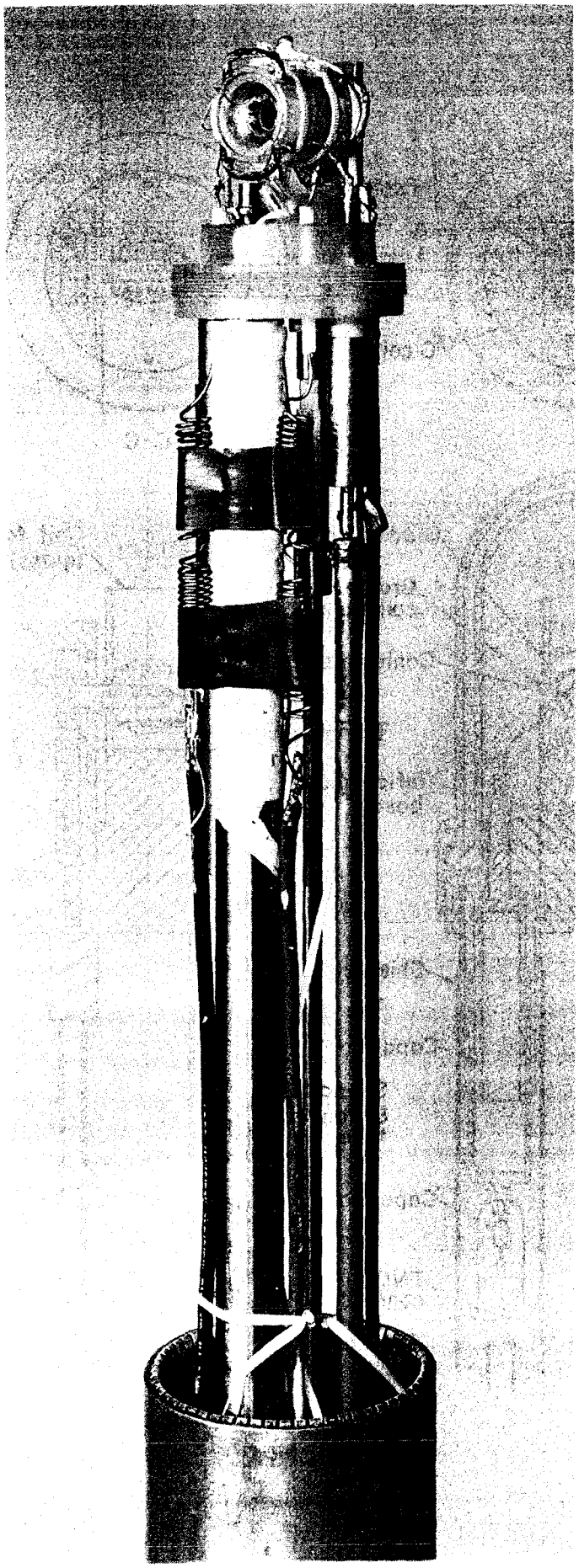

CBB 748-5643

Figure 6

wheel on which the sample is mounted. The entire rotation is precise to within 1° and can be controlled outside the magnet bore.

Temperature is controlled by a stream of dry nitrogen gas. This passes over a main heater at the base of the probe and reaches the sample cavity through an evacuated support and transfer tube. Mounted in the top of the transfer tube is a small auxiliary heater (made of platinum resistors) which is controlled by a feedback circuit. The temperature sensor for the feedback circuit is a thermocouple mounted in the sample cavity. The cavity is enclosed by a glass dewar which is mounted tightly on the base with a teflon/glass cup. Temperature control and gradients with this system within 1°C and the temperature range which has been covered in our liquid crystal work is -20°C to 200°C.

An additional feature of the probe is a quadrupole current coil system for producing pulsed magnetic field gradients of varying directions for diffusion studies. This will not be described here.

3. Samples

The samples (n-alkoxyazoxybenzenes and diethylazoxydibenzoate (DEAB)) were obtained commercially from Eastman Kodak Company. The nematic liquid crystals (n-alkoxyazoxybenzenes) and the smectic-A liquid crystal (DEAB) were recrystallized repeatedly from a 3/1 benzene/ethanol mixture until the melting points were within 1° of literature values. Small pyrex ampuoles of length 12mm and

outside diameter of 6mm were prepared to conform to the geometry of the magnet and heated in a flame to drive off adsorbed water. The material was then sealed in the ampuoles under vacuum after several freeze-thaw cycles. Several sealed ampuoles for each liquid crystal were prepared and used throughout the course of the experiments since it was found that decomposition sometimes occured, particularly after prolonged maintenance of the sample in the isotropic phase. The sample purity was monitored by following the clearing temperature.

B. Molecular Ordering and Even-Odd Effect in a Homologous Series of Nematic Liquid Crystals.

Although molecular end chains are known to have perceptible and important effects on the properties of liquid crystals, until recently, theories of the liquid crystal phase have not included their effects explicitly. Rather, their influence was taken into account indirectly by assuming simply that they "take up space" and thus affect the average interaction between essentially rigid molecules.[5]

Marčelja has presented a mean field theory which accounts specifically for the effects of the end chains on the anisotropic interactions between the molecules.[6] In his theory, a molecule is considered to consist of both rigid parts and flexible alkyl chains which take part in the ordering process. For the chain, this ordering is calculated by exact summation over all the conformations of a chain in the mean field due to neighboring

molecules. The nematic orientational ordering is obtained within a self-consistent mean field approximation.

This theory provides good agreement with experimental data on isotropic-nematic transition temperatures and entropies, and explains for the first time the "even-odd" effect in these quantities along a homologous series.[7] A quantity of prime concern in the structure of the nematic phase is the degree of orientational molecular ordering, described by an order parameter:[8]

$$S \equiv \langle D^{(2)}_{00}(\Omega) \rangle = \langle \frac{3}{2} \cos^2\theta - \frac{1}{2} \rangle \qquad (1)$$

where θ is the angle between the long axis and the nematic director. (See discussion just following (B19) and appendix D.) A striking prediction of the theory is that S should also exhibit the even-odd effect in a homologous series. In this section, results of measurements of S for a homologous series of nematic liquid crystals at the isotropic-nematic transition in the nematic phase are shown. These data provide the first convincing manifestation of the even-odd effect for the ordering near the transitions, and a reliable basis for the quantitative examination of microscopic theories of liquid crystal phases. In addition, some conclusions regarding conformational motion of the liquid crystal molecules and ^{14}N spin relaxation in the nematic phase are presented. The series of liquid crystals studied is shown in Figure 7, p-alkoxyazoxybenzenes,

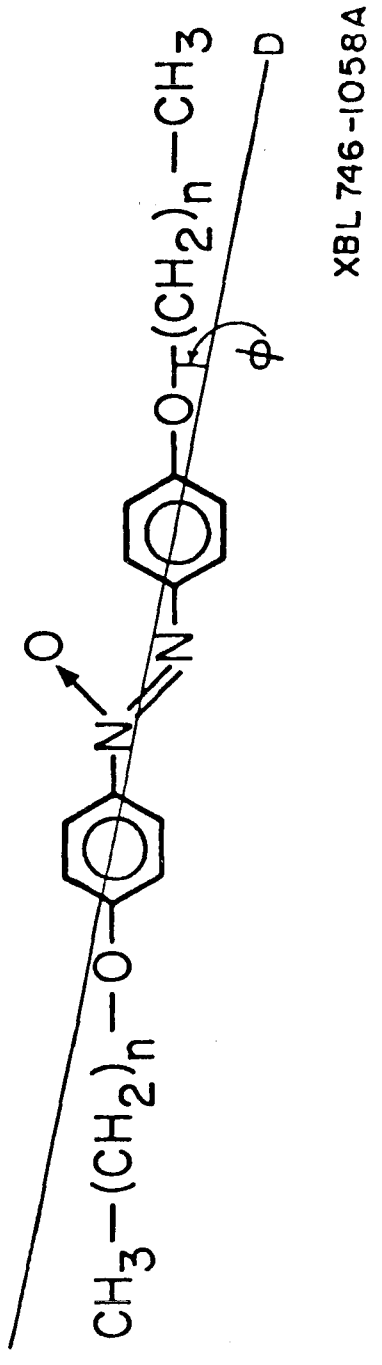

Figure 7

with n + 1 from 1 to 7.[9] Previously, high resolution nmr has not been generally possible in liquid crystals and limited approaches employing wideline nmr, deuterated materials and small probe molecules have been used. In some recent experiments, we demonstrated that with high power proton spin decoupling, high resolution and tractable ^{13}C nmr spectra can be obtained, and that they are sensitive to molecular ordering through the strongly anisotropic ^{13}C chemical shielding tensors.[2,10]

To obtain a qualitative idea of the behavior expected, Figure 8 shows the directional trends of $\underset{\approx}{\sigma}$ tensors for the important carbon functional groups occuring in liquid crystal molecules, namely aromatic core and aliphatic side chains. These were obtained from single crystal experiments on model systems.[11] The meaning of the symbols are as follows: σ_{ii} are the elements of $\underset{\approx}{\sigma}$ with the convention $\sigma_{11} \leq \sigma_{22} \leq \sigma_{33}$. Higher σ_{ii} implies higher diamagnetic shielding, i.e., lower resonance frequency at fixed field. In the aliphatic case, $\sigma_{11} \approx \sigma_{22} = \sigma_{\perp}$. Thus, for the aromatic carbons, the heaviest shielding occurs with the magnetic field perpendicular to the π-model plane, and the lightest shielding with the field radially outwards from the ring. The anisotropy $\sigma_{33} - \sigma_{11}$ is large for these carbons, $\sim$ 200 ppm typically.

For the aliphatic chains, details of the conformation are of course critical; the behavior of $\underset{\approx}{\sigma}$ for the R group in Figure 8 is intended to imply that the heaviest shielding occurs with the magnetic field more or less "along the chain". The anisotropy

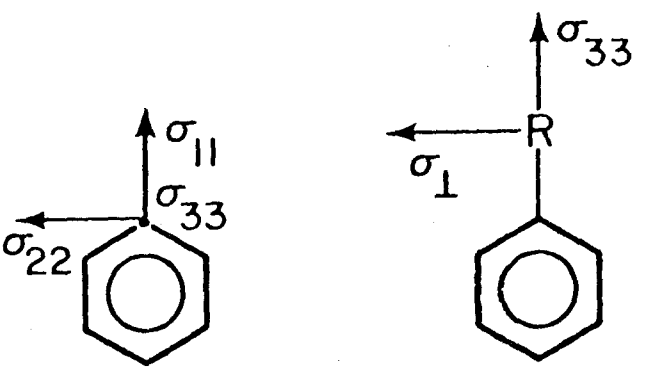

Figure 8

$\sigma_{33} - \sigma_{\perp}$ is smaller for the chains, ranging from $\sim$ 20 ppm for C-C bonds to $\sim$ 60 ppm for O-C bonds.

Recent work done by Pines and Chang[2] confirmed this expected trend. Figure 9 shows this vividly. The spectra are interpreted in the caption. Figure 10 shows Fourier-transform ^{13}C nmr spectra in the isotropic and nematic phases of series I. The line assignments appear in the caption. In the nematic phase, some of the spectra were acquired with proton-enhancement to improve the signal/noise for the low abundance ($\sim$ 1%) ^{13}C nuclei.[4] Without intense spin decoupling, broad, featureless spectra normally characteristic of the nematic phase were observed. In the isotropic phase, the chemical shifts σ_i for each of the carbon positions in the molecule are given, according to appendix A, by:

$$\sigma_i = \frac{1}{3} \mathrm{Tr}\, \underset{\approx}{\sigma} \qquad \text{(A11)}$$

where $\underset{\approx}{\sigma}$ are the chemical shielding tensors.[12] In the nematic phase, we assume rapid reorientation of the molecules about their long axes, yielding averaged tensors $\underset{\approx}{\bar{\sigma}}$ with elements $\bar{\sigma}_{\parallel}$ and $\bar{\sigma}_{\perp}$ relative to the long axis. From appendix B, the observed chemical shifts σ are given by

$$\sigma = \sigma_i + \frac{2}{3} S\, (\bar{\sigma}_{\parallel} - \bar{\sigma}_{\perp}) \qquad \text{(B22)}$$

where S is the order parameter in (1). For the aromatic rings, it has been shown that $\bar{\sigma}_{\parallel} < \bar{\sigma}_{\perp}$[2,4] and thus a downfield shift of

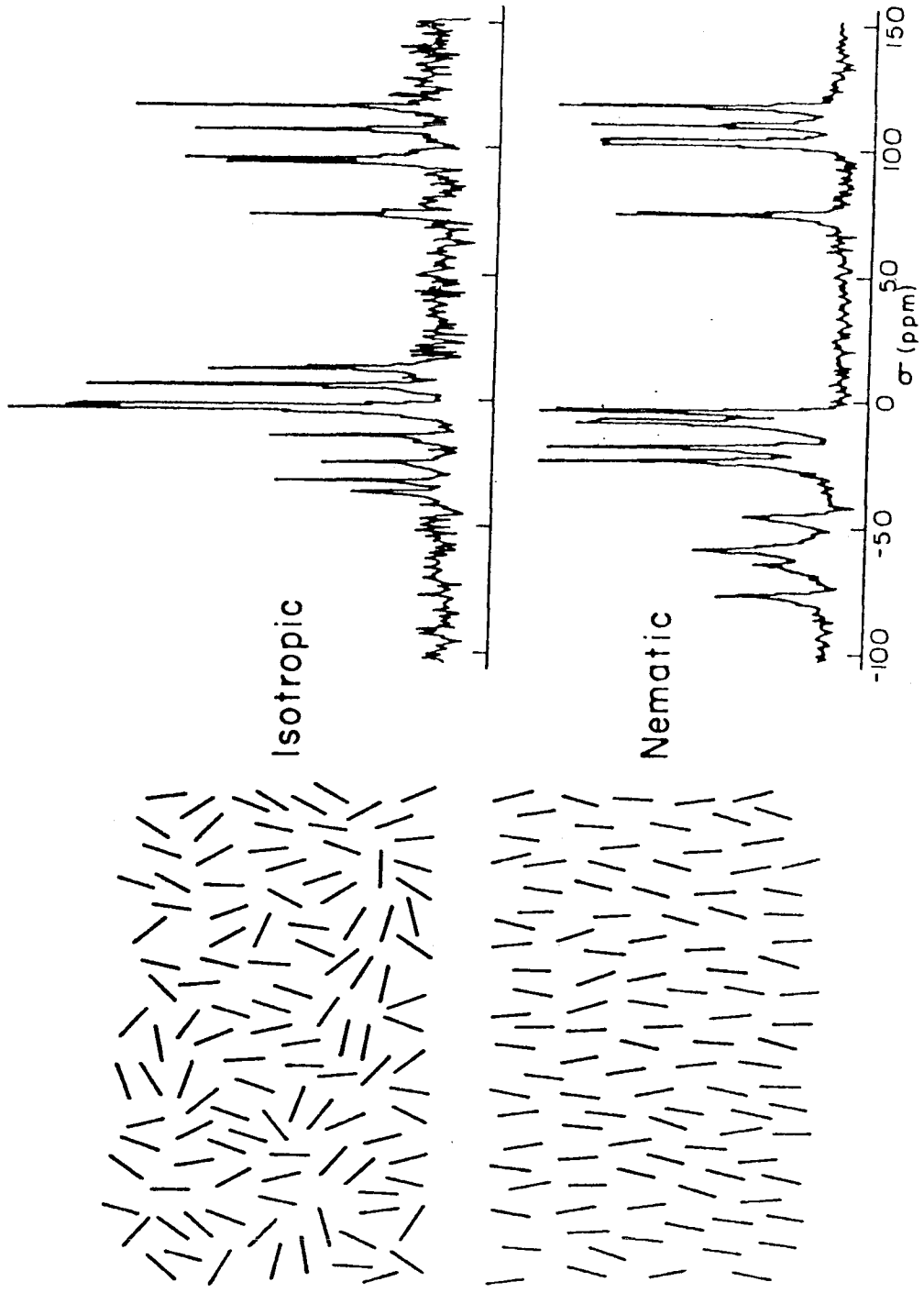

XBL 751-5492

Figure 9

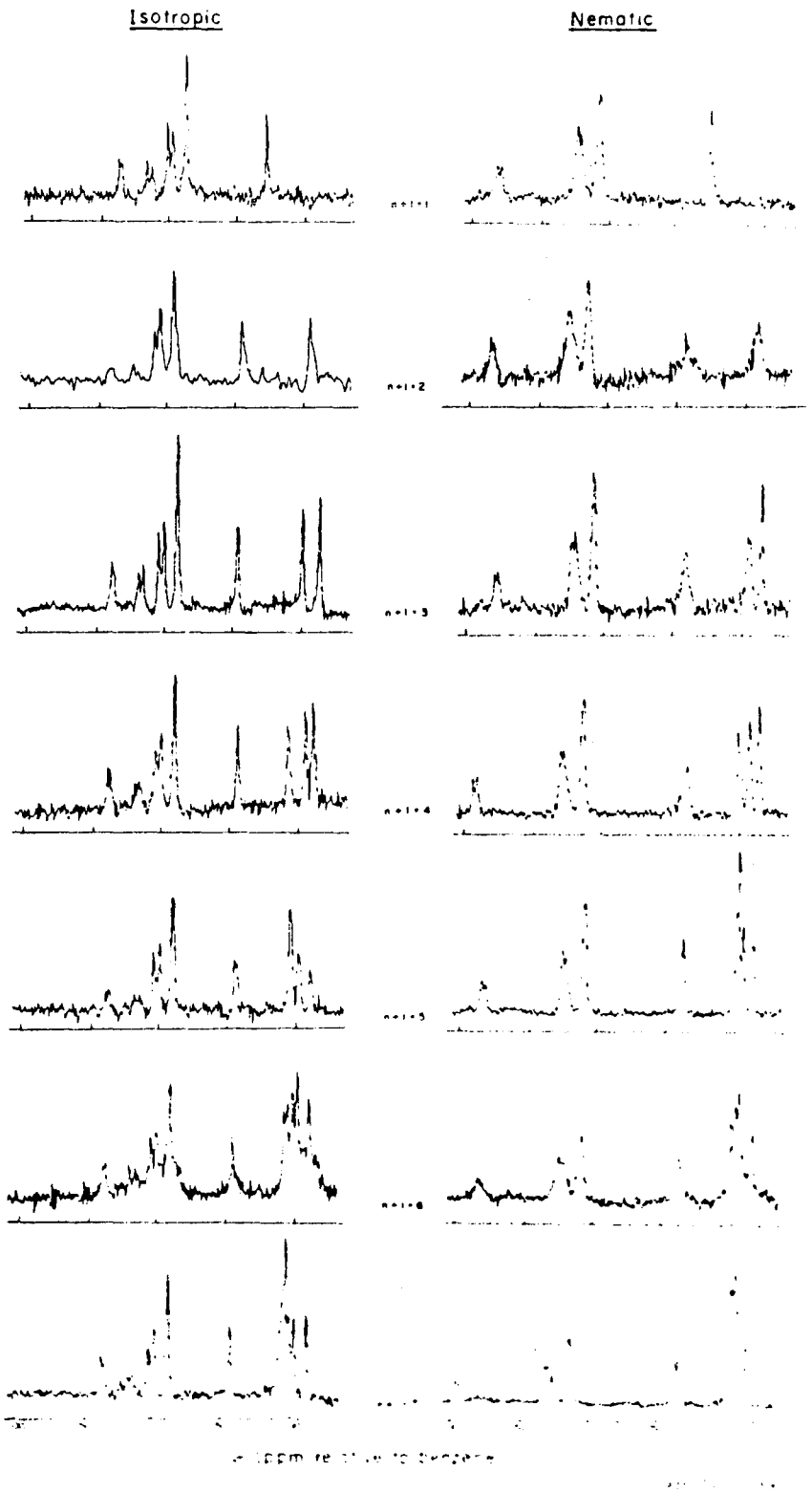

Figure 10

the lines is expected in the isotropic-nematic transition, exactly as observed for the whole series in Figure 10. Further conclusions are presented from these spectra at the end of this section.

The dependence of chemical shifts on temperature for the lines in the series studied is depicted in Figure 11, reflecting the first-order isotropic-nematic transitions and the marked effect of ordering on the chemical shifts observed for the whole series. In order to extract quantitative values of the order parameters for comparison with theory, we make the assumptions that the aromatic $\underset{\sim}{\sigma}$ tensors remain the same and that the geometry of the aromatic region of the molecules is similar throughout the homologous series. The values of σ for the low field lines can then be used to calculate relative values for S from (B22). Such values at the isotropic-nematic transitions and 5°C below are shown in Figure 12, normalized to 0.43, the Maier-Saupe value for n + 1 = 1. The values at the transition temperatures were obtained in a separate set of experiments with ^{13}C spectra displaying two sets of lines from the isotropic and nematic phases in equilibrium. Also shown are the transition values calculated by Marčelja.[6] Although these are not expected to be accurate in a mean field theory near the transitions, the correspondence in general trend and in the even-odd effect is gratifying.[13] Value of S over the entire temperature ranges are available from our data and appear in Table 1 below.

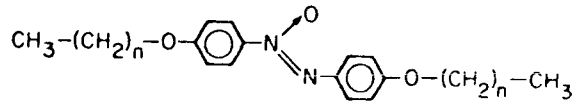
CH3-(CH2)n-O
N
O
N
O-(CH2)n-CH3

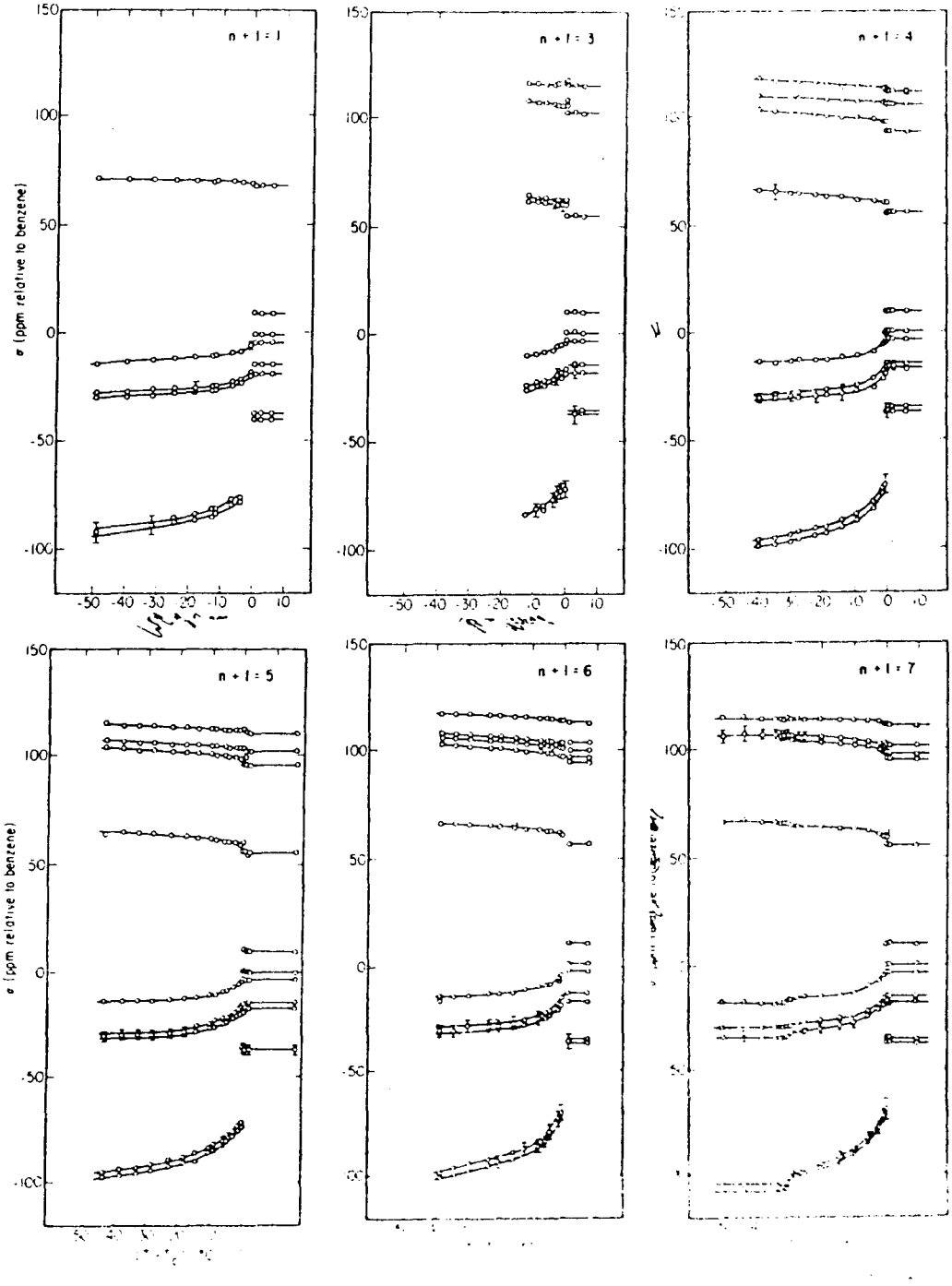
n + l = 1
n + l = 3
n + l = 4
n + l = 5
n + l = 6
n + l = 7
σ (ppm relative to benzene)
150
100
50
0
-50
-100
-50 -40 -30 -20 -10 0 10

Figure 11

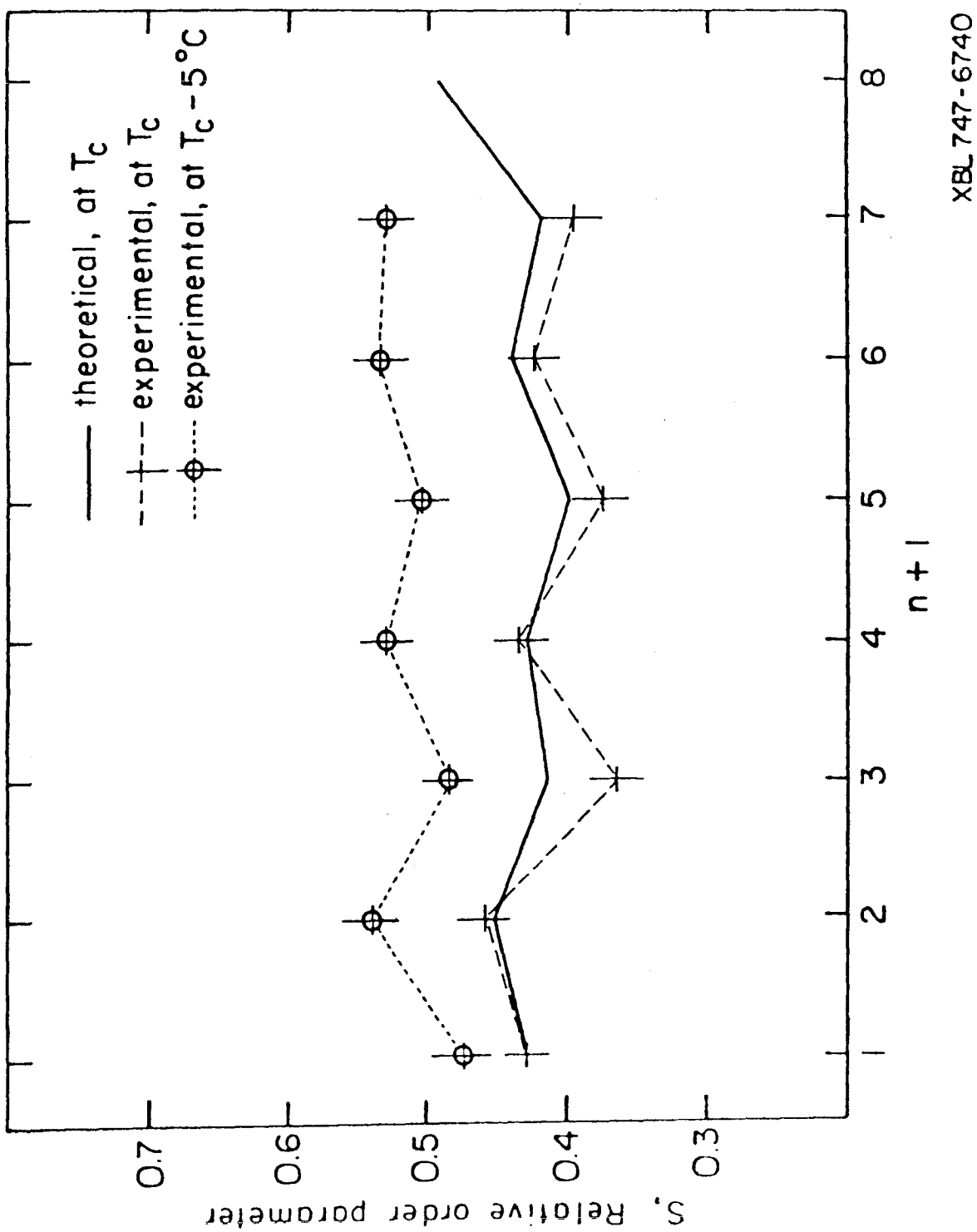
theoretical, at T_c
experimental, at T_c
experimental, at $T_c - 5°C$
S, Relative order parameter
0.7
0.6
0.5
0.4
0.3
1
2
3
4
5
6
7
8
n + 1
XBL 747-6740

Figure 12

TABLE 1. Order Parameters of Alkoxy-azoxybenzenes[a]

$(T-T_C)$	σ_1	σ_2	σ_3	$\Delta\sigma_1$	$\Delta\sigma_2$	$\Delta\sigma_3$	S_1	S_2	S_3	$\bar{S}$
n + 1 = 1										
isotropic	202	251.5	267	0	0	0	0	0	0	0
0	-	-	-	46.0	26.0	22.0	0.43	0.43	0.43	0.43
4.0	149.5	224.0	243.0	52.5	27.5	24.0	0.49	0.46	0.47	0.47
5.0	-	-	-	52.5	28.0	24.0	0.49	0.46	0.47	0.47
6.5	148.5	223.0	243.0	53.5	28.5	24.0	0.50	0.47	0.47	0.48
11.5	142.5	220.5	241.0	59.5	31.0	26.0	0.56	0.51	0.51	0.53
12.5	141.5	219.5	240.5	60.5	32.0	26.5	0.57	0.53	0.52	0.54
18.0	139.0	220.0	240.0	63.0	31.5	27.0	0.59	0.52	0.53	0.55
24.5	137.5	218.5	239.0	64.5	33.0	28.0	0.60	0.55	0.55	0.57
31.5	134.0	217.0	238.0	68.0	34.5	29.0	0.64	0.57	0.57	0.59
39.5	-	216.0	236.5	-	35.5	30.5	-	0.59	0.60	0.59
49.0	130.0	216.0	235.5	72.0	35.5	31.5	0.67	0.59	0.62	0.63
n + 1 = 2										
isotropic	202	250.5	266	0	0	0	0	0	0	0
0	-	-	-	54.0	25.5	23.0	0.51	0.42	0.45	0.46
2.0	146	221	241	56.0	29.5	25.0	0.52	0.49	0.49	0.50
4.0	143	219	239	59.0	31.5	27.0	0.55	0.52	0.53	0.53
5.0	-	-	-	62.0	31.5	26.5	0.58	0.52	0.52	0.54
6.0	139	218	238	63.0	32.5	28.0	0.59	0.54	0.55	0.56
8.0	136	217	237	66.0	33.5	29.0	0.62	0.55	0.57	0.58
12.0	133	216	236	69.0	34.5	30.0	0.65	0.57	0.59	0.60
n + 1 = 3										
isotropic	204	251.5	267.5	0	0	0	0	0	0	0
0	-	-	-	43.0	21.0	18.0	0.40	0.35	0.35	0.37
1.5	155	227.5	247	49.0	24.0	20.5	0.46	0.40	0.40	0.42
3.0	153	227	246	51.0	24.5	21.5	0.48	0.41	0.42	0.43
4.0	149	224	243	55.0	27.5	24.5	0.51	0.46	0.48	0.48
5.0	-	-	-	55.5	28.0	24.5	0.52	0.46	0.48	0.49
7.0	143.5	222	242	60.5	29.5	25.5	0.57	0.49	0.50	0.52
9.0	143	222	241	61.0	29.5	26.5	0.57	0.49	0.52	0.53
12.5	140	219.5	240	64.0	32.0	27.5	0.60	0.53	0.54	0.56
n + 1 = 4										
isotropic	204.5	251.5	267	0	0	0	0	0	0	0
0	-	-	-	52.0	24.5	21.0	0.49	0.41	0.41	0.43
1.0	153.5	226.5	245.5	51.0	25.0	21.5	0.48	0.41	0.42	0.44
4.0	144	221	241	60.5	30.5	26.0	0.57	0.50	0.51	0.53
5.0	-	-	-	61.5	30.5	26.0	0.58	0.50	0.51	0.53
9.0	137	218.5	239	67.5	33.0	28.0	0.63	0.55	0.55	0.58
14.0	133	215	238	71.5	36.5	29.0	0.67	0.60	0.57	0.61
19.0	129	215.5	236	75.5	36.0	31.0	0.71	0.60	0.61	0.64
22.5	128	213	236	76.5	38.5	31.0	0.72	0.64	0.61	0.65
27.5	125.5	213.5	236	79.0	38.0	31.0	0.74	0.63	0.61	0.66
30.0	124	213	235	80.5	38.5	32.0	0.75	0.64	0.63	0.67
34.5	122	213	234	82.5	38.5	33.0	0.77	0.64	0.65	0.68
39.5	121	212	235	83.5	39.5	32.0	0.78	0.65	0.63	0.69

n + 1 = 5

isotropic	204.0	252.5	268	0	0	0	0	0	0	0
0	-	-	-	45.0	21.5	18.0	0.42	0.36	0.35	0.38
0.5	155.5	229.5	249	48.5	23.0	19.0	0.45	0.38	0.37	0.40
1.5	153.5	228	247	50.5	24.5	21.0	0.47	0.41	0.41	0.43
3.0	149.5	226	245	54.5	26.5	23.0	0.51	0.44	0.45	0.47
4.0	147	223.5	243	57.0	29.0	25.0	0.53	0.48	0.49	0.50
5.0	-	-	-	57.5	29.0	25.5	0.54	0.48	0.50	0.51
6.0	145	223	242	59.0	29.5	26.0	0.55	0.49	0.51	0.52
9.0	141	221	240	63.0	31.5	28.0	0.59	0.52	0.55	0.55
11.0	139.5	220	240	64.5	32.5	28.0	0.60	0.54	0.55	0.56
15.0	134.5	218	238	69.5	34.5	30.0	0.65	0.57	0.59	0.60
18.5	133	216	238	71.0	36.5	30.0	0.66	0.60	0.59	0.62
23.0	131	215	237	73.0	37.5	31.0	0.68	0.62	0.61	0.64
29.0	128	214	236	76.0	38.5	32.0	0.71	0.64	0.63	0.66
33.5	126	214	236	78.0	38.5	32.0	0.73	0.64	0.63	0.66
38.5	125	214	236	79.0	38.5	32.0	0.74	0.64	0.63	0.67
44.0	123.5	213	236	80.5	39.5	32.0	0.75	0.65	0.63	0.68

n + 1 = 6

isotropic	207	256	271	0	0	0	0	0	0	0
0	-	-	-	47.0	26.0	21.0	0.44	0.43	0.41	0.43
1.0	161	223.5	251	46.0	22.5	20.0	0.43	0.37	0.39	0.40
1.5	157	230	249	50.0	26.0	22.0	0.47	0.43	0.43	0.44
4.5	148	225.5	245	59.0	30.5	26.0	0.55	0.50	0.51	0.52
5.0	-	-	-	62.0	31.0	26.5	0.58	0.51	0.52	0.54
5.5	-	224	244	-	32.0	27.0	-	0.53	0.53	0.53
8.0	139	222	243	68.0	34.0	28.0	0.64	0.56	0.55	0.58
12.0	-	219.5	241	-	36.5	30.0	-	0.60	0.59	0.60
15.5	132.5	218.5	239	74.5	37.5	32.0	0.70	0.62	0.63	0.65
20.5	-	217	238	-	39.0	33.0	-	0.65	0.65	0.65
23.5	128	217	238	79.0	39.0	33.0	0.74	0.65	0.65	0.68
30.0	125.5	217	237	81.5	39.0	34.0	0.76	0.65	0.67	0.69
34.5	123	214	236	84.0	42.0	35.0	0.79	0.70	0.68	0.72
39.0	120.5	214	235.5	86.5	42.0	35.5	0.81	0.70	0.68	0.73

n + 1 = 7

isotropic	204.5	253	268	0	0	0	0	0	0	0
0	-	-	-	47.0	21.5	20.0	0.44	0.36	0.39	0.40
0.5	160	232	250	44.5	21.0	18.0	0.42	0.35	0.35	0.37
1.0	156	230.5	248	48.5	22.5	20.0	0.45	0.37	0.39	0.41
2.5	148	227.5	244	56.5	25.5	24.0	0.53	0.42	0.47	0.47
5.0	-	-	-	63.0	29.0	26.5	0.59	0.48	0.52	0.53
6.0	141	222.5	241	63.5	30.5	27.0	0.59	0.50	0.53	0.54
10.5	132.5	-	236	72.0	-	32.0	0.67	-	0.63	0.65
14.5	128	217.5	235	76.5	35.5	33.0	0.72	0.59	0.65	0.65
20.5	123	215.5	234.5	81.5	37.5	33.5	0.76	0.62	0.66	0.68
26.0	119.5	214	234	85.0	39.0	34.0	0.80	0.65	0.67	0.70
28.0	118	213.5	233	86.5	39.5	35.0	0.81	0.65	0.68	0.72
30.0	117.5	212.5	231.5	87.0	40.5	36.5	0.81	0.67	0.71	0.73
31.0	111	211.5	232	93.5	41.5	36.0	0.87	0.69	0.70	0.76
32.0	109.5	210.5	230	95.0	42.5	38.0	0.89	0.70	0.74	0.78
33.0	110	210.5	230	94.5	42.5	38.0	0.88	0.70	0.74	0.78
35.0	109.5	210.5	229	95.0	42.5	39.0	0.89	0.70	0.76	0.78
39.0	109	210.5	230	95.5	42.5	38.0	0.89	0.70	0.74	0.78
44.5	110	210	231	94.5	43.0	37.0	0.88	0.71	0.72	0.77
51.0	109	211	230.5	95.5	42.0	37.5	0.89	0.70	0.73	0.77

(a) σ_i are the chemical shifts of the aromatic peaks, $\Delta\sigma_i$ are the shifts from isotropic, S_i are the microscopic order parameters and $\bar{S}$ is average order parameter for the full aromatic core.

Finally, it is interesting to comment on some aspects of conformational motion and spin relaxation which can be studied by our technique:

1. Molecular reorientation about the long axes is certainly rapid, but there is a question of conformational rigidity. In particular, are the benzene rings fixed or do they rotate rapidly about the para axes? In PAA, Rowell et al. have found that they rotate rapidly, by deuteron magnetic resonance.[14] Similar conclusions were reached regarding MBBA[2] and the center ring of TBBA.[15] If the rings are fixed for the series I which has been studied, then in the nematic phase we expect a chemical shift difference $\Delta\sigma$ for the two carbon positions ortho to the N = N linkage. From (B22) the difference $\Delta\sigma$ is given by

$$\Delta\sigma = \frac{2}{3} S \left(\bar{\sigma}_{11}^{(2)} - \bar{\sigma}_{\perp}^{(2)} - (\bar{\sigma}_{11}^{(1)} - \bar{\sigma}_{\perp}^{(1)})\right) \tag{2}$$

where the superscript denotes the ortho carbon. From (A7), (A8), Figure 8, and letting ϕ be the angle between the long axis and the para axis, we get

$$\sigma_{11}^{(2)} = \cos^2(60° + \phi)\sigma_{11} + \sin^2(60° + \phi)\sigma_{22} \tag{3}$$

$$\sigma_{11}^{(1)} = \cos^2(60° - \phi)\sigma_{11} + \sin^2(60° - \phi)\sigma_{22}$$

$$\sigma_{\perp}^{(2)} = \frac{1}{2}\left(1 - \cos^2(60° + \phi)\right)\sigma_{11} + \frac{1}{2}\left(1 - \sin^2(60° + \phi)\right)\sigma_{22} + \frac{1}{2}\sigma_{33}$$

$$\sigma_{\perp}^{(1)} = \frac{1}{2}\left(1 - \cos^2(60° - \phi)\right)\sigma_{11} + \frac{1}{2}\left(1 - \sin^2(60° - \phi)\right)\sigma_{22} + \frac{1}{2}\sigma_{33} .$$

Substituting these back into (2) we get

$$\Delta\sigma = 1.73 \cdot S \cdot \sin\phi \cos\phi \, (\sigma_{22} - \sigma_{11}) \quad . \qquad (4)$$

It is assumed that one of the rings does not deviate from planarity[16] and that the ring angles are 120°. Taking values of $\phi = 8°$, $\sigma_{11} = -98$ ppm, $\sigma_{22} = -13$ ppm[17] and $S = 0.6$, we see from (4) that $\Delta\sigma \approx 12$ ppm which is clearly within the limits of our resolution. Since no such additional splittings occur in the nematic phase, we conclude that the benzene rings rotate or flip about the para axes at a rate greater than 1 kHz for the whole series throughout the nematic ranges.

2. A striking observation from the spectra in Figure 10 is that one set of lines appears to disappear consistently for the whole series in the isotropic-nematic transitions. These are the lines assigned to ^{13}C nuclei bonded to the N = N group and thus coupled to ^{14}N nuclei. A possible explanation for this effect is the combination of ^{13}C-^{14}N magnetic dipolar coupling and ^{14}N spin relaxation by fluctuating electric field gradients. The threefold splitting in ^{13}C lines expected from the coupling is $\sim$ 1 kHz and thus ^{14}N spin relaxation with $T_1 \sim 1$ ms would cause a severe broadening of the ^{13}C lines making the resonance essentially unobservable. Much slower or more rapid ^{14}N spin relaxation would yield three or one sharp lines respectively. ^{14}N spin relaxation has been measured in the isotropic phase of PAA,[18] and it would be interesting to check our contention directly in the nematic phases.

We have carried out one set of experiments with results which are consistent with our explanation. Di-ethylazoxybenzoate, the analog of series I (Figure 7) with -COO C_2H_5 constituting the side chains, exhibits a smectic A phase. In the isotropic-smectic transition the ^{13}C-^{14}N lines again disappear, but when the sample is rotated by 55° (the magic angle) in the smectic A phase they reappear. This is consistent with our explanation, since at this angle the ^{13}C-^{14}N magnetic dipolar coupling disappears rendering the three ^{13}C transitions degenerate and eliminating the broadening due to ^{14}N spin relaxation. This will be discussed in the next section.

C. Study of a Smectic-A Liquid Crystal

In this section, the application of ^{13}C nmr to a smectic-A liquid crystal is presented. Although deuterium nmr was shown to provide a great deal of information,[19,20] ^{13}C nmr has the advantage that it can be done without the use of probe molecules or labelling. As in the nematics, we obtain information on ordering as a function of temperature and molecular conformational motion. Furthermore, spin-relaxation by ^{14}N is elucidated and sample rotation in the magnetic field provides additional information. The value of sample rotation will become evident in this section and is bound to be of potential importance in future studies of smectic-C liquid crystals.

The compound studied was diethylazoxydibenzoate (DEAB) and is shown in Figure 13. DEAB was a convenient choice because: 1) it

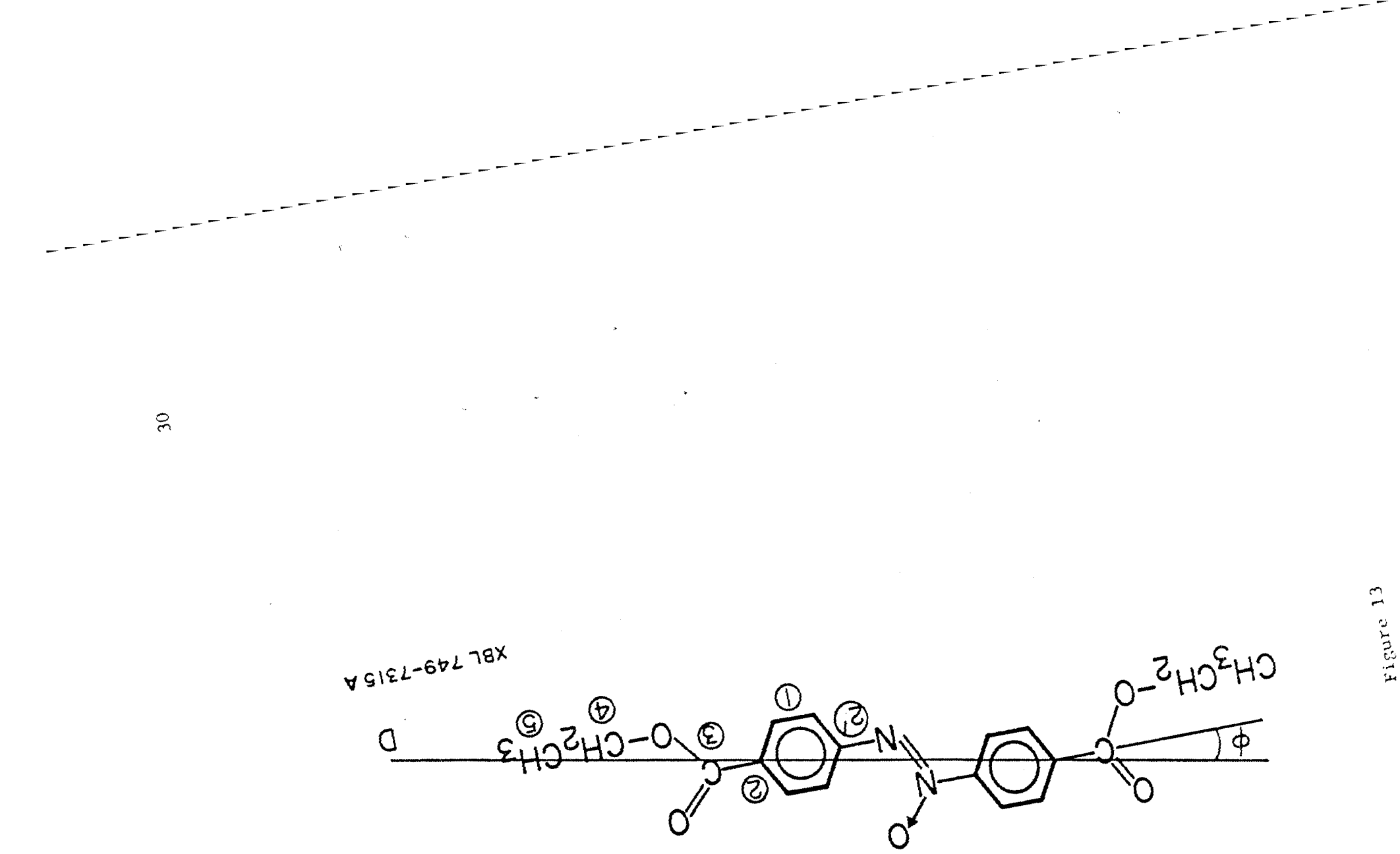

Figure 13

is an analog of the nematic liquid crystals studied, 2) it is a simple smectic-A, and 3) it contains groups about which we know something of $\underset{\approx}{\sigma}$.

1. Spectrum in Isotropic Phase

In the isotropic phase, ^{13}C spectra are obtained by conventional Fourier transform nmr with proton spin decoupling (Figure 4a). The isotropic-smectic-A transition temperatures of our samples were 122°C, and Figure 14 shows a proton-decoupled ^{13}C free induction decay and Fourier-transform spectrum in the isotropic phase at 124°C. The resolution is limited by the homogeneity of the magnet. The line assignments appear in the caption.

Since the only spin-spin couplings in this phase are through weak electron-coupled scalar interactions, the proton decoupling power required is low. The isotropic chemical shift is given by (A11).

2. Spectrum in Smectic-A Phase

The normal evolution of orientational order from isotropic to smectic-A mesophases is through a nematic mesophase as shown in Figure 1. In DEAB, the nematic phase is non-existent or else the temperature range is very narrow and it has not been observed. In high magnetic field, in our case $\sim$ 23 KG, as the temperature is lowered from the isotropic phase, a transition into the smectic-A phase occurs, exhibiting long-range orientational order about a smectic-A director, in this case along the magnetic field, as well as a layered structure. In the case of the smectic-A phase we

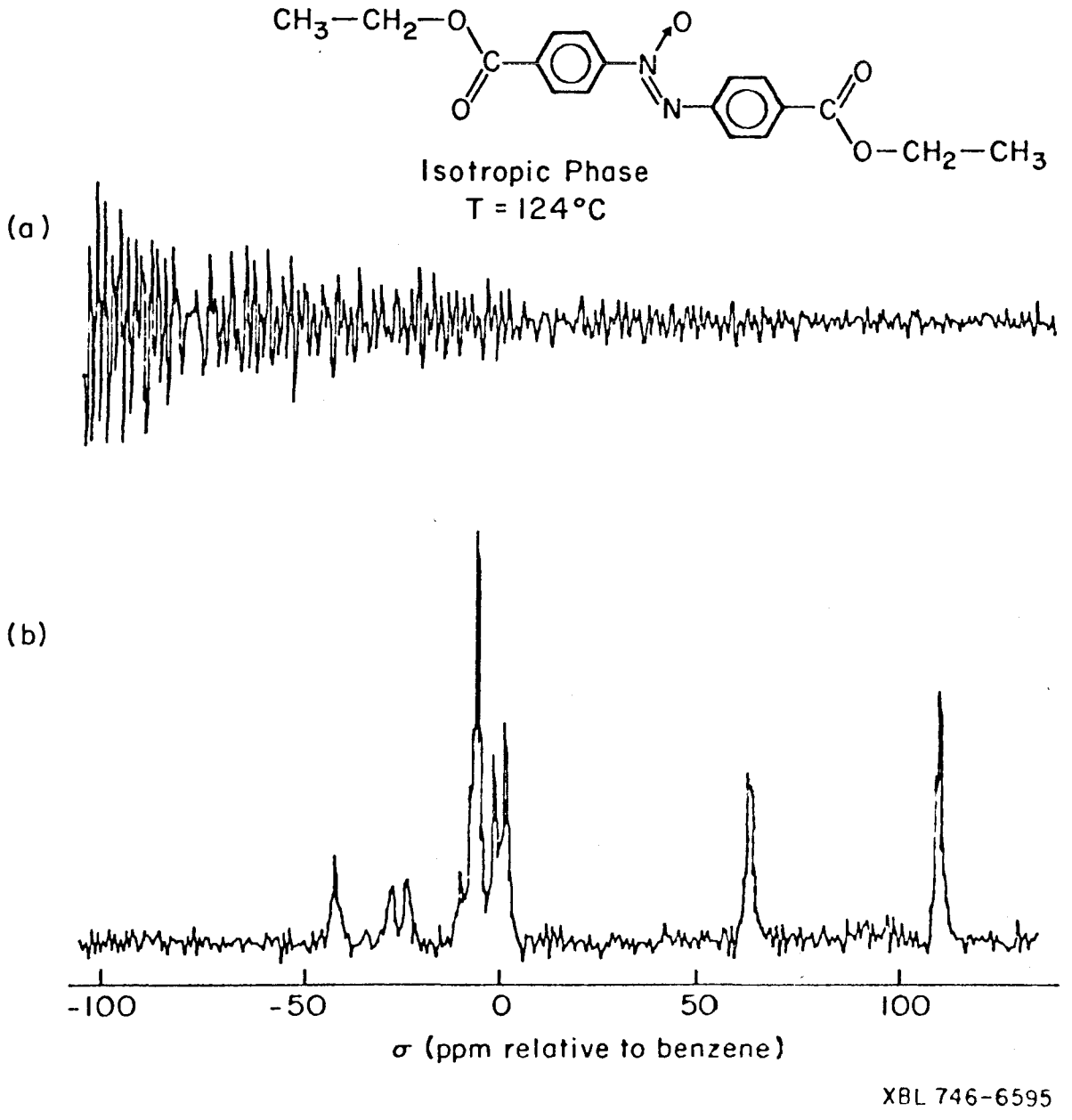
CH3—CH2—O
O
C
O
N
O
N
C
O
O—CH2—CH3
Isotropic Phase
T = 124°C
(a)
(b)
-100
-50
0
50
100
σ (ppm relative to benzene)
XBL 746-6595

Figure 14

consider three types of orientational motion:

a) rapid reorientation about the long molecular axis (Figure 15)

b) fluctuations of the long axis about the smectic-A director, the local average direction of the axis by angle $\theta'(t)$

c) internal conformational motion.

The chemical shift is derived in appendix B:

$$\sigma = \sigma_i + \frac{2}{3} S \, (\bar{\sigma}_{\parallel} - \bar{\sigma}_{\perp}) \qquad \text{(B22)}$$

where $\bar{\sigma}_{\parallel}$ and $\bar{\sigma}_{\perp}$ are the elements of the average shielding tensor over the motion in (a), and S is the order parameter given by (1). As shown in appendix A, $\bar{\sigma}_{\parallel}$ and $\bar{\sigma}_{\perp}$ depend only on $\underset{\approx}{\sigma}$, and on the orientation of the long axis in the principle axis system.

As in the nematic series studied, we can predict that in the isotropic smectic-A transition, with the molecular axes aligning on the average along the magnetic field, the aromatic lines should appear at lower field and the aliphatic side chain lines at higher field. The properties of $\underset{\approx}{\sigma}$ for the carboxyl group are similar to those of the aromatic, namely σ_{33} perpendicular to the π-nodal plane, so the carboxyl line should also shift downfield. Figure 16 bears out these qualitative predictions, showing a spectrum in the smectic-A phase at 114°C. This was obtained by proton-enhanced nmr, Figure 4(b), line assignments appear in the caption. This behavior is similar to that observed previously for nematic phases as discussed in the previous section.

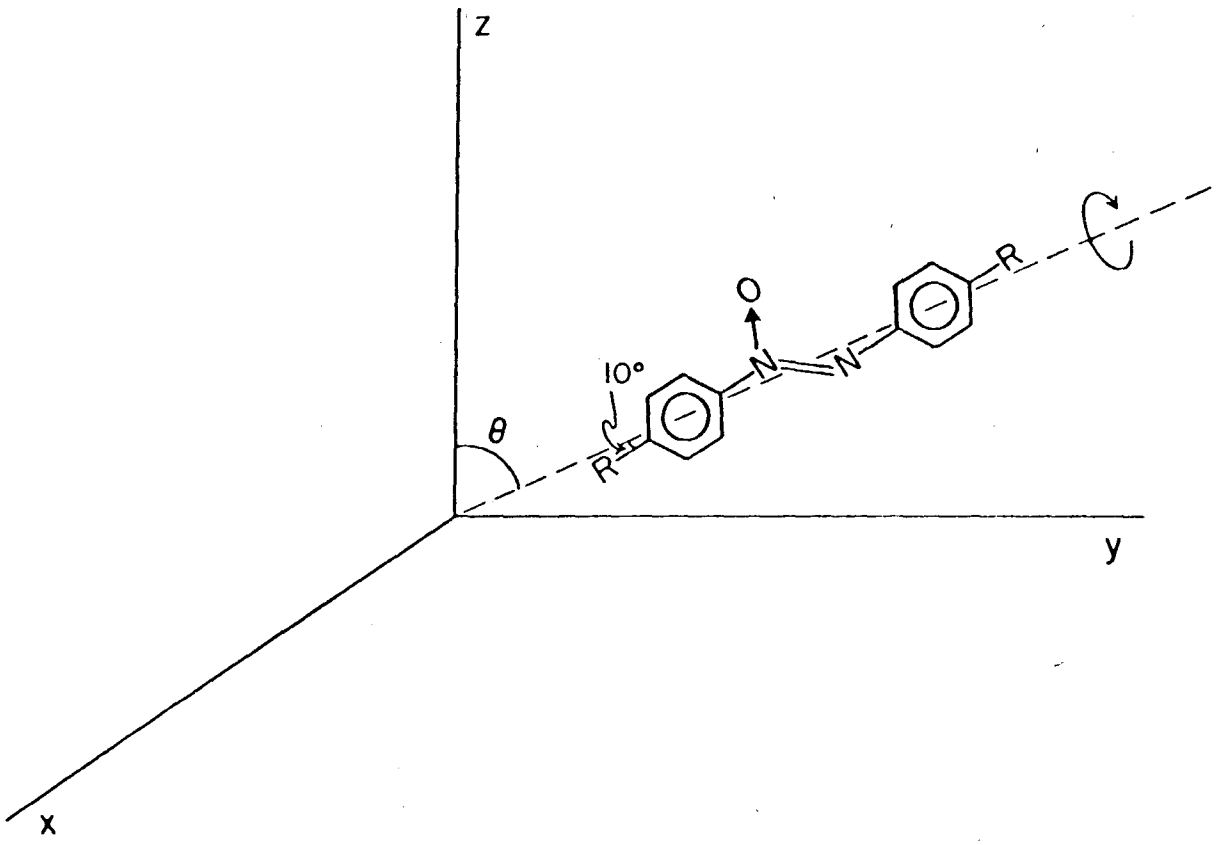

XBL 746-6598

Figure 15

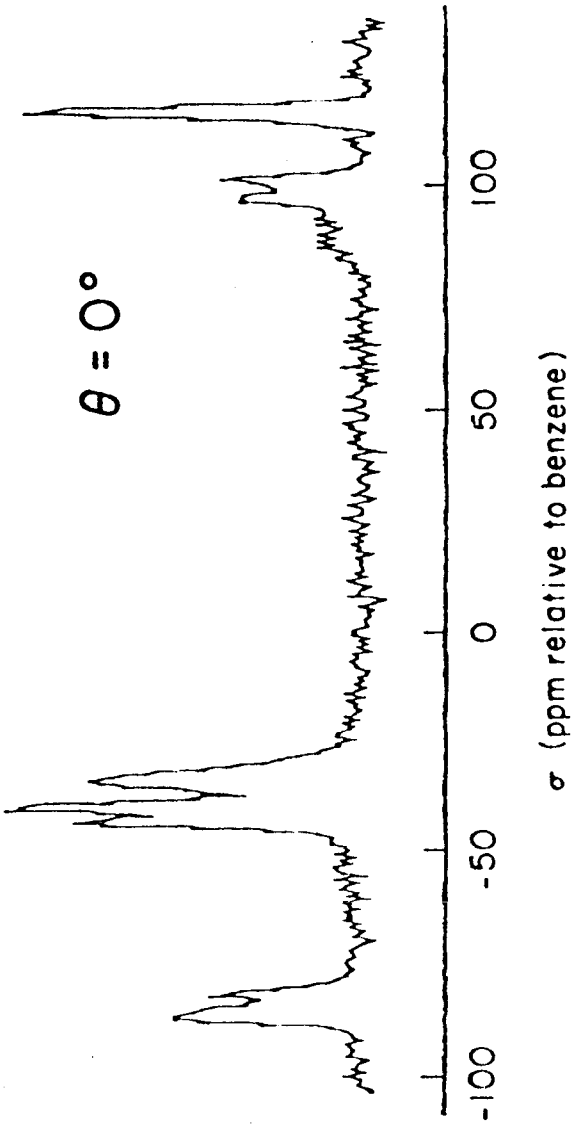

Figure 16

From more precise data about $\underset{\approx}{\sigma}$, and models for the molecular motion, we can clearly say considerably more about the ordering and motion in the smectic-A phase. Unfortunately, no data on $\underset{\approx}{\sigma}$ exist for the liquid crystal molecules; however, from quantitative data on model compounds some semiquantitative arguments are presented in this section.

Unlike the isotropic phase, the purpose of the proton irradiation in the smectic-A phase is to decouple the magnetic dipolar couplings between ^{1}H and ^{13}C. These are not averaged to zero as in the isotropic phase, and if the order parameter S is high, they can be substantial, of the order of many Gauss. Thus, the requisite decoupling power is high, otherwise yielding the broad, featureless spectra characteristic of proton nmr in liquid crystals. Figure 17 demonstrates this point, comparing a proton decoupled spectrum of DEAB in the smectic-A phase with that obtained when the proton-decoupling is eliminated. In the latter case, the main features of the sharp-line spectrum are broadened intractably.

An interesting effect observed in the isotropic-smectic-A transition is the disappearance of some of the lines. This can be concluded from the integrated intensities of the low field lines in Figures 14 and 16 assigned to aromatic carbons. Similar behavior was observed for the isotropic-nematic transitions in the p-alkoxyazoxybenzenes discussed previously and was explained by assuming that the lines for aromatic ^{13}C nuclei bonded directly to ^{14}N in the azoxy linkage are broadened to the extent that they

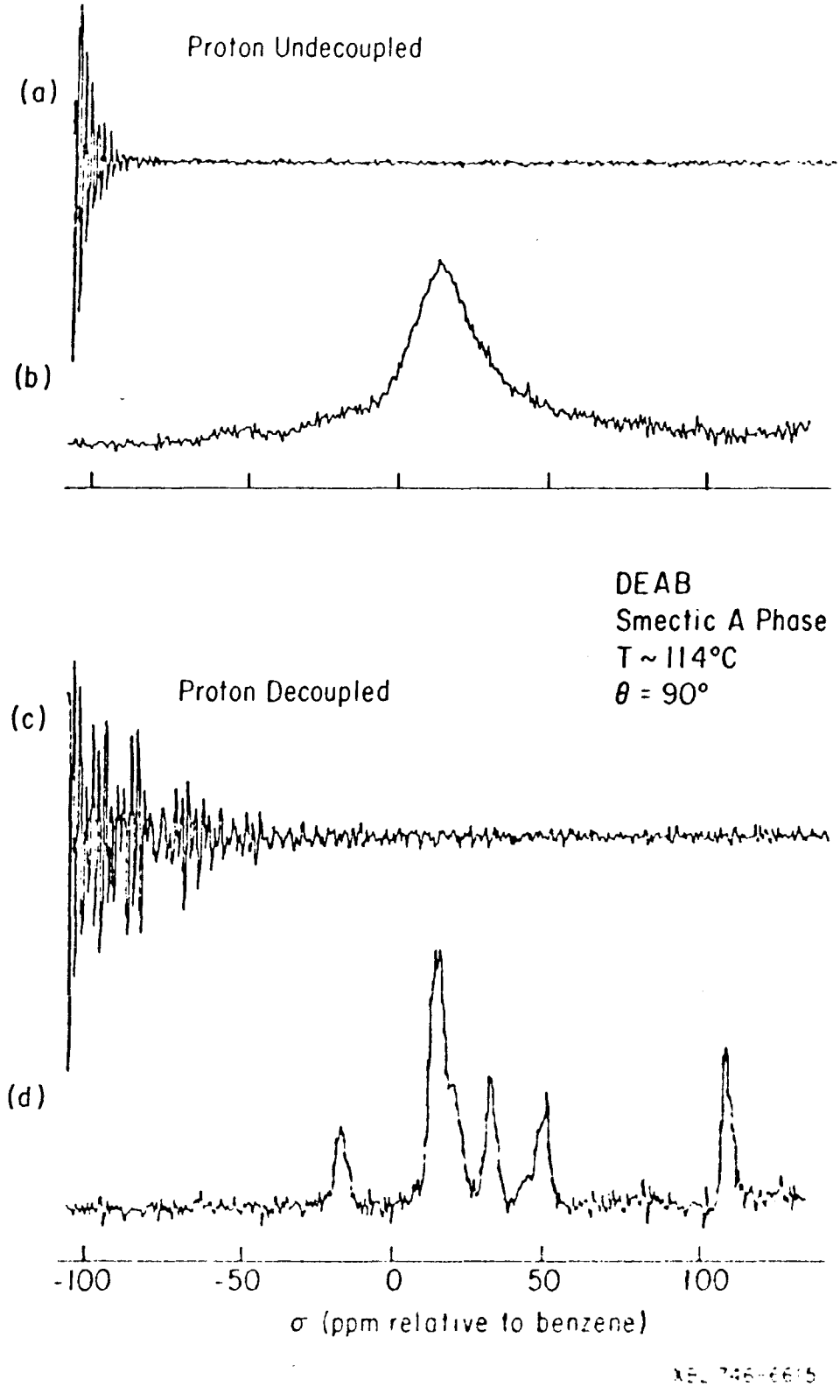
Proton Undecoupled
(a)
(b)
DEAB
Smectic A Phase
T ~ 114°C
θ = 90°
Proton Decoupled
(c)
(d)
-100
-50
0
50
100
σ (ppm relative to benzene)

Figure 17

become unobservable. This could occur by a combination of ^{14}N-^{13}C dipolar splittings together with rapid ^{14}N spin relaxation. Further evidence for this is presented in the next section.

3. Sample-Rotation in Smectic-A Phase

Consider a liquid crystal sample aligned in a magnetic field, by cooling from the isotropic phase. In nematic liquid crystals it is known that if the direction of the magnetic field is changed suddenly, the molecules rapidly realign with the field. The smectic phases on the other hand, are characterized by values the elastic constants[21] with the requirement that planes be maintained, and thus this realignment cannot occur. This behavior of the sample on rotation of a smectic-A phase in a magnetic field is depicted in Figure 18. The effects of this behavior on nmr and esr parameters are well known. However, all previous nmr work has employed either dissolved probe molecules, wideline spectra or deuterium labeling. Here, we show the effects of sample rotation on the high resolution ^{13}C nmr spectra, indicating that the line positions are sensitive to the reorientation and should provide a tool for local structural and dynamical studies in the smectic phases.

Figure 19 shows ^{13}C nmr spectra in the smectic-A phase as the sample is rotated about an axis perpendicular to the magnetic field. The sample was first heated to the isotropic phase in the magnetic field, then cooled into the smectic-A phase, producing an aligned sample, as in Figure 18(a). The sample rotation then reorients

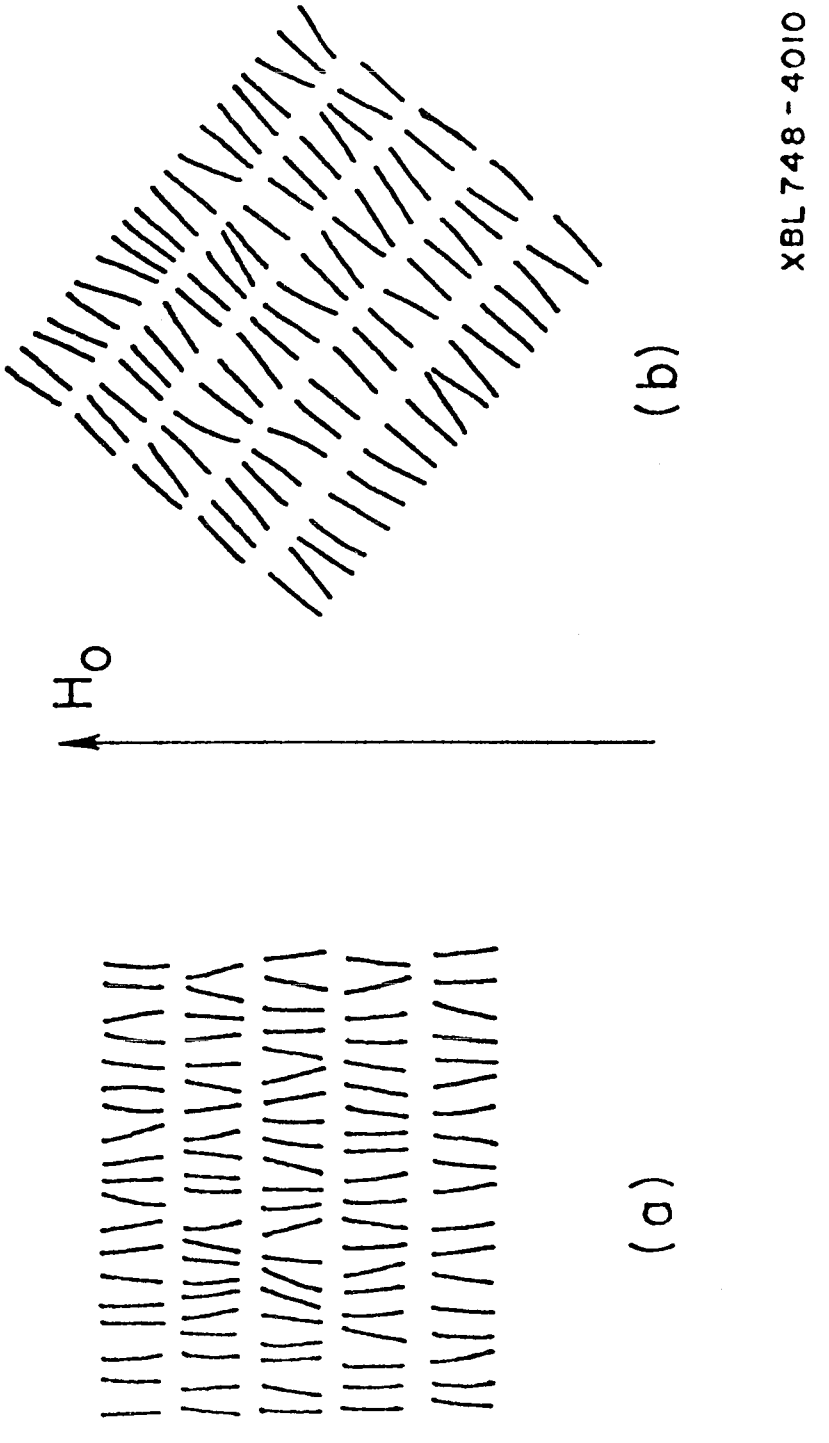

Figure 18

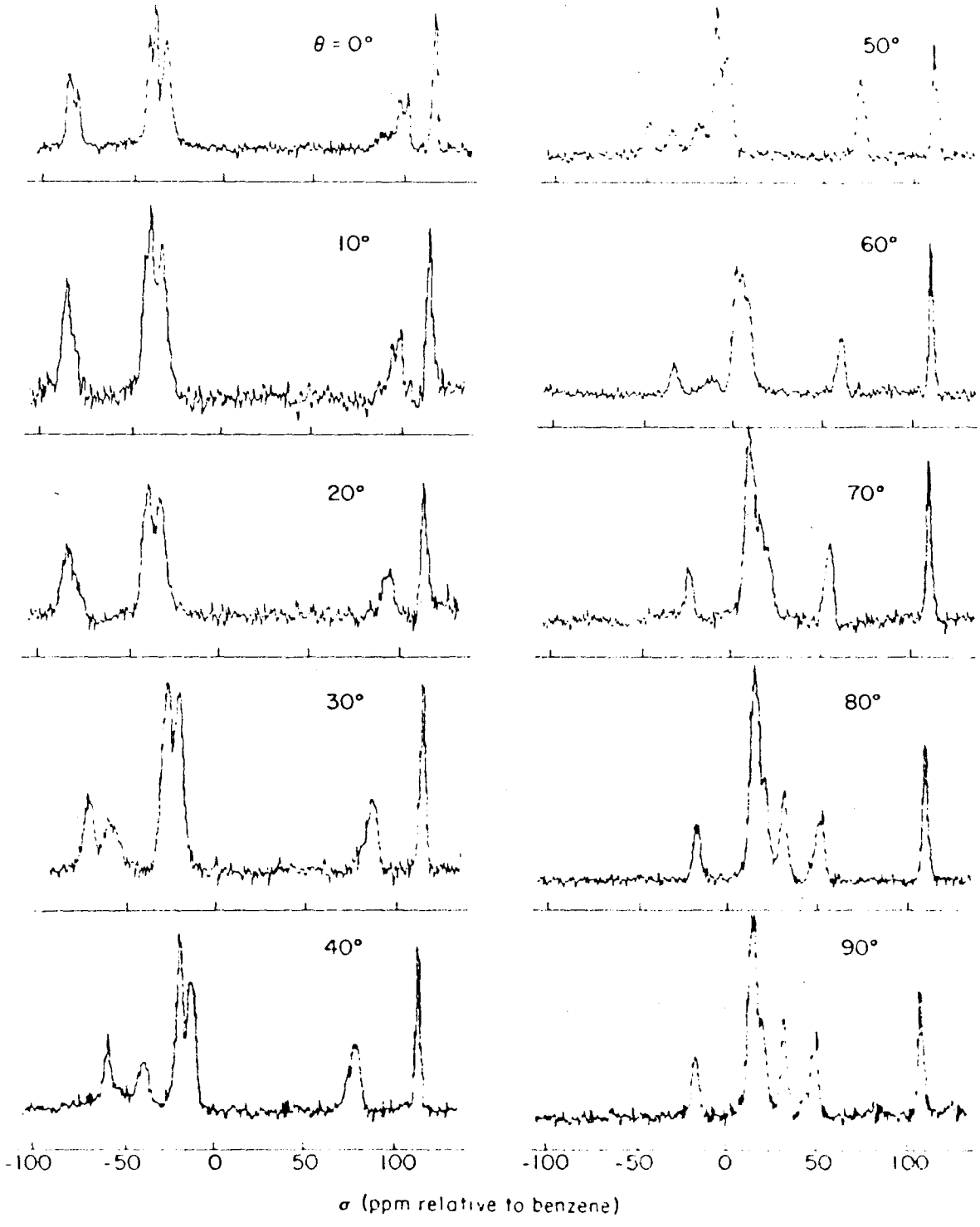
θ = 0°
10°
20°
30°
40°
50°
60°
70°
80°
90°
-100
-50
0
50
100
σ (ppm relative to benzene)

Figure 19

the layers as in 18(b), and as seen from Figure 20, the line positions are sensitive to this reorientation. In appendix B, it is shown that for a smectic-A (uniaxial molecular symmetry) that

$$\sigma = \sigma_i + \frac{2}{3} S P_2 (\cos\theta) (\bar{\sigma}_{\parallel} - \bar{\sigma}_{\perp}) \qquad \text{(B23)}$$

where θ is the angle of sample rotation, i.e., the angle between the director and the magnetic field. All spectra were obtained by proton-enhanced nmr Figure 4(b) except near $\theta = 55°$. In this region the ^{13}C-^{1}H dipolar coupling is weak and cross-polarization is inefficient.

The behavior of the spectra is fitted quantitatively to equation (B23) in Figure 20 using σ_i and $S (\bar{\sigma}_{\parallel} - \bar{\sigma}_{\perp})$ as two parameters. Thus, the behavior is exactly in accord with a well aligned sample, maintaining its orientation and layering undistorted on sample rotation, and with the molecules rotating rapidly about their long axes. Since $\bar{\sigma}_{\parallel}$, $\bar{\sigma}_{\perp}$ are related through (A7) and (A8) to $\underset{\sim}{\sigma}$, assumptions about $\underset{\sim}{\sigma}$ and the angle ϕ in Figure 13 can yield values of S. This problem is dealt with later in this section.

It was mentioned previously, that there appears to be a severe broadening of some of the lines in the isotropic-smectic-A transition. The secular dipolar coupling H_d between ^{14}N and ^{13}C for the aromatic carbons bonded to the azoxy group is:

$$Hd = \frac{\gamma_I \gamma_S \hbar^2}{\gamma_{IS}^3} P_2(\cos\theta) I_z S_z \qquad (5)$$

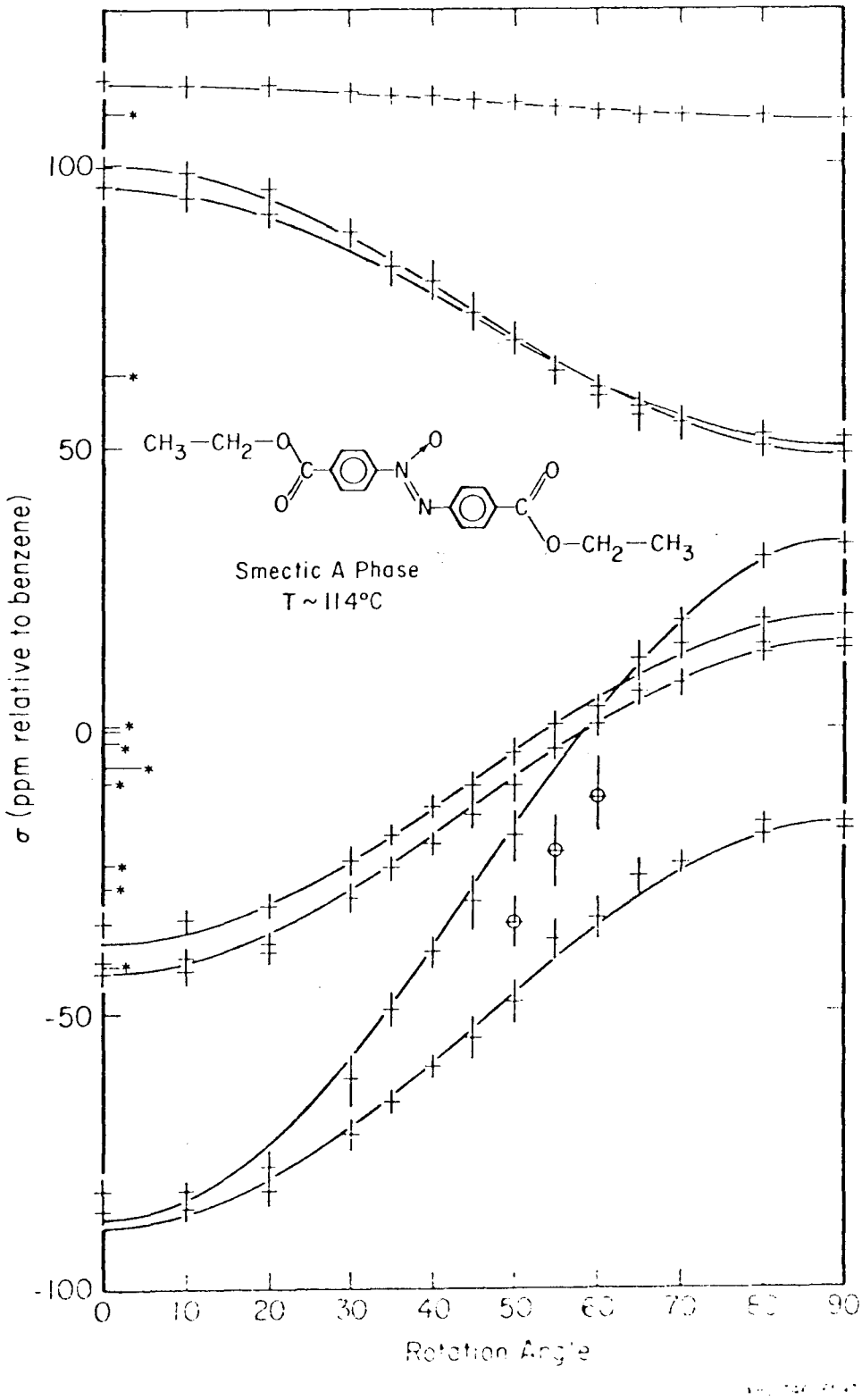
100
50
0
-50
-100
σ (ppm relative to benzene)
0
10
20
30
40
50
60
70
80
90
Rotation Angle
CH3—CH2—O
O—CH2—CH3
Smectic A Phase
T ~ 114°C

Figure 20

where I and S refer to the ^{14}N and ^{13} spins; this corresponds to a splitting of $\Delta\nu \sim 2$ KH_z for $\theta \sim \theta°$. If the ^{14}N spin lattice relaxation is very slow $T_1 >> \Delta\nu^{-1}$, then resolved ^{13}C lines should be observed, whereas for fast relaxation, $T_1 << \Delta\nu^{-1}$ a single sharp ^{13}C line would be seen. In the intermediate regime, $T_1 \sim \Delta\nu^{-1}$ exchange broadening yields a broad line from the merging of the dipolar split ^{13}C lines. For $\Delta\nu_2 \sim 2$ KH_z, this would certainly make the resonance unobservable in our spectra. This corresponds to a ^{14}N spin relaxation time in the range of several tenths of a milisecond. The exact analysis of this problem would require taking account of the ^{14}N quadrupole coupling and is not done here since it is not warranted by the data.

Although the above conclusion is far from unequivocal, Figures 19 and 20 show another feature which strengthens it. Spectra taken near $\theta = 54.7°$, the "magic angle", showed an additional line. This appears in Figure 10 at 50° and in the circuled points at 50°, 55° and 60° in Figure 20. This line is indeed assigned to the carbons adjacent to the -N=N-linkage. Looking at equation (5) this is easily understood since at the magic angle, H disappears thus eliminating the dipolar splitting and the ensuing broadening from ^{14}N spin relaxation. A direct measurement of ^{14}N spin relaxation would be interesting to check out this model, but such measurements have not yet been made to the best of our knowledge.

4. Self-Decoupling at Magic Angle

A characteristic feature of proton nmr of liquid crystals in the smectic-A phase, is a narrowing of the absorption line when the sample is rotated by $\theta = 54.7°$ the magic angle. Figure 15 depicts the situation with respect to one molecule. The ^{13}C-^{1}H dipolar coupling of a molecule rapidly rotating about an axis making an angle θ with H_o is given by an expression similar to equation (5), namely:

$$H_d \propto P_2(\cos\theta) \tag{6}$$

Thus without ^{1}H spin decoupling a narrowing of the lines is expected for $\theta = 54.7°$. This is in essence a self-decoupling by rapid molecular rotation similar in nature to the narrowing produced by rapid sample rotation at the magic angle.[22] This behavior is depicted in Figure 21. Shown are a proton uncoupled ^{13}C spectrum away from the magic angle (a), another near the magic angle (b), and, for comparison, a ^{1}H decoupled spectrum near the magic angle. The behavior is even more dramatic than that observed for proton nmr, since the line narrowing is accompanied by the appearance of new lines, which are too broad to be observed otherwise. Comparison of (b) with (c) shows that the resolution in (b) is not very high. This is due to the fact that the magic angle alignment is not very good, and there is probably a distribution or rotation angles for the various domains in the sample.

5. Spectrum in Solid Phase

In the transition from the smectic-A to the solid phase,

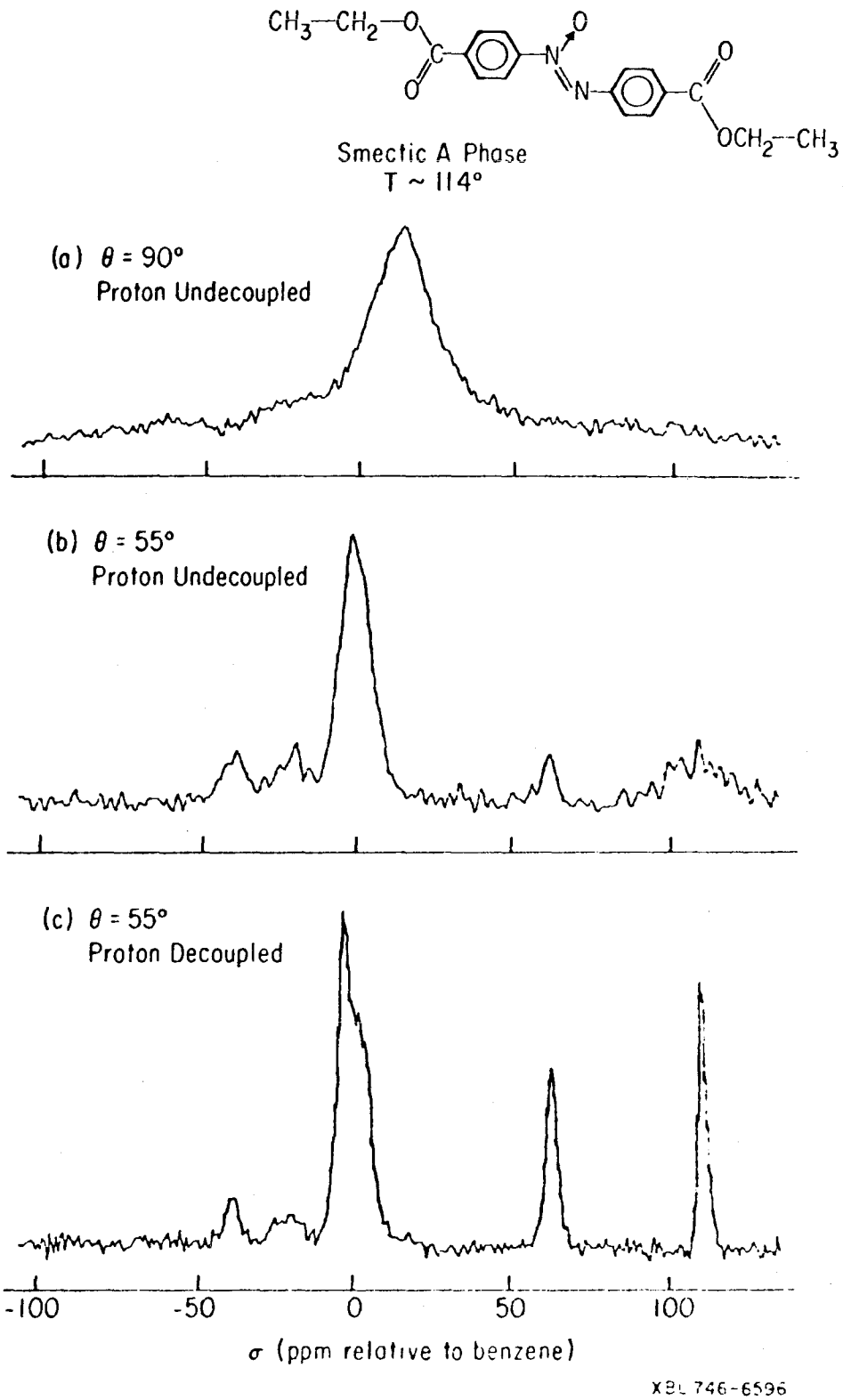
CH3—CH2—O
O
C
O
N
O
N
C
O
OCH2—CH3
Smectic A Phase
T ~ 114°
(a) θ = 90°
Proton Undecoupled
(b) θ = 55°
Proton Undecoupled
(c) θ = 55°
Proton Decoupled
-100
-50
0
50
100
σ (ppm relative to benzene)
XBL 746-6596

Figure 21

there is a sudden and severe broadening of the lines in the ^{13}C spectrum and most of the details are essentially lost. A typical spectrum is shown in Figure 22. The main features correspond to an aromatic and aliphatic region. The reason for this broadening is clear under the condition of our experiments, the sample from a polycrystalline distribution and thus all angles θ are represented. This yields a broad characteristic powder line for each carbon, and the large number of inequivalent overlapping lines is expected to yield a broad smeared out spectrum.

It would be extremely valuable to extract some orientational data, namely rigid values for $\underset{\sim}{g}$ from solid spectra, but single crystal studies are necessary for this. They are now underway.

6. Temperature-Dependence

The temperature dependence of the ^{13}C lines in the isotropic and smectic-A phases of DEAB is shown in Figure 23. In the isotropic phase, as expected, the chemical shift is independent of temperature. However, the dewar show that this is also true in the smectic-A phase. Looking at equation (B22), we see that this implies for the order parameter:

$$S = \text{const} \tag{7}$$

in the smectic-A phase, which is very different from the behavior in nematics and in other smectic phases.[19] This can be partially explained by a microscopic theory due to McMillan.[23] According to this theory the dependence of the order parameter

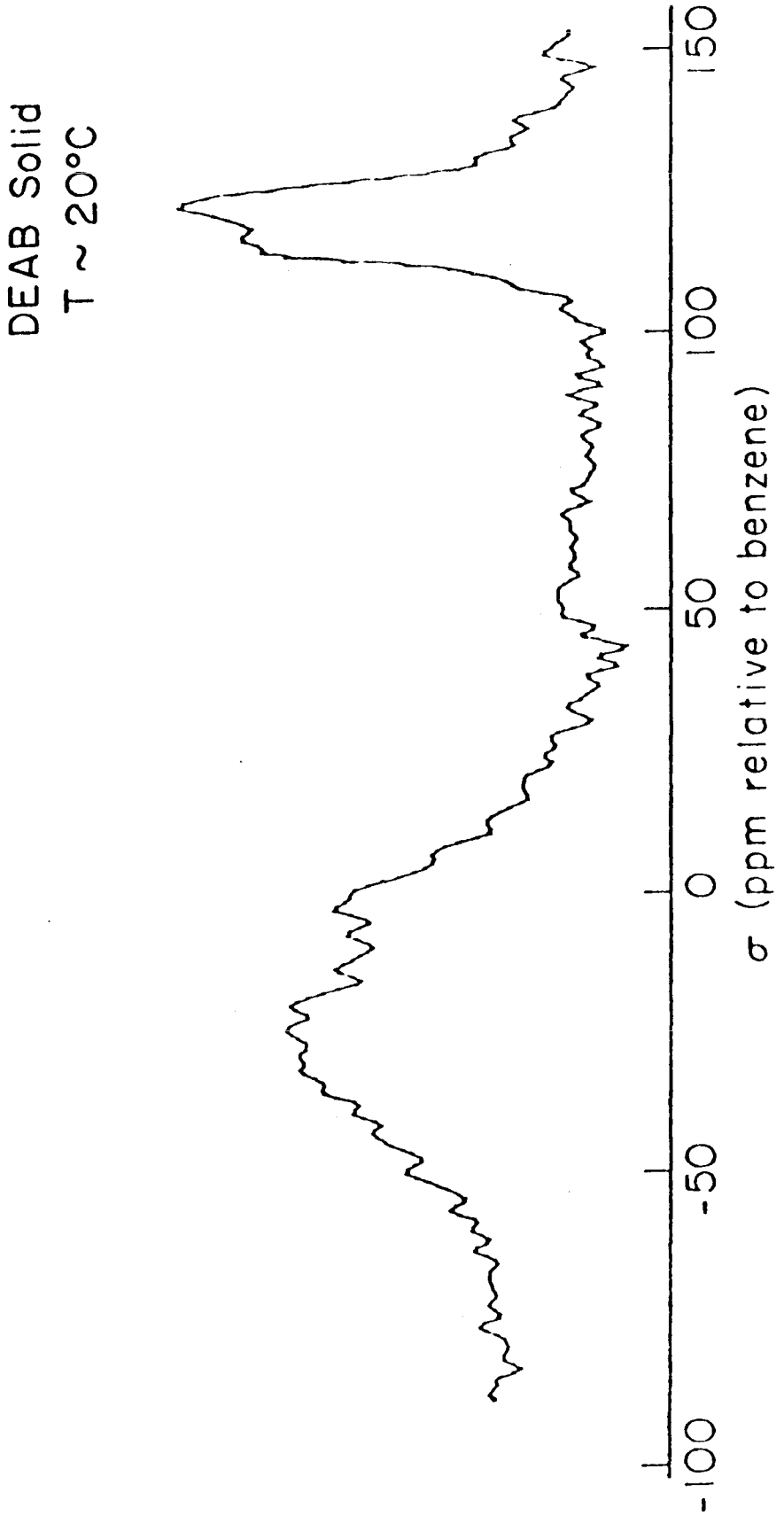

Figure 22

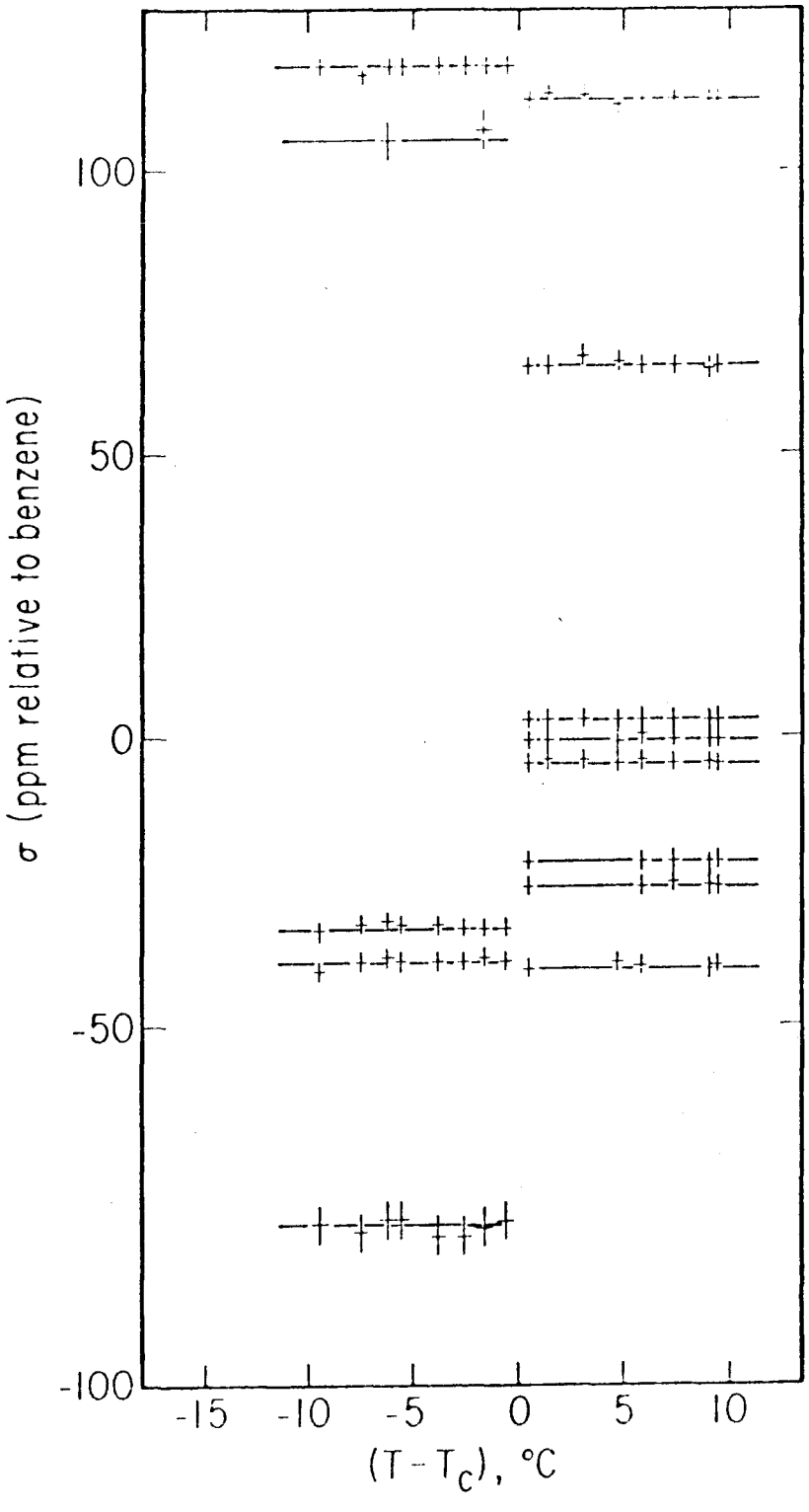
100
50
0
-50
-100
σ (ppm relative to benzene)
-15
-10
-5
0
5
10
(T - T_C), °C
XBL 748-6429

Figure 23

with temperature in the smectic-A phases decreases as the range of the nematic phase narrows and Figure 24, which was taken from McMillan's article demonstrates this. The experiments of Luckhurst et al.[24,25] confirm the prediction of the McMillan theory in the systems they studied. In their study of the nematic and smectic-A mesophase of 4-n-butyloxybenzylidene-4'-acetoaniline, for instance, the order parameter was strongly temperature dependent in the nematic phase but essentially independent of temperature in the smectic phase. Since our spectra are clearly very sensitive to ordering and orientation as shown in the previous sections, we believe this independence on temperature in the range studied to be quite unequivocal. Luz and Meiboom[19] observed a change in the order parameter for a dissolved probe molecule (methylene chloride); this indicates that care must be taken in extrapolating from the behavior of probe solutes to the liquid crystal sample itself.

The order parameter is quite high in the smectic-A phase, considerably higher than in the nematics we have studied, and the next section attempts a quantitative discussion of this point.

7. Order in the Smectic-A Phase

In this section we attempt a semiquantitative evaluation of the order parameter S in the smectic-A phase of DEAB. The ideal approach to this problem would be:

a) Determine $\underset{\approx}{\sigma}$ for all the carbons by ^{13}C nmr in a single crystal of DEAB

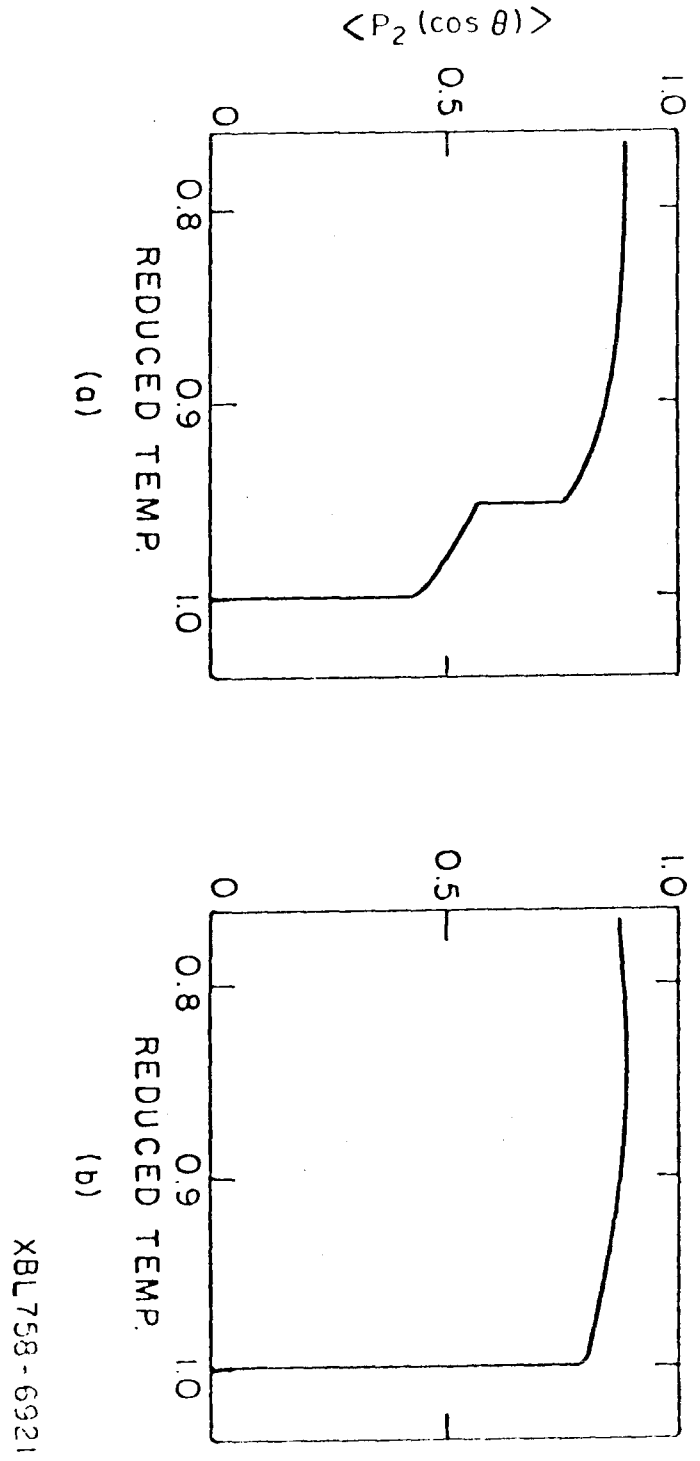
$\langle P_2(\cos\theta)\rangle$
0
0.5
1.0
0.8
0.9
1.0
REDUCED TEMP.
(a)
0
0.5
1.0
0.8
0.9
1.0
REDUCED TEMP.
(b)
XBL758-6921

Figure 24

b) Based on a model for the motion, calculate $\bar{\underset{\sim}{\sigma}}$ (i.e. $\bar{\sigma}_{\parallel}$ $\bar{\sigma}_{\perp}$) from $\underset{\sim}{\sigma}$.

c) Using equation (B22) and the observed chemical shifts, calculate S.

Unfortunately, the present state of the art regarding resolution of ^{13}C nmr spectra in crystals, does not allow a study of a single crystal with a large number of carbon nuclei. This is especially so when the limiting resolution is due to ^{14}N dipolar broadening and not magnetic field inhomogeneity or proton decoupling. Thus, higher magnetic fields are required and such developments are under way in our laboratory. It is possible, however, to make estimates of the order by using $\underset{\sim}{\sigma}$'s from measurements on crystals of small model molecules. This effectively replaces step (a) above, steps (b), (c) then proceed normally as above. From appendix A, we have

$$\bar{\sigma}_{\parallel} = \cos^2\alpha \sin^2\beta \sigma_{11} + \sin^2\alpha \sin^2\beta \sigma_{22} + \cos^2\beta \sigma_{33} \quad \text{(A7)}$$

$$\bar{\sigma}_{\perp} = \frac{1}{2}(1-\cos^2\alpha \sin^2\beta)\sigma_{11} + \frac{1}{2}(1-\sin^2\alpha \sin^2\beta)\sigma_{22} + \frac{1}{2}\sin^2\beta \sigma_{33}. \quad \text{(A8)}$$

The observed shifts $\Delta\sigma = \sigma - \sigma_i$ from Figure 23 can then be used with equation (B22) to yield S. The results for these calculations are shown in Table 2. The value for angle ϕ (Figure 13) was taken at 10°. The $\underset{\sim}{\sigma}$ tensors for each carbon characterized by values of (σ_{11},σ_{22},σ_{33},α,β,γ) were taken from model studies of aromatic carboxyl and methylene groups[3,10] and the known X-ray crystal structure of

TABLE 2. Shielding Tensors and Order Parameters for ^{13}C Nuclei in Smectic-A DEAB

Carbon[(a)]	σ_{11}[(b)]	σ_{22}	σ_{33}	α[(c)]	β	γ	$\bar{\sigma}_{\parallel}$[(c,d)]	$\bar{\sigma}_{\perp}$[(c,d)]	$\bar{\sigma}_{\parallel}-\bar{\sigma}_{\perp}$[(e)]	$\Delta\sigma_{obs}$[(f)]	S (order parameter)
2	- 98	-13	108	100°	90°	90°	- 95	46	-141	-81	0.9
				40°	90°	90°	- 48	23			
1	- 98	-13	108						- 52	-39	1.1[(g)]
				-20°	90°	90°	- 23	10			
				90°	3°	0°	120	59			
4	53	65	121						59	33	0.8
				90°	-17°	0°	118	61			
				67°	90°	90°	-121	-19			
3	-138	-31	9						- 77	-48	0.9
				47°	90°	90°	- 88	-36			

(a) From numbering in Figure 13.

(b) From model single crystal work; see text. The values in ppm relative to an external reference of liquid benzene.

(c) Where two values appear, they refer to the two conformations in Figure 25, namely $(\sigma_{\parallel}^{(a)}, \sigma_{\perp}^{(a)})$ $(\sigma_{\parallel}^{(b)}, \sigma_{\perp}^{(b)})$.

(d) Calculated from equations (A7) and (A8).

(e) Average of two conformations.

(f) $\Delta\sigma_{obs} = \sigma - \sigma_i = \frac{2}{3} S (\bar{\sigma}_{\parallel} - \bar{\sigma}_{\perp})$ from equation (B22).

(g) This clearly means the anisotropy $\bar{\sigma}_{\parallel} - \bar{\sigma}_{\perp}$ taken is too small.

DEAB.[26] The methyl group was not included since its directional shielding properties are not well characterized. For carbons 1, 3, 4, (see Figure 13) two conformations were considered, as shown in Figure 25. These correspond to the two sets of values of (α,β,γ) for these carbons in the table. If we denote the chemical shift in the smectic phase for each of these conformations $\sigma^{(a)}$, $\sigma^{(b)}$, then for rapid conformational motion with equal populations:

$$\sigma = \frac{1}{2}\,(\sigma^{(a)} + \sigma^{(b)}) \tag{8}$$

This is equivalent to an averaged tensor $\bar{\underset{\approx}{\sigma}}$, with:

$$\begin{aligned} \bar{\sigma}_{\parallel} &= \frac{1}{2}\,(\bar{\sigma}_{\parallel}^{(a)} + \bar{\sigma}_{\parallel}^{(b)}) \\ \bar{\sigma}_{\perp} &= \frac{1}{2}\,(\bar{\sigma}_{\perp}^{(a)} + \bar{\sigma}_{\perp}^{(b)}) \end{aligned} \tag{9}$$

These values, averaged over the conformational motion, are reported as 'averaged' in the table and are the ones used to calculate the order parameters from equation (B23). If the model and all assumptions were rigorous, then S values for carbons 1-3 should be equal. Of course this is not the case since the $\underset{\approx}{\sigma}$ tensors (probably σ_{ii} rather than angles) are not accurate. It is clear, however, that the order is high and a reasonable summary of the values is $S = 0.9 \pm 0.1$.

The question of the rapid conformational motion (Figure 25) requires another comment. If this motion is not assumed, then

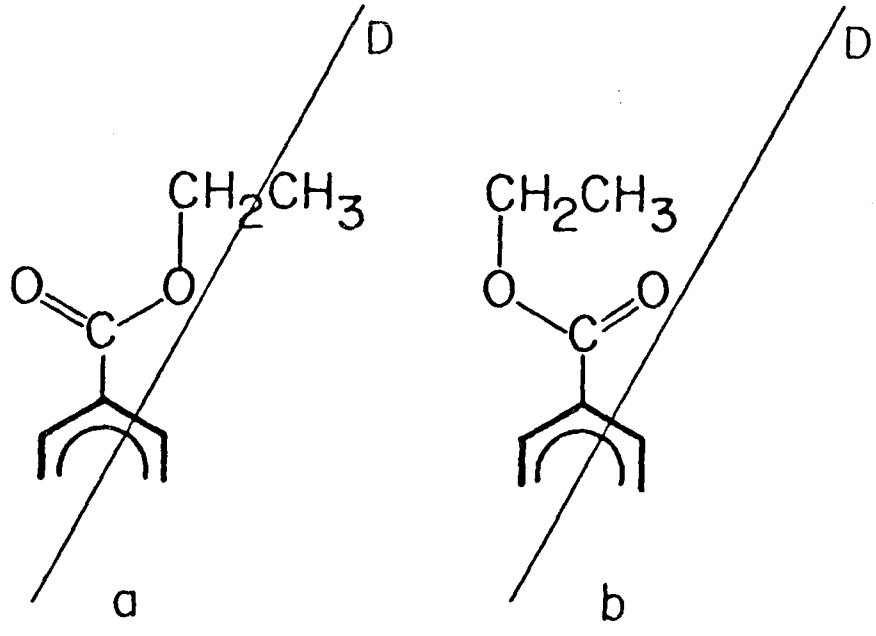

XBL 749-7316

Figure 25

(a) Table 1 shows that additional splittings would be expected for carbons 1, 3, 4 (b) the order parameters would be considerably higher or lower for these carbons and in stronger disagreement with carbon 2. Thus, although not unequivocal, it is quite probable that this conformational motion does exist. More experiments including characaterization of $\underset{\sim}{\sigma}$ in single crystals at high field[3] and spin-lattice relaxation[27] would contribute a great deal towards understanding this fully.

8. Summary

In summary,

1) We have shown that resolved tractable ^{13}C nmr spectra can be obtained in smectic liquid crystals and that they are sensitive to molecular ordering. The effects of sample rotation on the spectra have been demonstrated.

2) Some conclusions have been reached regarding molecular motion in DEAB. In particular, rapid conformational motion involving flipping of the benzene rings and carboxyl groups is very likely.

3) From the broadening of some lines in the isotropic-smectic-A transition and their reappearance on sample rotation near the magic angle, it is estimated that ^{14}N spin relaxation times are between 0.1 and 1 msec in the smectic-A phase of DEAB. Similar behavior was observed for nematics.

4) The order parameter S describing average order over fluctuation of the long molecular axes has been estimated at $S = 0.9 \pm 1$ in the smectic-A phase of DEAB. It is found

to be temperature-independent over the 10° temperature range studied.

III. CONCLUSION

In conclusion, high resolution ^{13}C nmr has successively been applied to nematic and smectic-A liquid crystals. From the spectra, it was possible to extract information concerning a) long range orientational order b) molecular conformational motion and c) spin relaxation of ^{14}N nuclei. At the present time, experiments on smectic-C liquid crystals are underway and it should be possible to extract the same type of information as the model presented demonstrates.

APPENDICES

A. Chemical Shift in Cartesian Coordinates

The directional properties and anisotropy of the observed chemical shift make it useful in studying liquid crystals. Given a nucleus, the observed chemical shift of that nucleus transforms upon rotation of the nucleus as a second rank cartesian tensor. For a strong field whose direction defines the z-axis in the laboratory frame, we have

$$\sigma = (\underset{\approx}{\sigma})_{zz} \tag{A1}$$

where σ is the observed chemical shift, $\underset{\approx}{\sigma}$ is the chemical shielding tensor, and the subscript, zz, denotes the zz-element of the chemical shielding tensor.

There exists a frame of reference in which this tensor is diagonal and this shall be called the principal axis (1,2,3) frame. Furthermore, the convention will be adopted that $\sigma_{11} \leq \sigma_{22} \leq \sigma_{33}$.

$$\underset{\approx}{\sigma}^{(p.a.)} = \begin{pmatrix} \sigma_{11} & 0 & 0 \\ 0 & \sigma_{22} & 0 \\ 0 & 0 & \sigma_{33} \end{pmatrix} \tag{A2}$$

In some new coordinate system (x,y,z) the chemical shielding tensor becomes

$$\underset{\approx}{\sigma} = \underset{\approx}{R}^{+} \underset{\approx}{\sigma}^{p.a.} \underset{\sim}{R} \tag{A3}$$

where $\underset{\approx}{R}$ is the Euler transformation matrix which takes the principal axis frame into the new frame. Adopting the usual notation,[28,29] where α denotes the first Euler rotation angle about the initial z axis, β denotes the second Euler rotation angle about the first intermediate y axis, and γ denotes the final Euler rotation angle about the final intermediate z axis necessary to arrive at the final frame of reference, we have

$$\underset{\approx}{R} = \begin{pmatrix} \cos\alpha\cos\beta\cos\gamma - \sin\alpha\sin\gamma & \sin\alpha\cos\beta\cos\gamma + \cos\alpha\cos\gamma & -\sin\beta\cos\gamma \\ -\cos\alpha\cos\beta\sin\gamma - \sin\alpha\cos\gamma & -\sin\alpha\cos\beta\sin\gamma + \cos\alpha\cos\gamma & \sin\beta\sin\gamma \\ \cos\alpha\sin\beta & \sin\alpha\sin\beta & \cos\beta \end{pmatrix} \quad (A4)$$

Frequently, it is necessary to determine an averaged tensor,

$$\bar{\underset{\approx}{\sigma}} = \langle \underset{\approx}{R}^{+} \underset{\approx}{\sigma}^{(p.a.)} \underset{\approx}{R} \rangle \quad (A5)$$

where the brackets serve to denote this average. In the nematic and smectic-A phases, where rapid rotation about the long axis occurs, it is worthwhile to transform $\underset{\approx}{\sigma}$ from the principal axis frame to a new frame in which the "z" axis lies along the long axis of the molecule. Averaging, then, over γ yields a new tensor

$$\bar{\underset{\approx}{\sigma}} = \begin{pmatrix} \bar{\sigma}_{\perp} & 0 & 0 \\ 0 & \bar{\sigma}_{\perp} & 0 \\ 0 & 0 & \bar{\sigma}_{\parallel} \end{pmatrix} = \langle \underset{\approx}{R}^{+} \underset{\approx}{\sigma}^{(p.a.)} \underset{\approx}{R} \rangle_{\gamma} \quad (A6)$$

where $\bar{\sigma}_{\parallel}$ and $\bar{\sigma}_{\perp}$ are the observed chemical shifts parallel and perpendicular to the long axis of the molecule respectively. Using (A2) through (A6), it can be shown

$$\bar{\sigma}_{\parallel} = \cos^2\alpha \sin^2\beta \sigma_{11} + \sin^2\alpha \sin^2\beta \sigma_{22} + \cos^2\beta \sigma_{33} \quad \text{(A7)}$$

$$\bar{\sigma}_{\perp} = \frac{1}{2}(1-\cos^2\alpha \sin^2\beta)\sigma_{11} + \frac{1}{2}(1-\sin^2\alpha \sin^2\beta)\sigma_{22} + \frac{1}{2}\sin^2\beta \sigma_{33} . \quad \text{(A8)}$$

The actual chemical shift in a nematic and non-rotated smectic-A turns out to be

$$\sigma = \sigma_i + \frac{2}{3} S (\bar{\sigma}_{\parallel} - \bar{\sigma}_{\perp}) \quad \text{(B22)}$$

where σ_i is the isotropic chemical shift and S is the uniaxial order parameter, $\langle P_2(\cos\theta)\rangle$. To derive (B22), an additional transformation from this molecule fixed frame to the lab frame would be necessary, but this turns out to be rather cumbersome. By rewriting the chemical shift in terms of spherical tensors, as is done in appendix B, the transformations are greatly simplified and (B22) is readily derived. For the more complicated smectic-C phase, use of spherical tensors becomes necessary even in computer calculations. The purpose of this appendix is more to give insight into the transformational properties of the chemical shielding tensor than to be of great practical value. Perhaps the one exception to this deals with the chemical shift in the isotropic phase. In the isotropic phase, the observed chemical shift is just the average of the 3 elements; σ_{11}, σ_{22}, σ_{33}.

$$\sigma_i = \frac{1}{3}(\sigma_{11} + \sigma_{22} + \sigma_{33}) \quad \text{(A9)}$$

This, however, is simply one third the trace of the shielding tensor in the principal axis frame:

$$\sigma_i = \frac{1}{3} \mathrm{Tr}\ (\underset{\approx}{\sigma}^{(p.a.)}) \quad , \tag{A10}$$

but the trace of a tensor is independent of the frame of reference and hence

$$\sigma_i = \frac{1}{3} \mathrm{Tr}\ (\underset{\approx}{\sigma}) \quad . \tag{A11}$$

Thus, knowing the diagonal elements <u>in any frame</u> will give, in a simple way, the isotropic chemical shift.

B. Theory of The Orientational Dependence of Chemical Shifts in Liquid Crystals.

1. The Hamiltonian in terms of spherical tensors.

It is frequently possible to express a Hamiltonian in a form which involves a cartesian tensor. The chemical shift Hamiltonian, for example, can be written

$$\mathcal{H} = \underset{\sim}{H} \cdot \underset{\approx}{\sigma} \cdot \underset{\sim}{I} = \sum_{i=1}^{3} \sum_{j=1}^{3} H_i \, \sigma_{ij} \, I_j \qquad \text{(B1)}$$

where $\underset{\sim}{H}$ is the applied field, $\underset{\approx}{\sigma}$ is the chemical shielding tensor, and $\underset{\sim}{I}$ is the spin operator of a particular nucleus. The disadvantage of writing the Hamiltonian as such is that one can form linear combinations of the components of this shielding tensor, $\underset{\approx}{\sigma}$, which transform differently upon rotation.[28] It is easy to show, for example, that the trace of $\underset{\approx}{\sigma}$ is invariant to rotation and hence transforms as a scalar. Likewise, certain linear combinations of the σ_{ij}'s can be formed which transform as second rank spherical harmonics. Consequently, it is possible to write the Hamiltonian in terms of spherical tensors. Such forms of the Hamiltonian can be found in the literature[19,29] and we outline how to go from the cartesian to the spherical form.

The first step involves writing the vector elements $H_i I_j$ as spherical vector (first rank tensor) products. The elements of a spherical vector are given by (B2).

$$V_x = -\frac{1}{\sqrt{2}}(V_{1-1} - V_{11})$$

$$V_y = \frac{i}{\sqrt{2}}(V_{1-1} + V_{11})$$

$$V_z = V_{10} \tag{B2}$$

Here the notation $V_{\ell m}$ means a spherical tensor of rank "ℓ" and projection "m". A particular linear combination of the products of two spherical tensors yield a new tensor and these linear combinations must satisfy (B3).[30]

$$T_{\ell m} = \sum_{\substack{\ell_1 \ell_2 \\ m_1 m_2}} \langle \ell m | \ell_1 \ell_2 m_1 m_2 \rangle \, V_{\ell_1 m_1} \, W_{\ell_2 m_2} \tag{B3}$$

Here, $T_{\ell m}$ is a new spherical tensor of rank "ℓ" and projection "m" formed by taking the stated linear combinations of tensor products $V_{\ell_1 m_1} W_{\ell_2 m_2}$, and $\langle \ell m | \ell_1 \ell_2 m_1 m_2 \rangle$ is the Clebsh-Gordon coefficient. The most familiar example of this comes from quantum mechanics and involves the coupling of two systems of angular momenta. The eigenvalues are the total angular momentum "ℓ" and projection "m" and the eigenvalues are expressed as a sum of products of the eigenfunctions of the two uncoupled systems.

Using (B3), new spin-field tensors, $T_{\ell m}$, can be formed from the products of the components of the field and spin spherical vectors $H_{1m} I_{1m}$. The result is

$$T_{00} = \frac{1}{\sqrt{3}} \sum_{k=-1}^{1} (-)^k H_{1k} I_{1-k}$$

$$T_{11} = \frac{1}{\sqrt{2}} (H_{11} I_{10} - H_{10} I_{11})$$

$$T_{10} = \frac{1}{\sqrt{2}} (H_{11} I_{1-1} - H_{1-1} I_{11})$$

$$T_{1-1} = \frac{1}{\sqrt{2}} (H_{10} I_{1-1} - H_{1-1} I_{10}) \qquad \text{(B4)}$$

$$T_{22} = H_{11} I_{11}$$

$$T_{21} = \frac{1}{\sqrt{2}} (H_{10} I_{11} + H_{11} I_{10})$$

$$T_{20} = \frac{1}{\sqrt{6}} (H_{1-1} I_{11} + 2H_{10} I_{10} + H_{11} I_{1-1})$$

$$T_{2-1} = \frac{1}{\sqrt{2}} (H_{1-1} I_{10} + H_{10} I_{1-1})$$

$$T_{2-2} = H_{1-1} I_{1-1}$$

and the converse relationships are

$$H_{11} I_{11} = T_{22}$$

$$H_{1-1} I_{1-1} = T_{2-2}$$

$$
\begin{aligned}
H_{11}I_{10} &= \frac{1}{\sqrt{2}}\,(T_{21} + T_{11}) \\
H_{10}I_{11} &= \frac{1}{\sqrt{2}}\,(T_{21} - T_{11}) \\
H_{1-1}I_{10} &= \frac{1}{\sqrt{2}}\,(T_{2-1} - T_{1-1}) \\
H_{10}I_{1-1} &= \frac{1}{\sqrt{2}}\,(T_{2-1} + T_{1-1}) \\
H_{10}I_{10} &= \frac{1}{\sqrt{3}}\,(\sqrt{2}\,T_{20} + T_{00}) \\
H_{11}I_{1-1} &= \frac{1}{\sqrt{6}}\,(T_{20} + \sqrt{3}\,T_{10} - \sqrt{2}\,T_{00}) \\
H_{1-1}I_{11} &= \frac{1}{\sqrt{6}}\,(T_{20} - \sqrt{3}\,T_{10} - \sqrt{2}\,T_{00}) \quad .
\end{aligned}
\tag{B5}
$$

By substituting these back into (B1)

$$
\begin{aligned}
H = {} & \frac{1}{\sqrt{3}}\,T_{00}\,(\sigma_{11} + \sigma_{22} + \sigma_{33}) \\
& + \frac{1}{2}\,T_{11}\,(i(\sigma_{23} - \sigma_{32}) + (\sigma_{31} - \sigma_{13})) \\
& + {}^{i}/_{2}\,T_{10}\,(\sigma_{21} - \sigma_{12}) \\
& + {}^{1}/_{2}\,T_{1-1}\,(i(\sigma_{32} - \sigma_{23}) + (\sigma_{31} - \sigma_{13})) \\
& + \frac{1}{2}\,T_{22}\,(\sigma_{11} - \sigma_{22} - i(\sigma_{12} + \sigma_{21})) \\
& + \frac{1}{2}\,T_{21}\,(i(\sigma_{32} + \sigma_{23}) - (\sigma_{31} + \sigma_{13})) \\
& + \frac{1}{\sqrt{6}}\,T_{20}\,(2\sigma_{33} - \sigma_{11} - \sigma_{22}) \\
& + \frac{1}{2}\,T_{21}\,(i(\sigma_{23} + \sigma_{32}) + (\sigma_{13} + \sigma_{31})) \\
& + \frac{1}{2}\,T_{2-2}\,(\sigma_{11} - \sigma_{22} + i(\sigma_{12} + \sigma_{21})) \quad .
\end{aligned}
\tag{B6}
$$

The components of the first term transform as scalars, those of the second as vectors, and those of the third as second rank tensors. The linear combinations of the σ's are also spherical tensor elements. The Hamiltonian is a scalar and from (B6) it is possible to show that

$$H = U_{00} = \sum_{\ell,m} (-)^m F_{\ell m} T_{\ell -m} \quad . \tag{B7}$$

Comparing (B6) and (B7) it can readily be seen

$$H = H^{(0)} + H^{(1)} + H^{(2)} \tag{B8}$$

where

$$H^{(0)} = F_{00} T_{00}$$

$$H^{(1)} = \sum_{m=-1}^{+1} (-)^m F_{1m} T_{1-m}$$

$$H^{(2)} = \sum_{m=-2}^{+2} (-)^m F_{2m} T_{2-m} \quad . \tag{B9}$$

Here, $F_{\ell m}$ is a spherical tensor involving linear combinations of the elements of the chemical shielding tensors and $T_{\ell m}$, as stated previously, are functions of the field vector and spin operators.

Since the Hamiltonian is a scalar, it is independent of the reference frame we choose. Choosing a frame of reference corresponding to the principal axis of the shielding tensor yields

$$F_{00}^{(p.a.)} = \frac{1}{\sqrt{3}} (\sigma_{11} + \sigma_{22} + \sigma_{33})$$

$$F_{1m}^{(p.a.)} = 0$$

$$F_{2\pm2}^{(p.a.)} = \frac{1}{2} (\sigma_{11} - \sigma_{22})$$

$$F_{2\pm1}^{(p.a.)} = 0$$

$$F_{20}^{(p.a.)} = \frac{1}{\sqrt{6}} (2\sigma_{33} - (\sigma_{11} + \sigma_{22})) \quad . \tag{B10}$$

The superscripts denote the frame of reference. To transform from the p.a. frame to the lab frame, use is made of a modified version of the Addition Theorem of Spherical Harmonics.[28]

$$F_{\ell m}^{(lab)} = \sum_{m'} D_{m'm}^{(\ell)} (\Omega) F_{\ell m'}^{(p.a.)} \tag{B11}$$

where Ω denotes the Euler angles which take the p.a. frame into the lab frame and $D_{m'm}^{(\ell)} (\Omega)$ is an element of the Wigner rotation matrix. Those matrix elements of importance to this work are given in appendix D.

Thus the Hamiltonian, with the field in the z direction becomes

$$H = F_{00} T_{00} + \sum_{m,m'=-2}^{+2} (-)^m D_{m'm}^{(2)} (\Omega) F_{2m'}^{(p.a.)} T_{2-m} \tag{B12}$$

and from (B4)

$$T_{00} = \frac{1}{\sqrt{3}} HI_z$$

$$T_{2\pm2} = 0$$

$$T_{2\pm1} = \frac{1}{\sqrt{2}} HI_{\pm}$$

$$T_{20} = \sqrt{\frac{2}{3}} HI_z \quad . \tag{B13}$$

In high fields, it is valid to neglect $T_{2\pm1}$ since they involve only second order corrections to the energy by mixing non-diagonal states. Recognizing that

$$H = H_0 \sigma_{zz} I_z \tag{B14}$$

it is simple to show that

$$\sigma_{zz} = \frac{1}{3} \mathrm{Tr} \underset{\approx}{\sigma} + \sqrt{\frac{2}{3}} \sum_m D^{(2)}_{m0} (\Omega) F_{2m}^{(p.a.)} \tag{B15}$$

or

$$\sigma_{zz} = \sigma_i + \sqrt{\frac{2}{3}} F_{20}^{(lab)} \tag{B16}$$

where σ_i is the isotropic chemical shift.

2. Liquid Crystal Chemical Shifts.

a. Nematic and Smectic A.

A molecule in the nematic or smectic-A phase rotates about its long axis. At the same time, the long axis of the molecule tends to align along the direction of the field. To derive the observed

chemical shift, it is necessary to introduce two Euler transformations. Let Ω_0 take the p.a. frame to a molecule fixed frame and let Ω take the molecule fixed frame into the lab frame. Examples of the p.a. frame were shown previously (Figure 8). The molecule fixed frame is shown in Figure 26. Using (B11) and transforming first by Ω and then by Ω_0, we get

$$F_{20}^{(lab)} = \sum_m \sum_n D_{m0}^{(2)} (\Omega) D_{nm}^{(2)} (\Omega_0) F_{2n}^{(p.a.)} \quad . \tag{B17}$$

Due to fluctuations rapid on the nmr timescale, (B17) must be averaged.

These fluctuations involve deviations of the long axis of the molecule from its mean orientation along the direction of the field. Consequently, an average over Ω must be made. Equation (B17) then becomes

$$\langle F_{20}^{(lab)} \rangle = \sum_{m,n} \langle D_{m0}^{(2)} (\Omega) \rangle D_{nm}^{(2)} (\Omega_0) F_{2n}^{(p.a.)} \quad . \tag{B18}$$

From appendix D

$$\langle D_{mn}^{(2)} (\Omega) \rangle = \langle e^{-i(m\alpha+n\gamma)} d_{mn}^{(2)} (\beta) \rangle = \int_0^{2\pi} d\alpha \int_0^{2\pi} d\gamma \int_0^{1} d(\cos\beta) \; P(\alpha,\beta,\gamma) e^{-i(m\alpha+n\gamma)} d_{mn}^{(2)} (\beta) \tag{B19}$$

where $P(\alpha,\beta,\gamma)$ is the orientational distribution function. In the nematic and smectic-A phase, the molecule reorients rapidly about its long axis. Assuming free rotation about the long axis insures that

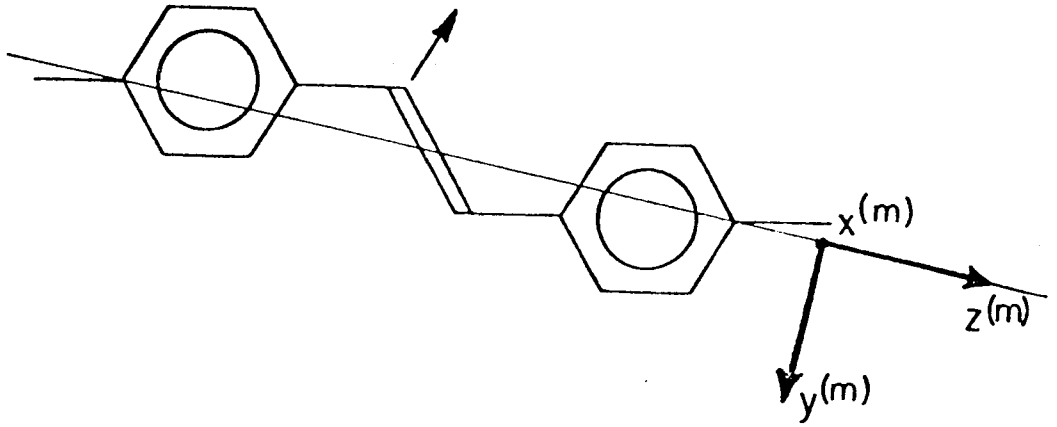

XBL757-6739

Figure 26

the orientational distribution function is independent of α and γ. From (B19) then, it can be seen that only $\langle D_{00}^{(2)}(\Omega)\rangle$ remains. Equation (B18) then becomes

$$\sigma_{zz} = \sigma_i + \sqrt{\frac{2}{3}} \sum_n \langle D_{00}^{(2)}(\Omega)\rangle \; D_{n0}^{(2)}(\Omega_0) \; F_{2n}^{(p.a.)} \qquad \text{(B20)}$$

Remembering that $S = \langle P_2(\cos\beta)\rangle = \langle D_{00}^{(2)}(\Omega)\rangle$, it is simple to show that

$$\sigma_{zz} = \sigma_i + \frac{2}{3} S \left[(\sigma_{33} - \frac{1}{2}(\sigma_{11}+\sigma_{22}))P_2(\cos\beta_0) + \frac{3}{4}\cos 2\alpha_0 \sin^2\beta_0 (\sigma_{11}-\sigma_{22})\right] \qquad \text{(B21)}$$

where $(\alpha_0,\beta_0,\gamma_0)$ are the Euler angles which take the p.a. frame into the molecule fixed frame and $P_2(\cos\beta_0) = \frac{3}{2}\cos^2\beta_0 - \frac{1}{2}$. Making use of (A7) and (A8) in (B21) finally yields the familiar expression

$$\sigma_{zz} = \sigma_i + \frac{2}{3} S (\bar{\sigma}_{\parallel} - \bar{\sigma}_{\perp}) \quad . \qquad \text{(B22)}$$

In order to determine the chemical shift of a rotated smectic A, an additional transformation is necessary. The procedure is analogous to that given above and the result is

$$\sigma_{zz} = \sigma_i + \frac{2}{3} P_2(\cos\theta) S (\bar{\sigma}_{\parallel} - \sigma_{\perp}) \qquad \text{(B23)}$$

where "θ" is the angle through which the sample was rotated.

b. Smectic-C.

Before discussing the transformations necessary to best treat

the smectic-C phase, it will be wise to consider carefully the model which best describes it. The model to be discussed is a microscopic one and combines the model of Luz and Meiboom[19] and Wise et al.[31] with that of McMillan.[32]

When a sample is cooled from the nematic or isotropic phase down to the smectic-C phase, the molecules remain aligned along the direction of the field. The molecules layer into planes as in the smectic-A phase, but unlike the smectic-A phase, these planes are tilted relative to the direction of the field as shown in Figure 27. The tilting of the smectic planes is assumed to be caused by electric transverse or steric interactions between the molecules as shown in Figure 28. As a result of this collective interaction, rotation about the long axis becomes biased.

Since there is no preferred orientation of the smectic planes about the field direction, all azimuthal orientations of the planes are present. Each azimuthal orientation of a smectic plane will be called a domain. The domain structures is shown schematically as the cone in Figure 29.

If the interplanar spacing is negligible, the tilt angle "α" is also the angle between the normal to the plane and the director of the domain. (As in the case of the nematic phase, the director is the mean orientation of the long axis of the molecules.) Since the molecules are tilted by "α" in these planes, the director is free to reorient. The allowed orientations lie on a cone with half the vertex angle of this cone equal to the tilt angle "α" as shown in Figure 30. The azimuthal orientation which the director assumes

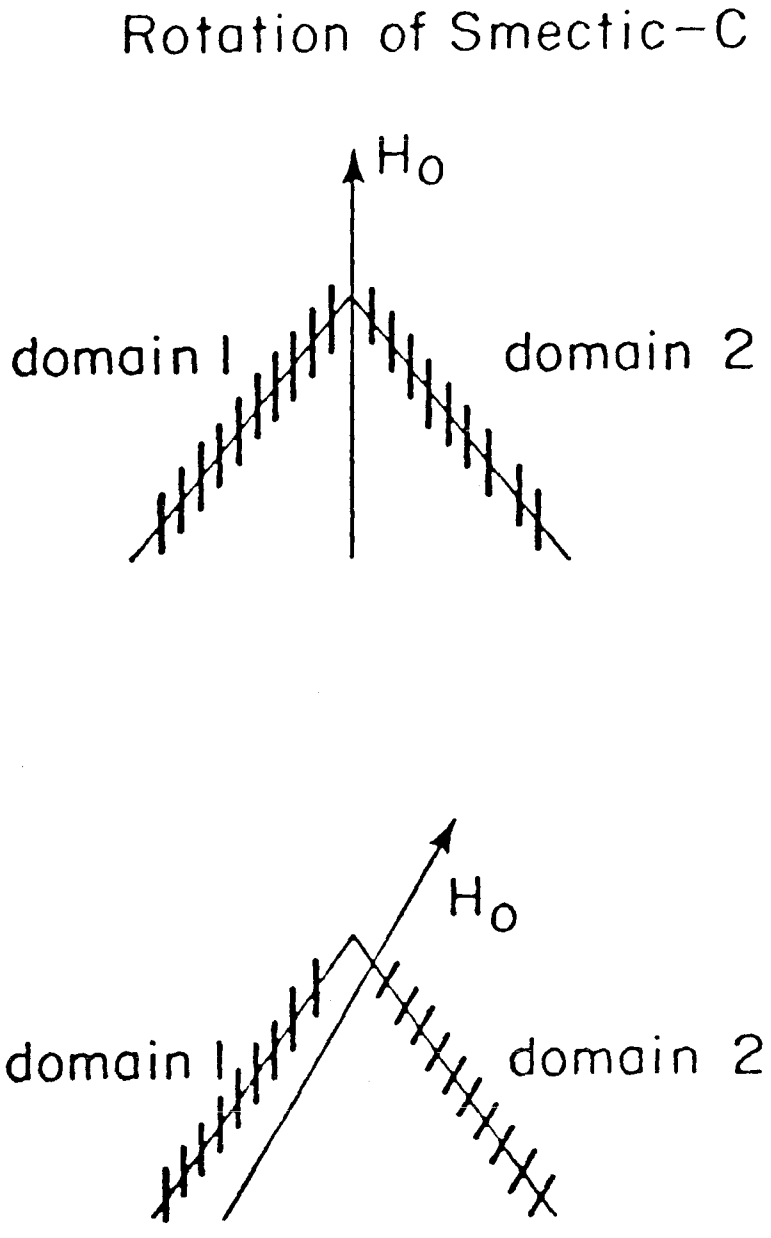

XBL 751-5494

Figure 27

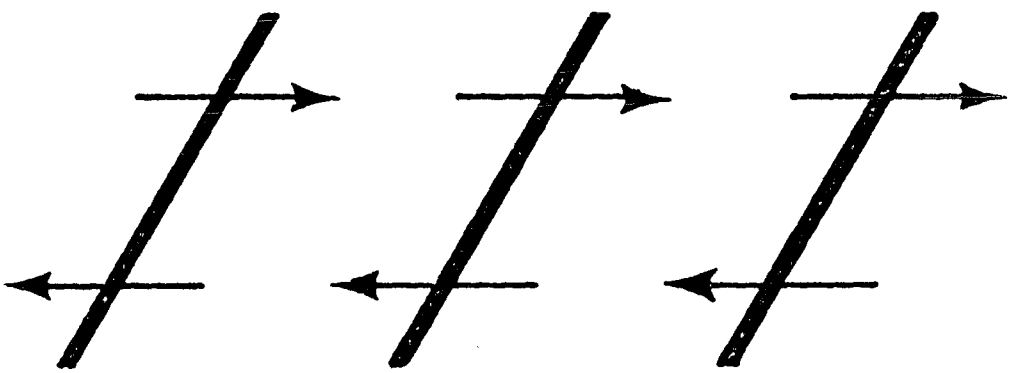

XBL 751-5550

Figure 28

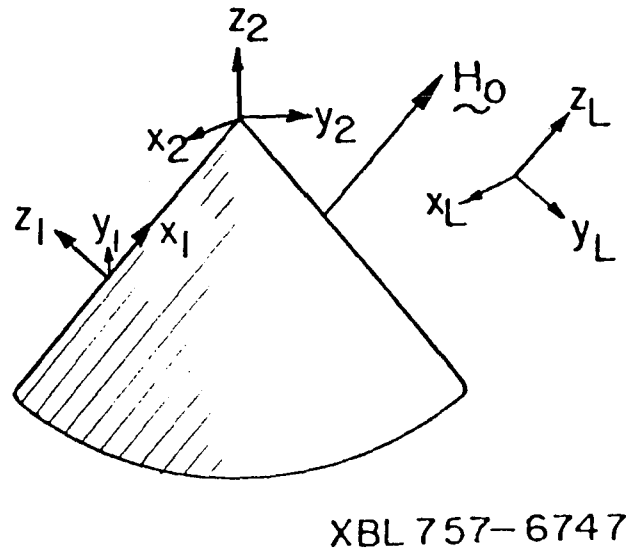

Figure 29

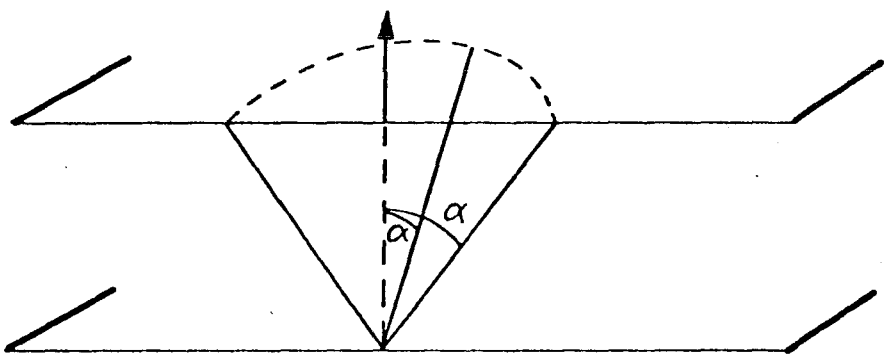

XBL 758-6922

Figure 30

will be that which maximizes its projection along the direction of the field and thereby minimizes its magnetic anisotropy energy according to Equation (B24).

$$E_m = -\underset{\sim}{H} \cdot \underset{\approx}{\chi} \cdot \underset{\sim}{H} \qquad \text{(B24)}$$

The work of Luckhurst et al.[25] confirms this. For the same reason, the mean orientation of the plane of the molecule will usually orient in such a way that the average direction of the unit vector normal to the plane of the molecule is perpendicular to the direction of the field as illustrated in Figure 31. According to the McMillan theory[32] the tilt is induced by the freezing out of the rotation about the long axis. Indeed, McMillan derived equations which predict that the tilt passively follows this orientational order. Consequently, the plane of the molecules will tend to allign in the way stated to minimize their magnetic anisotropy energy.

Finally, when the sample is rotated, the domain structure is not altered or destroyed in any way. The works of others[19,25,31] confirm that this is true when pure samples are used in a field of 24 kG.

From this model, it will be possible to extract not only the type of information obtained from our studies of the nematics and DEAB, but it will also be possible to learn about hindered rotation.

On the basis of the model just discussed it will be necessary to make five successive transformations:

(1) the Euler angles, $(\Omega_0) = (\alpha_0, \beta_0, \gamma_0)$, take the p.a. frame into the molecule fixed frame. These 2 frames are depicted in Figures 8 and 26.

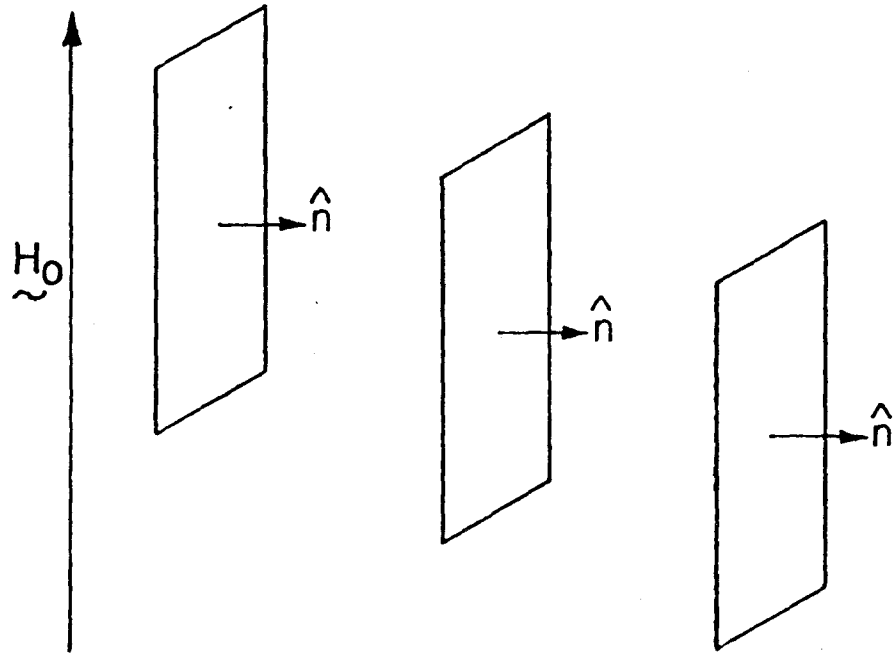

XBL 757-6741

Figure 31

(2) the Euler angles $(\Omega) = (\alpha', \beta, \gamma)$ takes the molecule fixed frame into a new frame which characterizes the averaged geometry of the molecules in a particular domain. (Note that α' is used instead of α since α will denote the tilt angle.) This frame of reference will be called the symmetry frame. In the symmetry frame, the z axis is chosen to lie along the director, x is chosen to lie along a vector which is normal to the mean molecular plane, and y is chosen to complete a right-handed coordinate system. In the case of a completely ordered system, $(\alpha', \beta, \gamma) = (0,0,0)$.

(3) The Euler angles $(\Omega_1) = (\alpha_1, \beta_1, \gamma_1)$ take the symmetry frame into a frame which specifies a particular domain. This new frame will be called the domain frame. This third transformation is necessary since changing the direction of the applied field will cause the position of the director in a domain fixed frame to change. Put in another way, domains which differ in their orientation relative to an applied field will have different (Ω_1)'s. The axis of the domain frame are chosen in the following conventional way: z_1 is normal to the domain plane, x_1 points radially toward the vertex of the cone which represents schematically all the possible domains, and y_1 is chosen to complete a right handed coordinate system. Figure 29 serves to illustrate this frame and also the last 2 frames of reference to be discussed. Figure 32 and its caption describe the Euler transformation (Ω_1). From the particular choice of the angles given,

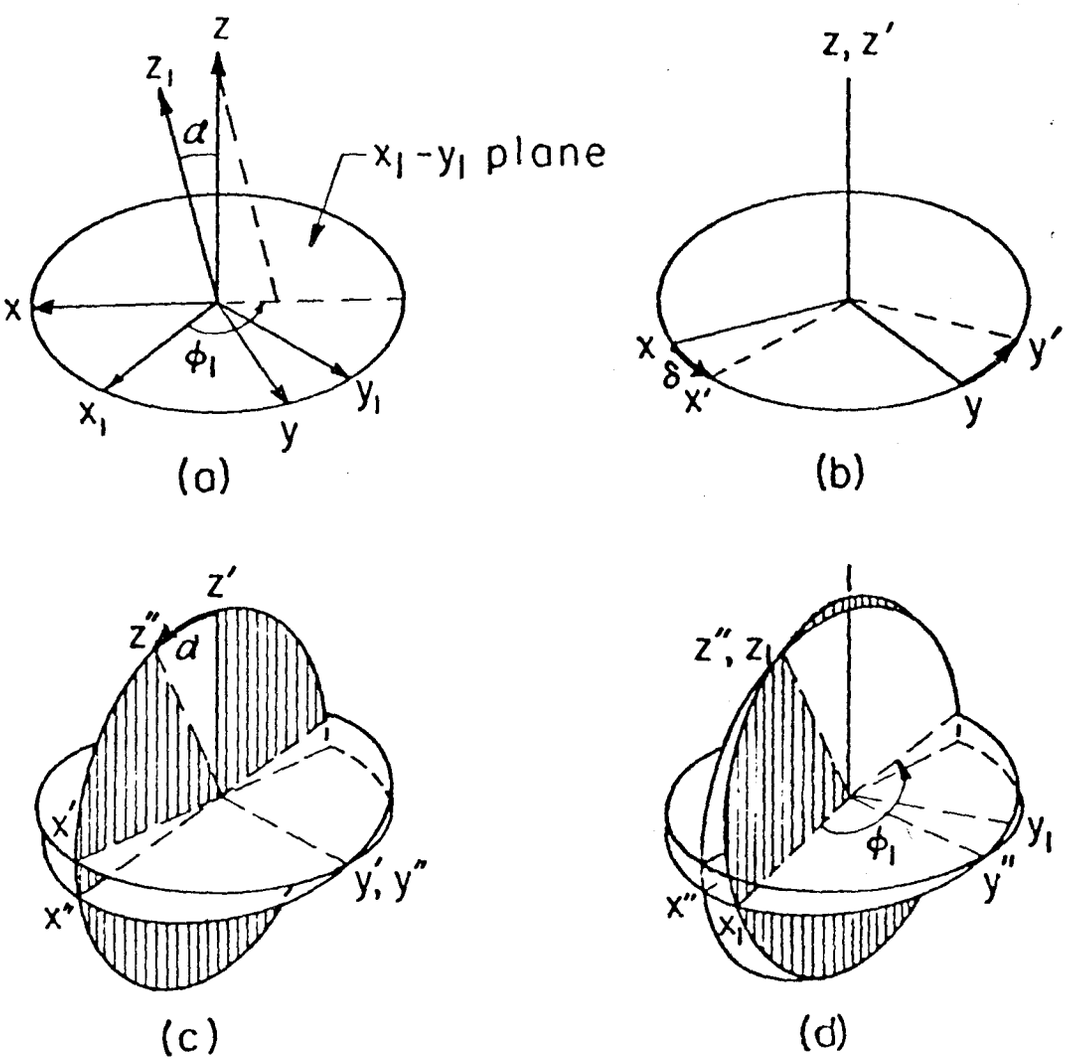
z
z_1
α
x_1 - y_1 plane
x
ϕ_1
x_1
y_1
y
(a)
z, z′
x
δ
x′
y′
y
(b)
z′
z″
α
x′
x″
y′, y″
(c)
z″, z_1
ϕ_1
y_1
y″
x″
x_1
(d)
XBL 757-6740

Figure 32

$$(\Omega_1) = (\alpha_1, \beta_1, \gamma_1) = (\delta, \alpha, \pi - \phi_1) \tag{B25}$$

$$D_{nm}(\Omega_1) = (-)^m d_{nm}(\alpha) e^{i(m\phi_1 - n\delta)} . \tag{B26}$$

Here, α represents the tilt angle and δ and ϕ_1 will be determined later subject to the constraints of the model.

(4) The Euler angles $(\Omega_2) = (\alpha_2, \beta_2, \gamma_2)$, take the domain frame into a new frame. From Figure 29 and the previous discussion of the model, it is seen that this new frame and laboratory frame of a non-rotated sample coincide. Consequently, this new frame will be called the initial lab frame. (Ω_2), by inspection, turns out to be

$$(\Omega_2) = (0, \alpha, \phi_2) \tag{B27}$$

so

$$D_{m\ell}(\Omega_2) = d_{m\ell}(\alpha) e^{-i\ell\phi_2} . \tag{B28}$$

Here, ϕ_2 serves to identify a particular domain and was chosen to vary between $\pm \frac{\pi}{2}$. This choice gives all possible domains. It is the presence of different domains which give rise to a broadening of the line as the sample is rotated.[19,31]

(5) The final Euler transformation (Ω_2), takes the initial lab frame into the lab frame. It accounts for the rotation of the sample in a magnetic field by an angle θ. Since x_2 and x_L are chosen to lie on the axis of sample rotation and z_2 and z_L are chosen to

lie initially and finally along the field respectively (see Figures 29 and 33),

$$(\Omega_L) = (\frac{\pi}{2}, \theta, -\frac{\pi}{2}) \quad . \tag{B29}$$

Consequently

$$D_{\ell 0}(\Omega_L) = i^{-\ell} \, d_{\ell 0}(\theta) \quad . \tag{B30}$$

This completes the description of the necessary transformations.

From successive use of (B11) we get

$$F_{20}^{(lab)} = \sum_{\ell,m,n,p,q} D_{\ell 0}(\Omega_L) \; D_{m\ell}(\Omega_2) \; D_{nm}(\Omega_1) \langle D_{qn}(\Omega) \rangle \times D_{pq}(\Omega_0) F_{2p}^{(p.a.)} . \tag{B31}$$

In the smectic-C phase the order parameter $S = \langle D_{00}(\Omega) \rangle$ is high--probably around 0.9. Consequently, the off-diagonal elements $\langle D_{qn}(\Omega) \rangle$ are small and to a good approximation, can be neglected. (See appendix E). Making this approximation, (B31) becomes

$$F_{20}^{(lab)} = \sum_{\substack{\ell \; m \\ n \; p}} D_{\ell 0}(\Omega_2) \; D_{m\ell}(\Omega_2) \; D_{nm}(\Omega_1) \langle D_{nn}(\Omega) \rangle D_{pn}(\Omega_0) F_{2p}^{(p.a.)} \tag{B32}$$

Using (B30), (B28), (B26), and writing out the other elements ($D_{pn}(\Omega_0) = e^{-i(p\alpha_0 + n\gamma_0)} d_{pn}(\beta_0)$, etc.) (B32) becomes

$$F_{20}^{(lab)} = \sum_{\substack{\ell \; m \\ n \; p}} (-)^{\ell+m} \, i^{\ell} \, e^{-i(\ell\phi_2 - m\phi_1 + n\delta + p\alpha_0 + n\gamma_0)} d_{\ell 0}(\theta) \; d_{m\ell}(\alpha) \times d_{nm}(\alpha) \; \langle D_{nn}(\Omega) \rangle \; d_{pn}(\Omega_0) F_{2p}^{(p.a.)} \quad . \tag{B33}$$

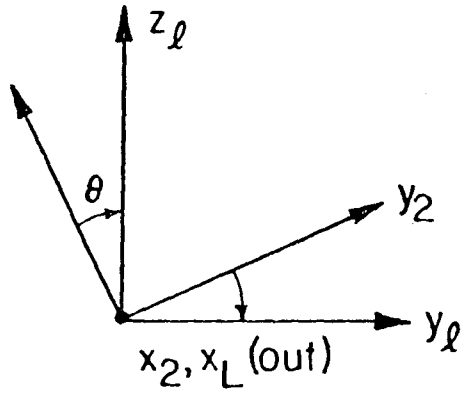

XBL757-6746

Figure 33

Since the chemical shift is real and so then is $F_{20}^{(lab)}$,

$$F_{20}^{(lab)} = \frac{1}{2}(F_{20}^{(lab)} + F_{20}^{(lab)}\ (c.c.)) \qquad (B34)$$

Since β-fluctuations are small, it is valid to neglect the complex part of $<D_{nn}(\Omega)>$ so

$$<D_{nn}(\Omega)> = <\cos n(\alpha'+\gamma)\ d_{nn}(\beta)> + i<\sin n(\alpha'+\gamma) d_{nn}(\beta)>$$

$$= <\cos n(\alpha'+\gamma)\ d_{nn}(\beta)> \qquad (B35)$$

Substituting (B35) and (B34) into (B33) yields, after rearrangement,

$$F_{20}^{(lab)} = \sum_{\substack{\ell\ m \\ n\ p}} (-)^{\ell+m} d_{\ell 0}(\theta) d_{\ m}(\alpha) d_{nm}(\alpha) d_{pn}(\beta_0) <\cos n\ (\alpha'+\gamma)\ d_{nn}(\beta)>$$

$$x\ \cos\varepsilon\ F_{2p}^{(p.a.)}$$

$$\varepsilon \equiv \ell(\phi_2 - \pi/2) - m\phi_1 + n(\delta+\gamma_0) + p\alpha_0 \quad . \qquad (B36)$$

Now ϕ_1 and δ will be determined subject to the constraints of the model.

If $\underset{\sim}{z}_L$ is a unit vector along the direction of the field and $\underset{\sim}{z}$ and $\underset{\sim}{x}$ are unit vectors pointing along the z and x axi of the symmetry frame, then to maximize the projection of the director along the field requires

$$|\underset{\sim}{z}_L \cdot \underset{\sim}{z}| = \text{maximum.} \qquad (B37)$$

Furthermore, the constraint that the normal to the mean-molecular

plane is perpendicular to the direction of the field requires

$$\underset{\sim}{z}_L \cdot \underset{\sim}{x} = 0 \quad . \tag{B38}$$

The first step is to rewrite these unit vectors in terms of their spherical components. Perhaps the best discussion of this method can be found in Tinkham.[33] If $\underset{\sim}{\ell}$ is a unit vector with cartesian components ℓ_x, ℓ_y, and ℓ_z, then transforming to spherical components yields

$$\ell_x = -\frac{1}{\sqrt{2}} (\ell_{-1} - \ell_{+1})$$

$$\ell_y = +\frac{i}{\sqrt{2}} (\ell_{-1} + \ell_{+1})$$

$$\ell_z = \ell_0 \tag{B39}$$

The spherical components transform in a manner analogous to second rank spherical tensors. If the components of some vector $\underset{\sim}{\ell}$ are known in one frame of reference (Σ_1) and (Ω) represents the Euler transformation which takes the Σ_1 frame into a new frame (Σ_2), then the spherical components of this same vector in Σ_2 will be

$$\ell_m^{(2)} = \sum_n D_{nm}^{(1)}(\Omega)\ \ell_n^{(1)} \quad . \tag{B40}$$

The vector superscript denotes the frame of reference and the subscript the component of our vector. $D_{nm}^{(1)}(\Omega)$ is a component of the first rank Wigner rotation matrix. (See appendix D).

The scalar product of two vectors in spherical form is

$$\underset{\sim}{z}_1 \cdot \underset{\sim}{z}_2 = \sum_{\ell} (-)^{\ell} z_{1\ell} z_{2-\ell} \quad . \tag{B41}$$

The scalar product is independent of the frame of reference in which it is taken. To determine $\underset{\sim}{z}_1 \cdot \underset{\sim}{z}$, it will be useful to transform $\underset{\sim}{z}$ from the lab frame to the symmetry frame. By successively applying (B40) through the three transformations discussed previously, we get

$$z_{-\ell}^{(\ell)} = \sum_{m,n,p} D^{(1)}_{m-\ell}(\Omega_L)\, D^{(1)}_{nm}(\Omega_2)\, D^{(1)}_{pn}(\Omega_1) z_p^{(s)} \quad . \tag{B42}$$

The vector superscripts (ℓ) and (s) denote the lab and symmetry frames respectively. Using (B42) and (B41), the vector scalar product, $\underset{\sim}{z}_L \cdot \underset{\sim}{z}$, in the lab frame is

$$\underset{\sim}{z}_L \cdot \underset{\sim}{z} = \sum_{\substack{\ell\ m \\ n\ p}} (-)^{\ell} z_{L\ell}^{(\ell)}\, D^{(1)}_{m-\ell}(\Omega_1)\, D^{(1)}_{nm}(\Omega_2)\, D^{(1)}_{pn}(\Omega_1) z_p^{(s)} \quad . \tag{B43}$$

From the definitions of $\underset{\sim}{z}_L$ and $\underset{\sim}{z}$ and Equation (B39)

$$\begin{aligned} z_{L\ell}^{(\ell)} &= \delta_{\ell 0} \\ z_p^{(s)} &= \delta_{p0} \end{aligned} \tag{B44}$$

Substituting (B44) into (B43) and writing out the matrix elements $(D^{(1)}_{nm}(\Omega_2) = e^{-i(n\alpha_2 + m\alpha_2)} d^{(1)}_{nm}(\beta_2)$, etc.) we find

$$\underset{\sim}{z}_L \cdot \underset{\sim}{z} = \sum_{mn} (-)^{m+n} (i)^m d_{0n}(\alpha) d_{nm}(\alpha) d_{m0}(\theta) e^{-i(n\phi_2 + p\phi_1)} \tag{B45}$$

Maximizing the absolute value with respect to the variable ϕ_1 requires

$$0 = \frac{\partial |\underset{\sim}{z}_L \cdot \underset{\sim}{z}|}{\partial \phi_1} = \frac{\underset{\sim}{z}_L \cdot \underset{\sim}{z}}{|\underset{\sim}{z}_L \cdot \underset{\sim}{z}|} \frac{\partial (\underset{\sim}{z}_L \cdot \underset{\sim}{z})}{\partial \phi_1} \tag{B46}$$

Substituting (B45) into (B46) yields

$$\tan \phi_1 = \frac{\sin\theta \cos\phi_2}{\sin\theta \cos\alpha \sin\phi_2 + \cos\theta \sin\alpha} \quad . \tag{B47}$$

Since ϕ_1 ranges between 0 and 2π, two values of ϕ_1 will satisfy (B47). To determine the maximum, both values must be substituted into (B45) to distinguish the maximum. An analogous derivation follows for (B38) and the result is

$$\tan\delta = \frac{\cos\theta\sin\alpha\cos\alpha(\cos\phi_1 - 1) - \sin\theta(\sin^2\theta\sin\phi_2 + \cos\alpha(\sin\phi_1\cos\phi_2 + \cos\alpha\cos\phi_1\sin\phi_2))}{\cos\theta\sin\alpha\sin\phi_1 + \sin\theta(\cos\phi_1\cos\phi_2 - \cos\alpha\sin\phi_1\sin\phi_2)} \tag{B48}$$

This completes the theory of the smectic-C. At present, application of this theory has been restricted to a few special cases and these will now be discussed.

Case 1 - uniaxial symmetry, free rotation.

The model of the smectic-A phase was adopted for which the tilt angle is zero and the molecules rotate freely about their long axis. In this case, solving (B48), (B47), and (B36) yields (B23).

$$\sigma_{zz} = \sigma_i + \frac{2}{3} S P_2(\cos\theta) (\bar{\sigma}_{\parallel} - \bar{\sigma}_{\perp}) \tag{B23}$$

Case 2 - Smectic C, free rotation.

A tilt angle of 45° and $\langle D_{00} \rangle = 1$ were assumed. Due to the free rotation about the long axis, $\langle D_{11} \rangle$ and $\langle D_{22} \rangle$ are identically zero.

In the case of free rotation, the elements of the shielding tensor ($\sigma_{11}, \sigma_{22}, \sigma_{23}$) can be written in terms of $\bar{\sigma}_{\parallel}$ and $\bar{\sigma}_{\perp}$ as shown in (A7) and (A8). Consequently, $\bar{\sigma}_{\parallel}$ and $\bar{\sigma}_{\perp}$ were chosen to be 50 and 150 respectively. The results of this calculation are shown in Figure 34. For comparison, similar spectra calculated by Luz and Meiboom[19] are shown in Figure 35. Their calculations and ours are seen to be in good qualitative agreement.

At zero degrees rotation, the line shape is a delta function at $\sigma_{zz} = \bar{\sigma}_{\parallel}$. As the sample is rotated, different domains assume different alignments relative to the field. In the calculation (appendix G), 3600 different domains were included ranging from $\phi_2 = -\pi/2$ to $+\frac{\pi}{2}$ in increments of .05 degree. For each domain, the chemical shift was determined. All domains giving a chemical shift in a narrow range ($\Delta\sigma = 1$ in this case) were lumped together and a histogram was formed. This histogram is then a normalized reproduction of the lineshape. It is worthwhile to try and interpret the features of Figure 34. As stated previously, the line broadening is caused by the different chemical shifts of the different domains. As the sample is initially rotated, some molecules can align with the field whereas others cannot depending on the domain they are in. An example of this is shown in Figure 36. When the sample has been rotated by an amount equal to the tilt angle, the molecules in domain

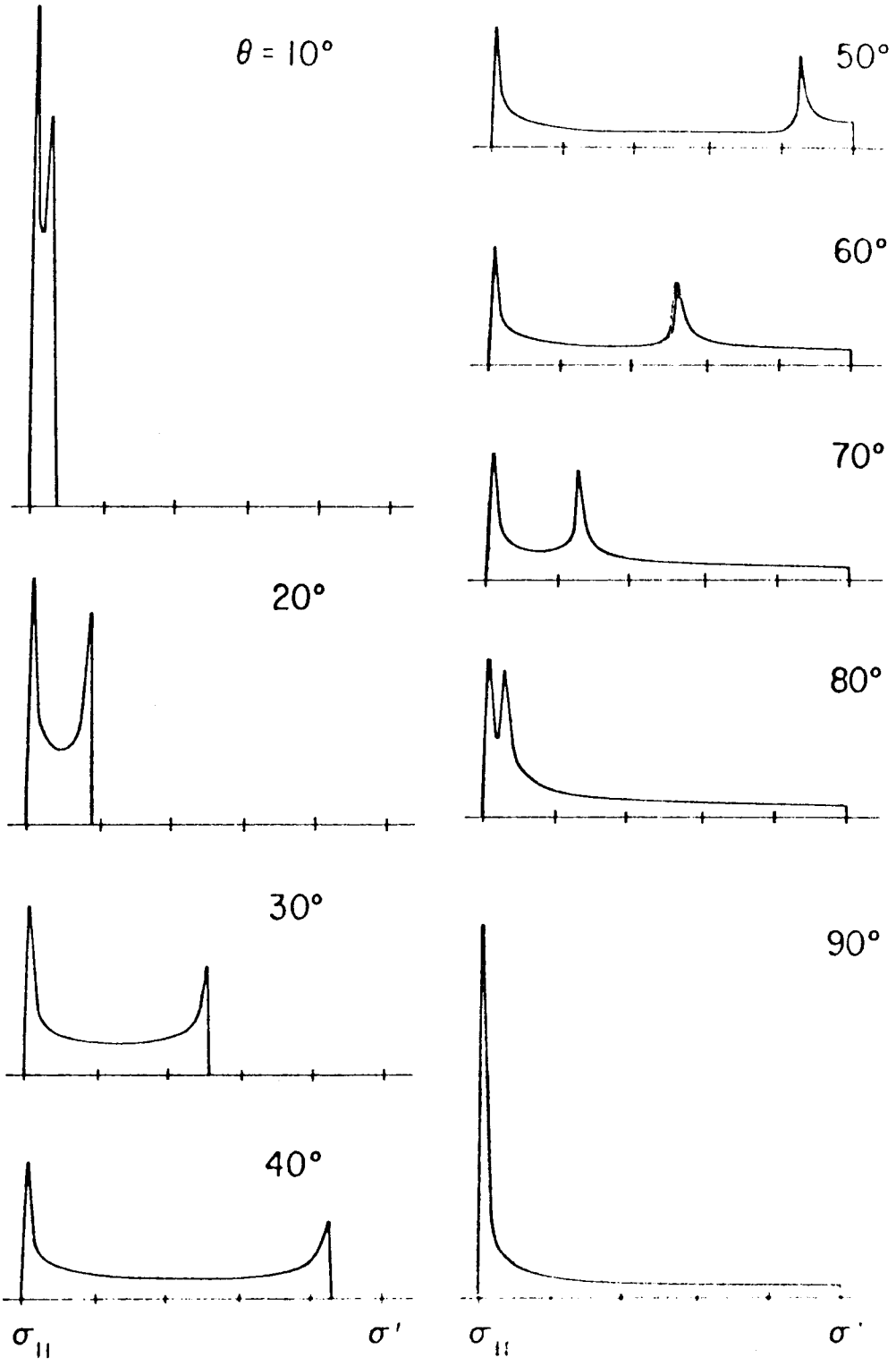

Figure 34

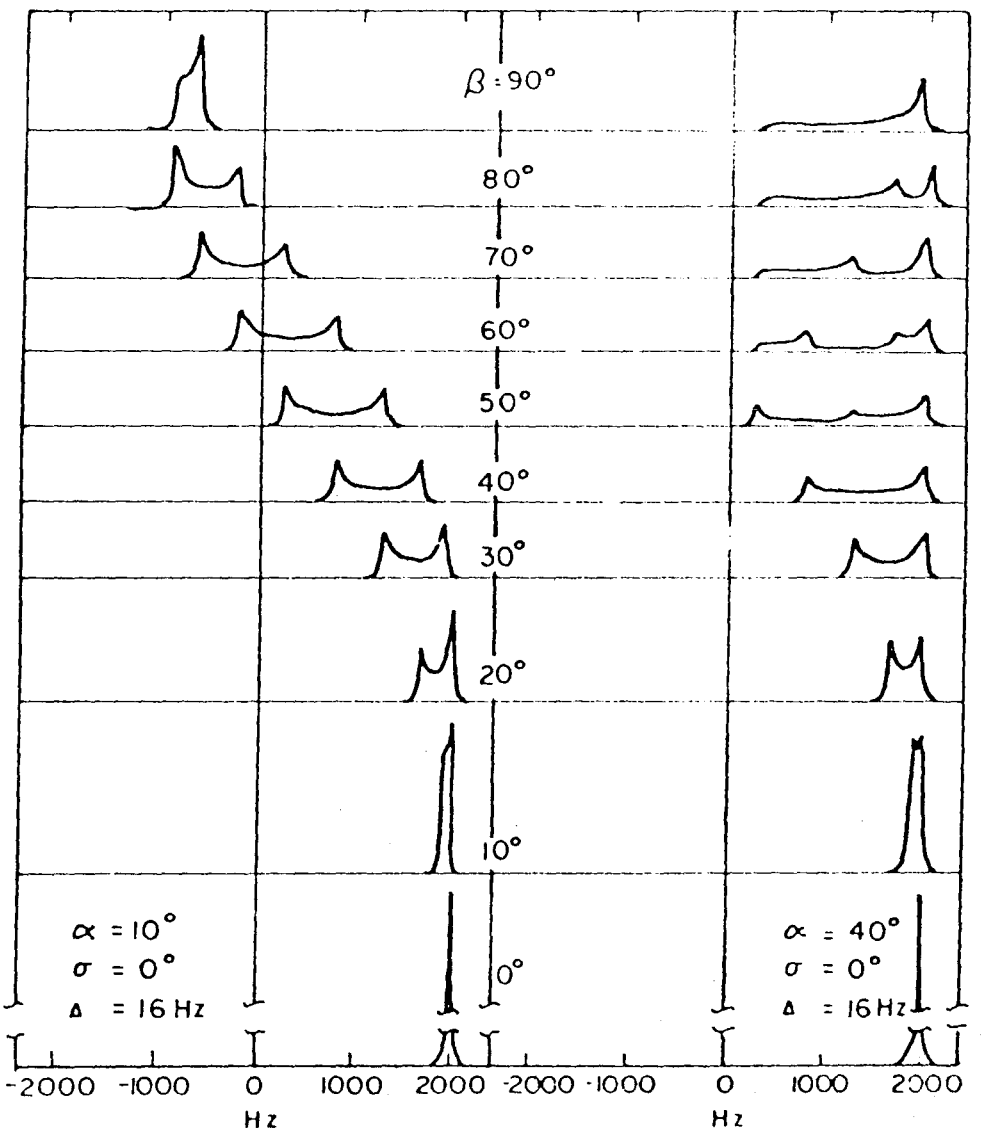

XBL758-6923

Figure 35

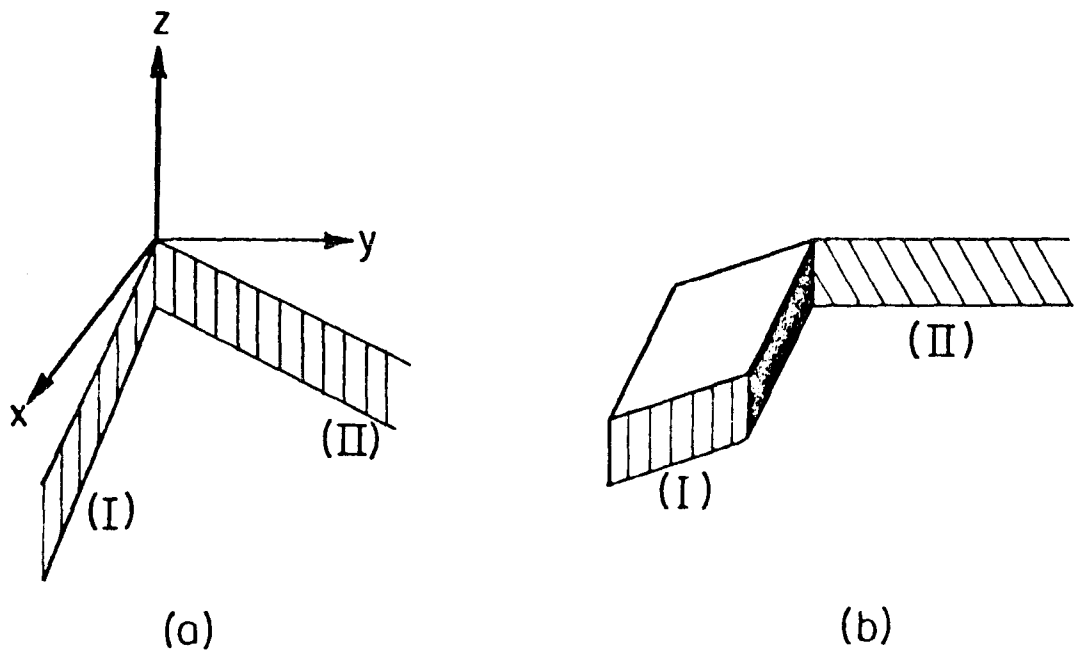

Figure 3b

"a" are just able to align along the direction of the field yielding $\sigma = \bar{\sigma}_{\parallel}$. The molecules in domain (b), on the other hand, are constrained to lie at an angle of 45° relative to the field and consequently $\sigma = \frac{1}{2}(\bar{\sigma}_{\parallel}+\bar{\sigma}_{\perp})$. For $0° < \theta < 45°$ then, the line shape broadens out with one edge at $\bar{\sigma}_{\parallel}$ and an outer edge intermediate between $\bar{\sigma}_{\parallel}$ and $\frac{1}{2}(\bar{\sigma}_{\parallel}+\bar{\sigma}_{\perp})$. The outer edge maximum cannot exceed $\frac{1}{2}(\bar{\sigma}_{\parallel}+\bar{\sigma}_{\perp})$ due to the ability of the molecules to reorient within the domain. Consider Figure 37 where a single domain at $\theta = 30°$, 45°, and 60° is shown. As θ approaches the tilt angle, the molecules align as shown in (a) and the chemical shift approaches $\frac{1}{2}(\bar{\sigma}_{\parallel}+\bar{\sigma}_{\perp})$. At θ equal to the tile angle, the molecules lie at an angle of 45° relative to the field so $\sigma = \frac{1}{2}(\bar{\sigma}_{\parallel}+\bar{\sigma}_{\perp})$. As θ passes beyond the tilt angle, the molecules "flip" by 180° thereby improving their alignment along the field and so σ drops below $\frac{1}{2}(\bar{\sigma}_{\parallel}+\bar{\sigma}_{\perp})$. It is this flipping which causes the outer peak to start moving inward as θ passes beyond 45°. The outer edge, however, remains at $\sigma = \frac{1}{2}(\bar{\sigma}_{\parallel}+\bar{\sigma}_{\perp})$ due to certain domains.

Case 3 - Smectic-C, no rotation.

As before, a tilt angle of 45° was chosen. The molecules were chosen to be completely frozen and so

$$\langle D_{00}^{(2)} \rangle = \langle D_{11}^{(2)} \rangle = \langle D_{22}^{(2)} \rangle = 1 \quad . \tag{B49}$$

The p.a. frame was chosen to coincide with the molecule fixed frame to simplify the calculation and is shown in Figure 38. The reason for choosing the elements of the shielding tensor as such is that this example would reduce to the previous one in the limit of free rotation.

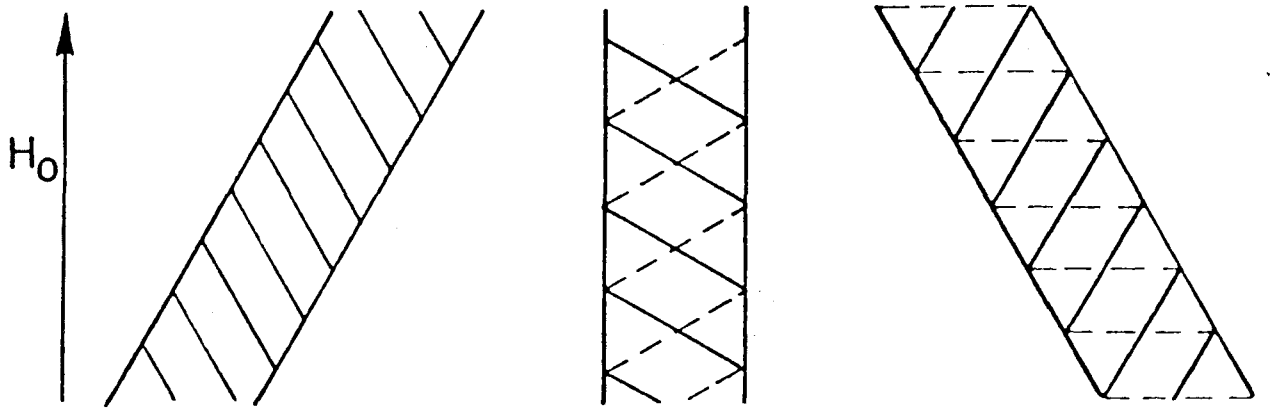

Figure 37

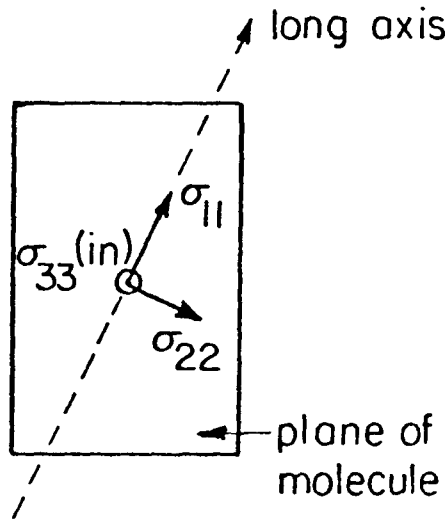

$\sigma_{33} = 175$
$\sigma_{22} = 125$
$\sigma_{11} = 50$

LBL 757-6743

Figure 38

The lineshapes of this example look the same as before except that they broaden to a lesser extent as the sample is rotated. Figure 39 contrasts the lineshapes for the freely rotating and frozen cases when the sample has been rotated by 50°. The reduction in line broadening was caused solely by the particular choice of σ_{22} and σ_{33}. The molecules will orient with the normal to the plane of the molecule perpendicular to the field. In effect, then, $\bar{\sigma}_{\perp} = 150$ is replaced by $\bar{\sigma}_{\perp} = 125$ and the outer band edge is reduced from $\frac{1}{2}(\bar{\sigma}_{\parallel}+\bar{\sigma}_{\perp}) = 100$ to $\frac{1}{2}(\bar{\sigma}_{\parallel}+\bar{\sigma}_{\perp}) = 87.5$. Had the values of σ_{22} and σ_{33} been interchanged, an outer band edge of $\frac{1}{2}(\bar{\sigma}_{\parallel}+\sigma_{\perp}) = 112.5$ would bave been observed. All other features would remain unchanged. Had a different choice of $\underset{\sim}{\sigma}$ been taken, the spectra would undoubtedly vary more markedly as the motion about the long axis freezes out.

From the preceding examples it is clear that the lineshape in a smectic-C will depend upon (a) the tilt angle, (b) the magnitudes of σ_{11}, σ_{22}, and σ_{33} and their orientations relative to the molecule fixed frame, (c) the diagonal order parameters $\langle D^{(2)}_{00}\rangle$, $\langle D^{(2)}_{11}\rangle$, $\langle D^{(2)}_{22}\rangle$ but not the off diagonal order parameters ($\langle D^{(2)}_{mk}\rangle$, $m \neq k$) which vanish to a good approximation and (d) the orientation of a sample in a magnetic field. Application of the foregoing theory to particular systems are currently under way in our laboratory.

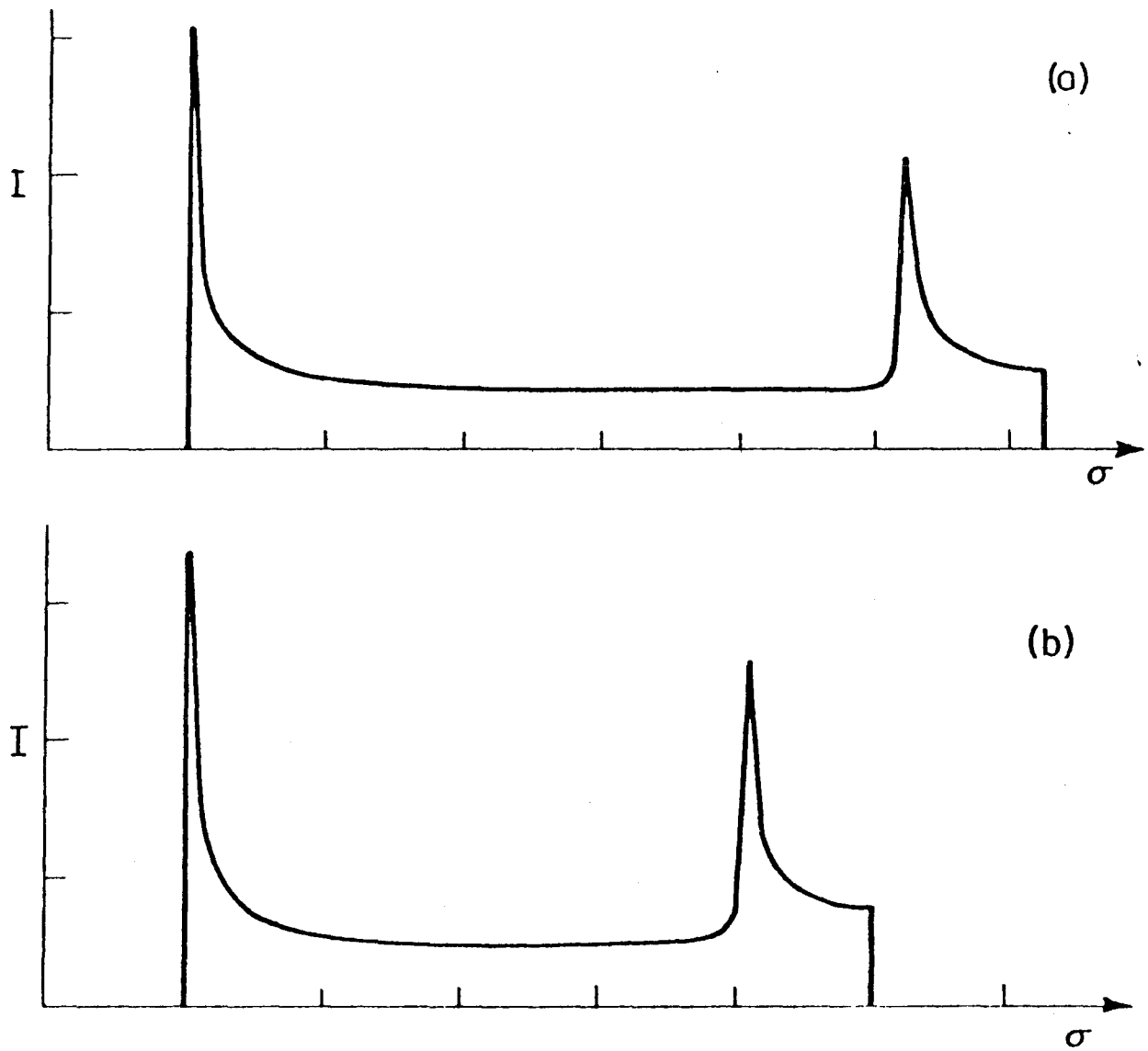

XBL 751-5498

Figure 39

C. Smectic-C Lineshape Program.

This program was used for the special cases in which (a) there was free rotation about the long axis and (b) motion about the long axis was completely frozen with the "molecule fixed" and "principal axis" frames coincident. Furthermore, it only treats the behavior of a single line as the sample is rotated. The final page in the appendix is an example of the output of the program. The angle of sample rotation appears in the upper right. I + 49 gives the chemical shift and the number to the left gives the number of domains whose 1 chemical shift lies between I + 49 and I + 50. A total of 3600 domains were considered. (See discussion at the end of appendix B.)

SPECT

```
      PROGRAM SPECT(INPUT,OUTPUT, TAPE 5=INPUT,TAPE6=OUTPUT)
      DIMENSION A(3,3) ,B1(3,3), B2 (3,3), D(3,3),RESULT(3,3),SIGMA(3,3)
      DIMENSION IS(125)
      REAL MAX1,MAX2
      INTEGER OUTPUT
      OUTPUT=6
    3 INPUT=5
    4 SMIN=90.0
    5 DELTA=1.0
    7 PI =4.0*ATAN(1.0)
   13 WRITE (OUTPUT,100)
  100 FORMAT(1X,*ENTER SIGMA PARALLEL AND PERPINDICULAR*)
   16 READ(INPUT,101) SIGPL,SIGPP,SIGP
  101 FORMAT (3F10.0)
   30 SIGMA(1,1)=SIGP
   31 SIGMA(1,2)=0.0
   32 SIGMA(1,3)=0.0
   33 SIGMA(2,1)=0.0
   33 SIGMA(2,2)=SIGPP
   35 SIGMA(2,3)=0.0
   35 SIGMA(3,1)=0.0
   36 SIGMA(3,2)=0.0
   37 SIGMA(3,3)=SIGPL
   41 WRITE(OUTPUT,102)
  102 FORMAT (1X,*ENTER ALPHA*)
   45 READ(INPUT,103) ALPHA
  103 FORMAT(F10.0)
   53 ALPHA=(PI/180.0)*ALPHA
   55 A(1,1)=COS(ALPHA)
   57 A(1,2)=0.0
   60 A(1,3)=SIN(ALPHA)
   63 A(2,1)=0.0
   63 A(2,2)=1.0
   65 A(2,3)=0.0
   66 A(3,1)=-A(1,3)
   67 A(3,2)=0.0
   70 A(3,3)=A(1,1)
   71 TDELTA = 10.0
   72 NTH=(90.0/TDELTA)+1.0
   75 DO 20 I=1,NTH
   77 DO 66 J=1,125
  103 IS(J)=0
  104 66 CONTINUE
  105 THETA=(PI/180.0)*((I-1)*TDELTA+0.1  )
  113 D(1,1)=1.0
  115 D(1,2)=0.0
  116 D(1,3)=0.0
  116 D(2,1)=0.0
  120 D(2,2)=COS(THETA)
  121 D(2,3)=-SIN(THETA)
  124 D(3,1)=0.0
  125 D(3,2)=-D(2,3)
  126 D(3,3)=D(2,2)
  127 PDELTA=.05
  131 PSTART=-90.0
  132 NPH=(180.0/PDELTA)+1.0
```

```
SPECT
    130         DO 10 J=1,NPH
    140         PHI2=(PI/180.0)*((J-1)*PDELTA+PSTART+0.1)
    146         ANUM=SIN(THETA)*COS(PHI2)
    153         XDENOM=SIN(THETA)*SIN(PHI2)*COS(ALPHA)-COS(THETA)*SIN(ALPHA)
    171         PHI1=ATAN(ANUM/XDENOM)
    175         PHIPI=PHI1+PI
    177         AA=-SIN(THETA)*SIN(PHI2)*COS(ALPHA)*SIN(ALPHA)
    212         BB=-SIN(THETA)*SIN(ALPHA)*COS(PHI2)
    223         CC=COS(THETA)*COS(ALPHA)*COS(ALPHA)
    231         DD=COS(THETA)*SIN(ALPHA)*SIN(ALPHA)
    237         MAX1=AA*(COS(PHI1)+1.0)+BB*SIN(PHI1)+CC+DD*COS(PHI1)
    253         MAX2=AA*(COS(PHIPI)+1.0)+BB*SIN(PHIPI)+CC+DD*COS(PHIPI)
    267         IF(MAX1.LT.0) MAX1=-MAX1
    271         IF (MAX2.LT.0) MAX2=-MAX2
    273         DEL=MAX1-MAX2
    274         IF(DEL.LT.0) PHI1=PHIPI
    300         B1(1,1)=COS(PHI1)
    302         B1(1,2)=-SIN(PHI1)
    305         B1(1,3)=0.0
    306         B1(2,1)=-B1(1,2)
    307         B1(2,2)=B1(1,1)
    310         B1(2,3)=0.0
    311         B1(3,1)=0.0
    312         B1(3,2)=0.0
    312         B1(3,3)=1.0
    314         B2(1,1)=COS(PHI2)
    316         B2(1,2)=-SIN(PHI2)
    321         B2(1,3)=0.0
    322         B2(2,1)=-B2(1,2)
    323         B2(2,2)=B2(1,1)
    324         B2(2,3)=0.0
    325         B2(3,1)=0.0
    326         B2(3,2)=0.0
    326         B2(3,3)=1.0
    330           CALL XFORM (A,SIGMA,RESULT)
    333         CALL XFORM (B1,RESULT,RESULT)
    336         CALL XFORM (A,RESULT,RESULT)
    341         CALL XFORM (B2,RESULT,RESULT)
    344         CALL XFORM (D,RESULT,RESULT)
    347         SHIFT=RESULT(3,3)
    350         IF(SHIFT.LT.SMIN) SHIFT=SMIN
    354         IPIDG=IFIX((SHIFT-SMIN)/DELTA)+1
    360         IS(IPIDG)=IS(IPIDG)+1
    362     10  CONTINUE
    364         THETA = (180.0/PI)*THETA
    367         WRITE(OUTPUT,200)  THETA,(K,IS(K),K=1,125)
         200    FORMAT(1X,*THETA=*,F6.1/(5(5X,*I=*,I4,*    *,I5)/))
    405         THETA=(PI/180.0)*THETA
    410     20  CONTINUE
    412         STOP
    414         END
```

PROGRAM LENGTH INCLUDING I/O BUFFERS

THETA= 50.1

I= 1	303	I= 2	126	I= 3	98	I= 4	83	I= 5	74
I= 6	67	I= 7	61	I= 8	59	I= 9	54	I= 10	53
I= 11	50	I= 12	49	I= 13	46	I= 14	46	I= 15	45
I= 16	42	I= 17	42	I= 18	42	I= 19	40	I= 20	40
I= 21	40	I= 22	38	I= 23	38	I= 24	38	I= 25	37
I= 26	36	I= 27	37	I= 28	36	I= 29	37	I= 30	36
I= 31	35	I= 32	35	I= 33	37	I= 34	35	I= 35	35
I= 36	35	I= 37	35	I= 38	36	I= 39	35	I= 40	37
I= 41	35	I= 42	36	I= 43	37	I= 44	37	I= 45	38
I= 46	39	I= 47	38	I= 48	41	I= 49	43	I= 50	47
I= 51	56	I= 52	213	I= 53	122	I= 54	93	I= 55	81
I= 56	75	I= 57	71	I= 58	67	I= 59	65	I= 60	63
I= 61	62	I= 62	62	I= 63	31	I= 64	0	I= 65	0
I= 66	0	I= 67	0	I= 68	0	I= 69	0	I= 70	0
I= 71	0	I= 72	0	I= 73	0	I= 74	0	I= 75	0
I= 76	0	I= 77	0	I= 78	0	I= 79	0	I= 80	0
I= 81	0	I= 82	0	I= 83	0	I= 84	0	I= 85	0
I= 86	0	I= 87	0	I= 88	0	I= 89	0	I= 90	0
I= 91	0	I= 92	0	I= 93	0	I= 94	0	I= 95	0
I= 96	0	I= 97	0	I= 98	0	I= 99	0	I= 100	0

D. Elements of the Wigner Rotation Matrices.

$$D^{(\ell)}_{jk}(\alpha,\beta,\gamma) = e^{-i\alpha j}\, d^{(\ell)}_{jk}(\beta) e^{-i\gamma k} \tag{D1}$$

$$d^{(0)}_{00}(\beta) = 1 \tag{D2}$$

$$d^{(1)}_{11}(\beta) = d^{(1)}_{-1-1}(\beta) = \frac{1}{2}(1 + \cos\beta) \tag{D3}$$

$$d^{(1)}_{1-1}(\beta) = d^{(1)}_{-11}(\beta) = \frac{1}{2}(1 - \cos\beta)$$

$$d^{(1)}_{01}(\beta) = d^{(1)}_{-10}(\beta) = - d^{(1)}_{0-1}(\beta) = -d^{(1)}_{10}(\beta) = \frac{1}{\sqrt{2}}(\sin\beta)$$

$$d^{(1)}_{00}(\beta) = (\cos\beta)$$

$$d^{(2)}_{22}(\beta) = d^{(2)}_{-1-2}(\beta) = \cos^4(\frac{\beta}{2}) \tag{D4}$$

$$d^{(2)}_{21}(\beta) = d^{(2)}_{-1-2}(\beta) = -d^{(2)}_{12}(\beta) = - d^{(2)}_{-2-1}(\beta) = - \frac{1}{2} \sin\ (1 + \cos\beta)$$

$$d^{(2)}_{20}(\beta) = d^{(2)}_{02}(\beta) = d^{(2)}_{-20}(\beta) = d_{0-2}(\beta) = \sqrt{\frac{3}{8}} \sin^2\beta$$

$$d^{(2)}_{2-1}(\beta) = d^{(2)}_{1-2}(\beta) = -d^{(2)}_{-21}(\beta) = - d^{(2)}_{-12}(\beta) = \frac{1}{2} \sin\beta(\cos\beta-1)$$

$$d^{(2)}_{2-2}(\beta) = d^{(2)}_{-22}(\beta) = \sin^4(\frac{\beta}{2})$$

$$d^{(2)}_{11}(\beta) = d^{(2)}_{-1-1}(\beta) = \frac{1}{2}(2\cos\beta-1)\ (1+\cos\beta)$$

$$d^{(2)}_{1-1}(\beta) = d^{(2)}_{-11}(\beta) = \frac{1}{2}(2\cos\beta+1)\ (1-\cos\beta)$$

$$d^{(2)}_{10}(\beta) = d^{(2)}_{0-1}(\beta) = -d^{(2)}_{01}(\beta) = - d^{(2)}_{10}(\beta) = -\sqrt{\frac{3}{2}} \sin\beta\ \cos\beta$$

$$d^{(2)}_{00}(\beta) = (\frac{3}{2} \cos^2\beta - \frac{1}{2})$$

E. Dependence of the Order Parameters on V_1 and V_2.

As a model of mean potential which a liquid crystal molecules sees we take two mean fields: a "nematic" or dipole induced dipole field and an electric field which arises from the alignment of the permanent dipole moments in a large collection of ℓ.c. molecules. The form of the potential is then

$$V = - V_1' \cos^2\theta - V_2' \cos\phi \qquad (E1)$$

where

V_1' ≡ nematic potential

V_2' ≡ electric potential

θ ≡ angle between long axis and director

ϕ ≡ angle between permanent dipole moment and mean electric field direction.

The angles, θ and ϕ, can be related to the Euler angles (α,β,γ) which take the molecule fixed frame into the symmetry frame. It should be simple enough to see that $\theta = \beta$, but ϕ has a more complex form. By a method analogous to that given in appendix B (equations B39-44), it is easy to show that

$$\cos\phi = \cos^2\alpha' (\cos\beta\cos\alpha\cos\gamma - \sin\alpha\sin\gamma) + \cos\alpha' \sin\alpha' \sin\beta \times (\cos\alpha - \cos\gamma) + \sin^2\alpha' \cos\beta \qquad (E2)$$

where α' denotes the tilt angle. The inclusion of the tilt angle complicates the theory considerably and so only the special case

of zero tilt angle will be treated in this appendix. For zero tilt angle, the previous equation simplifies to

$$\cos\phi = \cos\beta\cos\alpha\cos\gamma - \sin\alpha\sin\gamma \qquad \text{(E3)}$$

or

$$\cos\phi = \cos(\alpha+\gamma) - 2\sin^2(\frac{\beta}{2})\cos\alpha\cos\gamma \quad . \qquad \text{(E4)}$$

Substituting this into (E1) gives

$$V = V_1'\cos^2\beta - V_2'\cos(\alpha+\gamma) + 2V_2'\sin^2\frac{\beta}{2}\cos\alpha\cos\gamma \quad . \qquad \text{(E5)}$$

The orientational distribution function for the molecule is then

$$P(\alpha,\beta,\gamma) = \frac{1}{Z}(e^{V_1\cos^2\beta}\, e^{V_2\cos(\alpha+\gamma)}\, e^{-2^1/2\,\sin^2(\frac{\beta}{2})\cos\alpha\cos\gamma}) \qquad \text{(E6)}$$

where

$$Z \equiv \int_0^{2\pi} d\alpha \int_0^{2\pi} d\gamma \int_0^{1} d(\cos\beta)\; P(\alpha,\beta,\gamma) \qquad \text{(E7)}$$

and V_1 and V_2 are the reduced potentials,

$$V_1 = V_1'/kT$$
$$V_2 = V_2'/kT \quad . \qquad \text{(E8)}$$

For small β-fluctuations it is valid to make the approximation that

$$e^{-2V_2\sin^2(\frac{\beta}{2})\cos\alpha\cos\gamma} = 1 - 2V_2\sin^2(\frac{\beta}{2})\cos\alpha\cos\gamma \qquad \text{(E9)}$$

Substituting this into (B6) gives

$$P(\alpha,\beta,\gamma) = e^{V_1\cos^2\beta}\, e^{V_2\cos(\alpha+\gamma)}\,(1 - 2V_2\sin^2(\tfrac{\beta}{2})\cos\alpha\cos\gamma). \qquad \text{(E10)}$$

The first term represents the approximation that the β and α-γ fluctuations are uncoupled. The second term represents a first order coupling of the β and α-γ fluctuations. It turns out that the second term contributes little to the order parameters, $\langle D^{(2)}_{mn}(\Omega)\rangle$, yet complicates the mathematics considerably. Consequently, only the leading term will be considered. For a more complete treatment, consult with Professor Pines who has a copy of my original calculations.

1. Vanishing of off-diagonal terms.

Retaining only the leading term in (E10), we have

$$P(\alpha,\beta,\gamma) = e^{V_1\cos^2\beta}\, e^{V_2\cos(\alpha+\gamma)} \qquad \text{(E11)}$$

$$Z = \int_0^{2\pi} d\alpha \int_0^{2\pi} d\gamma\, e^{V_2\cos(\alpha+\gamma)} \int_0^{1} d(\cos\beta)\, e^{V_1\cos^2\beta} \quad . \qquad \text{(E12)}$$

(E12) will be solved in the next section. The order parameters are then

$$\langle D_{mn}(\Omega)\rangle = \frac{1}{z}\left(\int_0^{2\pi} d\alpha \int_0^{2\pi} d\gamma\ e^{-i(m\alpha+n\gamma)}\ e^{V_2\cos(\alpha+\gamma)}\right)\left(\int_0^1 d(\cos\beta) \times\right.$$

$$\left. d_{mn}(\beta)\ e^{V_1\cos^2\beta}\right) \tag{E13}$$

Now the integration over α-γ vanishes. To see this integrate first over γ and then over α. This enables you to make a change of variables.

$$\gamma' = \alpha + \gamma$$
$$d\gamma' = d\gamma \tag{E14}$$

The α-γ integral then becomes

$$\int_0^{2\pi} d\alpha\ e^{-i(m-n)\alpha} \int_\alpha^{2\pi+\alpha} d\gamma'\ e^{-in\gamma'}\ e^{V_2\cos\gamma'} \quad . \tag{E15}$$

But now, the integral over α vanishes unless n = m. This proves that to the lowest order of approximation, the off-diagonal order parameters vanish.

2. Solution of Z.

By the change of variables given by (E14), (E12) becomes

$$Z = \int_0^{2\pi} d\alpha \int_\alpha^{\alpha+2\pi} d\gamma'\ e^{V_2\cos\gamma'} \int_0^1 dx\ e^{V_1 x^2} \quad . \tag{E16}$$

The integral over γ' involves a periodic function. Hence, it is valid to change the limits of integration to give

$$Z = \int_0^{2\pi} d\alpha \int_0^{2\pi} d\gamma' \; e^{V_2 \cos\gamma'} \int_0^1 dx \; e^{V_1 x^2} \quad . \tag{E17}$$

From (F5) and (F6) we find

$$Z = 2\pi \; I_o(V_2) \; S_o(V_1) \tag{E18}$$

where $I_o(V_2)$ is a hyperbolic Bessel function and $S_o(V_1)$ is a special function tabulated in Table 1F.

3. Solution of $\langle D_{00}^{(2)} \rangle$, $\langle D_{11}^{(2)} \rangle$, and $\langle D_{22}^{(2)} \rangle$.

Solving for these order parameters involve the same methods used to obtain (E18). As an example, $\langle D_{11}^{(2)} \rangle$ will be derived and $\langle D_{00}^{(2)} \rangle$, $\langle D_{22}^{(2)} \rangle$ merely stated.

From appendix D and (E.3) we get

$$Z\langle D_{11}^{(2)} \rangle = \frac{1}{2} \int_0^{2\pi} d\alpha \int_0^{2\pi} d\gamma \; e^{-i(\alpha+\gamma)} \; e^{V_2 \cos(\alpha+\gamma)} \int_0^1 dx \; (2x-1) \; (x+1) \; e^{V_1 x^2}$$

$$= \pi \int_0^{2\pi} d\gamma' \; (\cos\gamma' + i \sin\gamma') \; e^{V_2 \cos\gamma'} \int_0^1 dx \; (2x^2+x-1) e^{V_1 x^2}$$

$$= \pi \; I_1(V_2) \; \{2 \; S_2(V_1) + S_1(V_1) - S_0(V_1)\} \tag{E19}$$

Consequently

$$\langle D_{11}^{(2)} \rangle = \frac{I_1(V_2)}{I_0(V_2)} \left(\frac{2S_2(V_1) + S_1(V_1) - S_0(V_1)}{2 \; S_0(V_1)} \right) \quad . \tag{E20}$$

In an analogous manner, we find

$$\langle D_{00}^{(2)} \rangle = \frac{3}{2} \frac{S_2(V_1)}{S_0(V_1)} - \frac{1}{2} \qquad \text{(E21)}$$

$$\langle D_{22}^{(2)} \rangle = \frac{I_2(V_2)}{I_0(V_2)} \left(\frac{S_0(V_1) + 2\, S_1(V_1) + S_2(V_1)}{4\, S_0(V_1)} \right) \quad .$$

From (E21), it is seen that $\langle D_{00}^{(2)} \rangle$ depends only upon V_1. For a non-rotated smectic-C, the only order parameter is $\langle D_{00}^{(2)} \rangle$. (Off diagonal elements would be small.) Thus, it should be possible to extract V_1 from non-rotated samples. Then, the sample could be rotated and V_2 extracted through determinations of $\langle D_{11}^{(2)} \rangle$ and $\langle D_{22}^{(2)} \rangle$. Suppose, for example, that $\langle D_{00}^{(2)} \rangle$ of a non-rotated sample was found to be 0.84. From Table 1E, this corresponds to $V_1 \cong 10$. From (E20), (E21), and Table 1F we get

$$\langle D_{11}^{(2)} \rangle = 0.86 \frac{I_1(V_2)}{I_0(V_2)}$$

$$\langle D_{22}^{(2)} \rangle = 0.94 \frac{I_2(V_2)}{I_0(V_2)} \quad . \qquad \text{(E22)}$$

Table 1E

V_1	$\langle D_{00} \rangle$
0	0.00
2	0.30
4	0.56
6	0.71
8	0.79
10	0.84
12	0.87
14	0.89
16	0.90

Figure 40 shows $\langle D_{00}^{(2)} \rangle$, $\langle D_{11}^{(2)} \rangle$ and $\langle D_{22}^{(2)} \rangle$ as function of V_2 for this value of V_1. From it, and a knowledge of $\langle D_{11} \rangle$ and $\langle O_{22} \rangle$, V_2 could be determined.

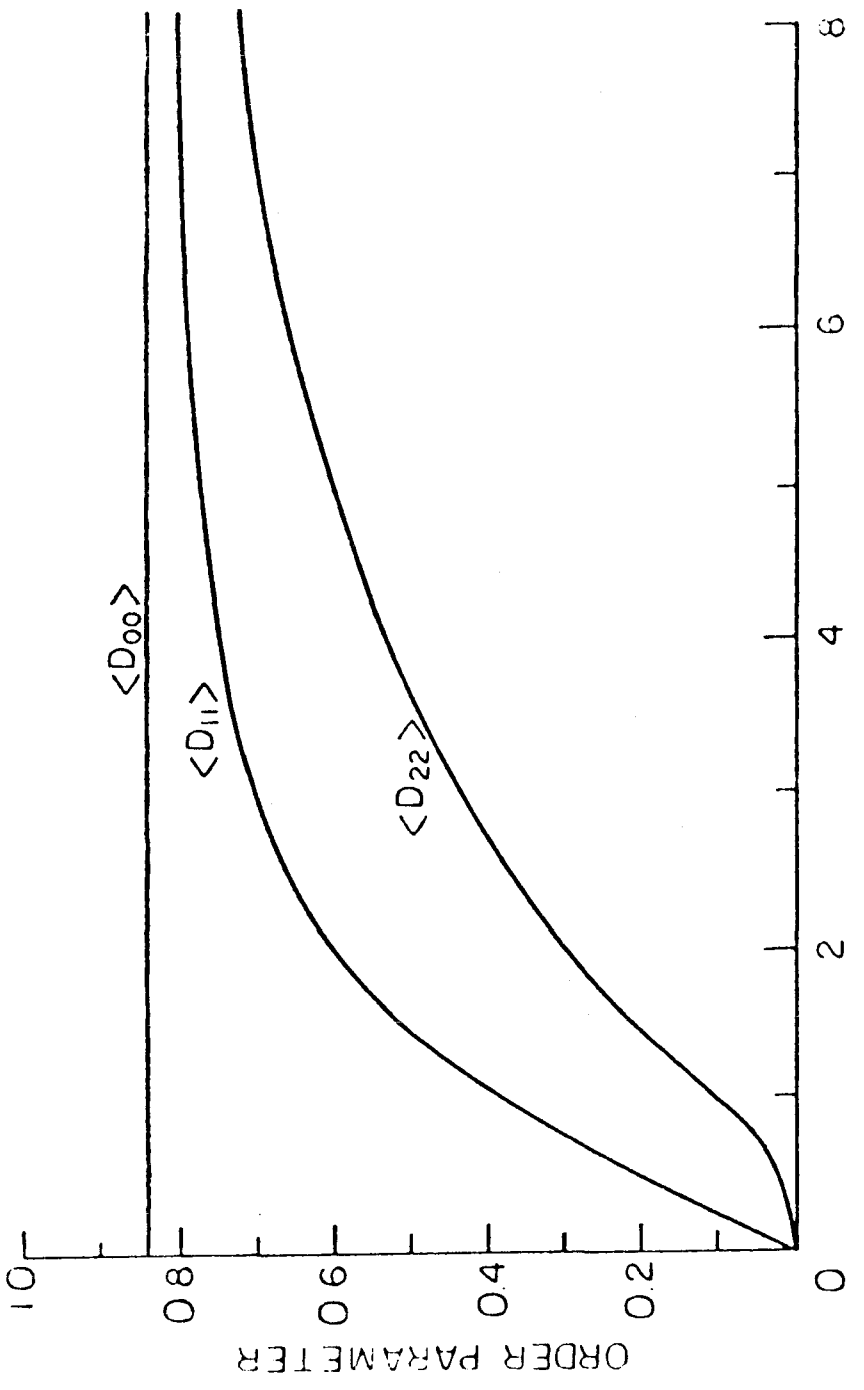

XBL 758-6920

Figure 40

F. Special Functions Used in Appendix-E.

Two classes of integrals appear in appendix-E. The first class arises in integration over α and γ and are of the form

$$I^{(n)}(V_2) \equiv \int_0^{2\pi} d\phi \; e^{V_2 \cos\phi} \cos^n\phi \tag{F1}$$

where n = 0, 1, or 2. The purpose of the superscript is well suited if note is taken of the property that

$$I^{(n)}(V_2) = \frac{d^n}{dV_2^n}\left(I^{(0)}(V_2)\right) \quad . \tag{F2}$$

Therefore, if we know the functional form of $I^{(0)}(V_2)$, we can determine the functional form of $I^{(n)}(V_2)$. By expanding the exponential in $I^{(0)}(V_2)$ as a power series and integrating, we find that

$$I^{(0)}(V_2) = \int_0^{2\pi} d\phi \; e^{V_2\cos\phi} = \sum_{j=0}^{\infty} \int_0^{2\pi} d\phi \; \frac{(V_2\cos\phi)^j}{j!} = \sum_{j=0}^{\infty} \left(\frac{V_2}{2}\right)^{2j} / (j!)^2 \tag{F3}$$

This however is just the zeroth order hyperbolic Bessel Function - $I_0(V_2)$. From the recursion relation of these functions

$$\frac{dI_n(x)}{dx} = \frac{1}{2}\left(I_{n-1}(x) + I_{n+1}(x)\right) \tag{F4}$$

we have

$$\int_0^{2\pi} d\phi\ e^{V_2\cos\phi} = I_0(V_2)$$

$$\int_0^{2\pi} d\phi\ e^{V_2\cos\phi}\ \cos\phi = I_1(V_2)$$

$$\int_0^{2\pi} d\phi\ e^{V_2\cos\phi}\ \cos^2\phi = \frac{1}{2}[I_0(V_2) + I_2(V_2)]_0 \qquad \text{(F5)}$$

The $I_n(V_2)$ is a hyperbolic Bessel function (sometimes called Bessel functions of the second kind) and can be found in any mathematical handbook.

The second class of integrals that appear involve V_1 and have the form

$$S_n(V_1) \equiv \int_0^1 d(\cos\beta)\ e^{V_1\cos^2\beta}\ d(\cos\beta) = \int_0^1 dx\ e^{V_1x^2}\ x^n \qquad \text{(F6)}$$

where n = 0, 1, or 2. The n = 1 case is trivial and gives:

$$S_1(V_1) \equiv \int_0^1 dx\ e^{V_1x^2}\ x = \frac{e^{V_1}-1}{2V_1} \quad . \qquad \text{(F7)}$$

The other two integrals, $S_0(V_1)$ and $S_2(V_1)$ were solved by expanding the exponential as a power series and integrating to give

$$S_0(V_1) = \sum_{j=0}^{\infty} \frac{V_1{}^j}{(2j+1)j!} \qquad \text{(F8)}$$

$$S_2(V_1) = \sum_{j=0}^{\infty} \frac{V_1{}^j}{(2j+3)j!} \quad . \qquad \text{(F9)}$$

These series could not be found and it was necessary to determine them with the aid of a computer by performing the indicated summations. Table 1F gives a list of these S values.

Table 1F

V_1	$S_0(V_1)$	$S_1(V_1)$	$S_2(V_1)$
0	1.000	0.500	0.333
2	2.364	1.597	1.256
4	8.226	6.700	5.796
6	37.73	33.54	30.47
8	201.5	186.2	173.7
10	1168	1101	1043
12	7111	6781	6485
14	44,690	42,950	41,350
16	287,400	277,700	268,700

References

1. Some recent reviews describing the application of nmr to liquid crystals are:

   a) S. Chandrasekhar and N. V. Madhusadana, Applied Spectroscopy Reviews, 6, 189 (1973).

   b) A. Saupe, Ann. Rev. Phys. Chem., 24, 441 (1973).

   c) G. H. Brown, J. W. Doane, and V. D. Neff, A Review of the Structure and Properties of Liquid Crystals, CRC Press, Cleveland, (1971).

   d) S. Meiboom and L. C. Snyder, Acct. Chem. Res., 4, 81 (1971).

   e) J. Lindon and J. Emsley, NMR in Liquid Crystals, Pergamon Press, New York, (1975).

2. A. Pines and J. Chang, Phys. Rev. A, 10, 946 (1974).

3. A. Pines, J. Chang, and R. Griffin, J. Chem. Phys., 61, 1021 (1974).

4. A. Pines, M. Gibby, and J. Waugh, J. Chem. Phys., 59, 569 (1973).

5. K. Kobayashi, J. Phys. Soc. Japan, 29, 101 (1970); W. McMillan, Phys. Rev. A, 4, 1238 (1971); 6, 936 (1972); F. Lee, H. Tom, Y. Shih and C. Woo, Phys. Rev. Lett., 31, 1117 (1973); H. Schroder, private communication.

6. S. Marčelja, Sol. St. Comm., 13, 759 (1973); J. Chem. Phys. 60, 3599 (1974).

7. H. Arnold, Z. Phys. Chem. (Leipzig), 226, 146 (1964); J. Van der Veen, W. de Jeu, M. Wanminkhof, and C. Tienhoven, J. Phys. Chem. 77, 17 (1973); W. de Jeu, J. Van der Vien, and W. Goossent, Sol. St. Comm., 12, 405 (1973).

8. W. Maier and A. Saupe, Z. Nat. A14, 882 (1959).

9. C. Weygand and R. Gabler, J. Prakt. Chem., 155, 332 (1940).

10. A. Pines, J. Chang, J. Am. Chem. Soc., 96, 5590 (1974).

11. A. Pines, M. Gibby, and J. Waugh, J. Chem. Phys., 59, 591 (1973).

12. N. Ramsey, Phys. Rev., 78, 699 (1950).

13. An even-odd variation has previously been observed by I. Chistyakov and V. Chaikovskii, Kristallographiya, 18, 293 (1973), using X-rays. However, these authors report single temperature values at equal points above the solid-nematic transitions. They thus contain inherently the variations in nematic range and are not useful for comparison with theory relative to the isotropic-nematic transitions.

14. J. Rowell, W. Phillips, L. Melby, and M. Panar, J. Chem. Phys., 43, 3442 (1965).

15. Z. Luz, R. Hewitt, and S. Meiboom, J. Chem. Phys., 61, 1758 (1974).

16. W. Krigbaum, Y. Chatani, and P. Barker, Act. Cryst., B26, 97 (1970); W. Krigbaum and P. Barker, Act. Cryst., B27, 1884 (1971).

17. A. Pines, M. Gibby, and J. Waugh, Chem. Phys. Lett., 15, 373 (1972).

18. B. Cabane and W. Clarke, Phys. Rev. Lett., 25, 91 (1970).

19. Z. Luz and S. Meiboom, J. Chem. Phys., 59, 275 (1973).

20. J. Seelig, and W. Niederberger, Biochem., 13, 1585 (1974); J. Seelig, A. Seelig, Biochem. and Biophys. Res. Comm., 57,

406 (1974); J. Charvolin, P. Manneville, and B. Deloche, Chem. Phys. Lett., 23, 345 (1973); R. Parker, J. Doane, and D. Fischel, preprint (to be published).

21. G. Brown, J. Doane, and V. Neff, A Review of the Structure and Properties of Liquid Crystals, CRC Press, Cleveland (1971).

22. E. Andrew, Progress in NMR Spectroscopy, Volume 8, Pergamon Press, New York (1971).

23. W. McMillan, Phys. Rev. A, 4, 1238 (1971).

24. G. Luckhurst and M. Setaka, Mol. Cryst. Liquid Cryst., 19, 179 (1972).

25. G. Luckhurst, M. Ptak, and A. Sanson, J. Chem. Soc., Faraday Trans. II, 69, 1752 (1973).

26. W. Krigbaum and P. Barber, Acta Cryst., B27, 1884 (1971).

27. G. Levy, R. Komoroski, and J. Halstead, J. Amer. Chem. Soc., 96, 5456 (1974).

28. M. Rose, Elementary Theory of Angular Momentum, John Wiley & Sons, New York, (1957).

29. A. Abragam, Principles of Nuclear Magnetism, Clarendon Press, Oxford (1960).

30. D. Brink, Angular Momentum, Clarendon Press, Oxford (1968).

31. R. Wise, D. Smith, and J. Doane, Phys. Rev. A, 7, 1366 (1973).

32. W. McMillan, Phys. Rev. A, 8, 1921 (1973).

33. M. Tinkham, Group Theory and Quantum Mechanics, McGraw Hill, New York (1964).

Figure Captions

1. Various high temperature liquid crystal phases. Molecules in the nematic phase differ from those in the isotropic in that the long axis of the molecules align preferentially in a particular direction. This direction is called the director. The smectic-A phase differs from the nematic in that the molecules orient in planes. The normal to the smectic plane coincides with the director. The smectic-C differs from the smectic-A in that the molecules are tilted in these planes.
2. Schematic diagram of double resonance spectrometer.
3. Schematic diagram of proton and carbon amplifiers.
4. Pulse sequences used in the experiments: (a) is a normal proton-decoupled ^{13}C free induction decay, while (b) is preceded by a cross-polarization step for signal enhancement. For most purposes the 90° pulse in (b) may be omitted.
5. Variable temperature probe for superconducting geometry. Details are presented in the text.
6. Photograph of probe.
7. p-Alkoxyazoxybenzenes, series I. D represents the long molecular axis and ϕ is the angle between this axis and the benzene 'para' axis.
8. Directional properties of chemical shielding tensors for characteristic ^{13}C nuclei, with convention $\sigma_{11} \leq \sigma_{22} \leq \sigma_{33}$. At left for aromatic group--the most shielded direction (corresponding) to σ_{33} is perpendicular to the plane. At right for aliphatic groups, σ_{33} is more or less along the

chain with $\sigma_{11} \approx \sigma_{22} = \sigma_{\perp}$.

9. Isotropic and nematic spectra of p-methoxybenzylidene p'-n-butylaniline.[2] On both spectra, the aromatic lines are at low field and the aliphatic lines at high field. Since the shielding of each nucleus perpendicular to the plane of the molecule is heaviest for the aromatic carbons and lightest for the aliphatic carbons, the aromatic lines shift downfield and the aliphatic lines shift upfield on going from the isotropic to the nematic phase.

10. Fourier transform ^{13}C nmr spectra of the series shown in Figure 7 with high power proton spin decoupling. Assignments in the isotropic phase are: $\sim$ -40 ppm, aromatic C-O; $\sim$ -20 ppm, C-N; $\sim$ -10 to 10 ppm, remaining 'ortho' aromatic carbons; 50-70 ppm, aliphatic C-O. In the nematic phase, the assignment order remains the same but the line assigned coupled to ^{14}N nuclei (C-N) appear to broaden and are unobservable, as discussed in the text. The nematic phase spectra were taken at various temperatures.

11. Dependence of chemical shifts, σ, on temperature for series I. T_c is the clearing (isotropic-nematic transition) temperature.

12. Relative order parameters calculated from the aromatic chemical shifts at T_c (normalized to 0.43 for n + 1 = 1) and 5°C below T_c in the nematic phase. The vertical bars depict the typical range of values for the different aromatic lines. The theoretical data are taken from the mean field calculations of Marčelja.[6]

13. Di-ethylazoxydibenzoate (DEAB) molecule. The long molecular axis is denoted D and the angle between this axis and the benzene 'para' axis is ϕ. 1 refers to the 'ortho' carbons, and 2, 2' to the 'para' carbons. The numbering is symmetrical on both sides of the molecule.

14. ^{13}C proton undecoupled free induction decay (a) and Fourier-transform (b) in the isotropic phase of DEAB. Resolution in this phase is limited only by magnetic field inhomogeneity. The line assignments, σ_i, are (refer to Figure 13 for carbon numbering): $\sim$ -45 ppm, carbons 3; $\sim$ -30 ppm, carbons 2'; $\sim$ 10 ppm, carbons 2; $\sim$ -5 to +5 ppm, carbons 1; $\sim$ 60 ppm, carbons 4; $\sim$ 110 ppm, carbons 5.

15. Rotation of molecule about the long molecular axis making an angle θ with the magnetic field.

16. ^{13}C Fourier-transform nmr spectrum in the smectic-A phase of DEAB at 114°C. This was obtained with signal enhancement by cross-polarization and with strong proton decoupling. The $\theta = 0°$ refers to the orientation of the sample, namely here the director is parallel to the magnetic field. The line assignments are (refer to Figure 13 for carbon numbering and refer to Figure 14 for comparison to isotropic line assignments): $\sim$ -80 ppm, carbons 2, 3; - 40 ppm, carbons 1; $\sim$ 100 ppm, carbons 4; and $\sim$ 120 ppm, carbons 5. Lines from carbons 2' were not identified and are believed to be broadened as explained in the text.

17. Effect of proton decoupling on ^{13}C nmr in the smectic-A phase of DEAB at 114°C. Here $\theta = 0°$, i.e., the director is perpendicular to the magnetic field (a) is a ^{13}C free induction decay with no proton decoupling, (b) the Fourier transform, (c), (d) the same with proton decoupling. Unlike the isotropic phase, proton-decoupling here is essential to a resolution of any features.

18. Schematic description of behavior of smectic-A phase under rotation of the sample. In (a), the sample is cooled into the smectic-A phase and aligns along the magnetic field. In (b), with sample rotation, the layer structure is preserved and the director rotates away from the field.

19. ^{13}C nmr spectra in the smectic-A phase of DEAB at 114°C at various sample orientations with proton decoupling. The rotation axis is perpendicular to the magnetic field. All spectra except those for $\theta = 50°$ and 60° were taken with cross polarization; the latter two together with all work near the magic angle were taken from a normal free induction decay since cross-polarization was inefficient as explained in the text. Note the appearance of a new line at $\theta = 50°$.

20. Dependence of ^{13}C chemical shift on orientation (see Figure 19) in the smectic-A phase of DEAB. The solid lines are fits using equation (B23). The lines with asterisks on the left denote the isotropic positions σ_i from Figure 14. Note that they correspond quite well to the average shifts on rotation: $\bar{\sigma} = \frac{1}{3}\bar{\sigma}_{\parallel} + \frac{2}{3}\bar{\sigma}_{\perp}$. The experimental points with circles at

θ = 5°, 55°, and 60° are thought to be from carbons 2' (Figure 13) with broadening by ^{14}N dipolar coupling.

21. Self-decoupling of ^{13}C-^{1}H dipolar couplings in the smectic-A phase of DEAB with sample orientation near the magic angle. (a) Away from magic angle with no proton decoupling. (b) Near the magic angle with no proton decoupling, showing line narrowing. (c) Same as (b) with proton decoupling.

22. ^{13}C nmr spectra in solid DEAB. This is a polycrystalline sample so the lines are strongly broadened by chemical shielding anisotropy.

23. Dependence of chemical shifts, σ, on temperature for DEAB. The discontinuity at T_c denotes the isotropic-smectic-A transition. Note the independence of line position on temperature in the smectic-A phase.

24. The order parameter, $S = \langle P_2(\cos\theta)\rangle$, in the nematic and smectic A phase as predicted by the McMillan theory.[23] In (a), both the nematic and smectic-A phases are present. S is seen to be much more temperature dependent in the nematic phase than in the smectic-A. In (b), the nematic phase is absent. Since the temperature dependence of S in the smectic-A phase decreases with decreasing nematic range, S is virtually independent of temperature.

25. Conformational motion involving either simultaneous or independent 180° flips of the benzene rings and carboxyl side groups.

26. Molecule fixed frame: $z^{(m)}$ chosen to lie along the long axis of the molecule, $x^{(m)}$ chosen to lie perpendicular to the plane

of the molecule, and $y^{(m)}$ chosen to complete a right handed coordinate system.

27. Two domains in a smectic-C liquid crystal. (a) and (b) show the arrangement of the molecules in a nonrotated and rotated sample respectively.

28. Ordering of the molecules in a smectic-C domain. As discussed in the text, the alignment of permanent electric dipoles is postulated to be responsible for the tilt angle.

29. Domain (Σ_1), initial lab (Σ_2), and lab frames (Σ_L). The cone represents all possible domains present since any plane drawn tangent to this cone represents a domain. The domain frame is described in the text. When the smectic-C phase is formed in the presence of an applied field, z_2 and z_L lie along both the field and the tip of the cone. As the sample is rotated about the axis which defines both x_2 and x_L, z_2 remains to point out from the tip of the cone and z_L serves to define the new direction of the field.

30. Molecular reorientation in a smectic-C domain. The molecules of a smectic-C domain may reorient as discussed in the text. The dotted hemicircle represents half the possible orientations of the long axis in this domain. The angle between the domain surface normal and the long axis is the tilt angle α' and two sample orientations are shown.

31. The normal to the molecular plane lies perpendicular to the field direction.

32. Euler transformation from the symmetry to the domain frame. This serves to illustrate the convention used throughout this thesis. The transformation which takes (x,y,z) into (x_1,y_1,z_1) as depicted in (a) is carried out in three steps: (1) rotation about z by δ (b), (2) rotation about the new intermediate y' axis by the tilt angle α (c), (3) and finally a rotation about the second intermediate z'' axis by $\pi-\phi_1$(d). As seen from (a), ϕ_1 represents the angle between the z_1-z plane and the x_1 axis for a particular domain. It serves to specify the orientation of the director in the domain frame whereas δ serves to specify the normal to the mean molecular plane in the domain frame.

33. Euler transformation from the initial lab frame to the lab frame. θ denotes the angle through which the sample was rotated.

34. Predicted line shape of rotated smectic-C. The tilt angle is 45° and the molecules rotate freely about their long axi. The angles given denote the angle through which the sample was rotated.

35. Luz and Meiboom calculated spectra.[19] Spectra are for a probe molecule containing two protons dissolved in a smectic-C. Only the high frequency component is shown; the complete spectrum is obtained by adding a image about zero frequency. The spectra on the left are for a tilt angle α of 10°, and those on the right for α = 40°.

36. Molecular alignment along the field in smectic-C domains. In (a), the molecules in both domains (I) and (II) are able to lie along the field. In (b), the sample has been rotated and though the molecules in (I) can align along the field, those in (II) cannot.
37. Molecular orientation in a domain changes as the sample is rotated. On going from (a) to (c), the molecules flip by 180°.
38. Case 3--principal axis and molecule fixed frames coincident.
39. Effect of the freezing out of motion about the long axis on lineshapes. The sample has been rotated 50°. In (a) free rotation occurs whereas in (b) the molecule is frozen.
40. Calculated order parameters. V_1 was chosen to be 10 and the dependence of the order parameters on V_2 is shown.